Generalized Stacked Sequential Learning

Eloi Puertas i Prats

Generalized Stacked Sequential Learning

Eloi Puertas i Prats

Department of Applied Mathematics and Analysis

Universitat de Barcelona

Doctoral advisors:

Dr. Oriol Pujol i Vila

Dr. Sergio Escalera Guerrero

A thesis submitted in the Mathematics and Computer Science Doctorate Program

Doctor in Mathematics - Computer Science (PhD)

Sep 2014

Abstract

In many supervised learning problems, it is assumed that data is independent and identically distributed. This assumption does not hold true in many real cases, where a neighboring pair of examples and their labels exhibit some kind of relationship. Sequential learning algorithms take benefit of these relationships in order to improve generalization. In the literature, there are different approaches that try to capture and exploit this correlation by means of different methodologies. In this thesis we focus on meta-learning strategies and, in particular, the stacked sequential learning (SSL) framework.

The main contribution of this thesis is to generalize the SSL highlighting the key role of how to model the neighborhood interactions. We propose an effective and efficient way of capturing and exploiting sequential correlations that take into account long-range interactions. We tested our method on several tasks: text line classification, image pixel classification, multi-class classification problems and human pose segmentation. Results on these tasks clearly show that our approach outperforms the standard stacked sequential learning as well as off-the-shelf graphical models such conditional random fields.

to my parents, brother and sister

All men by nature desire to know. An indication of this is the delight we take in our senses; for even apart from their usefulness they are loved for themselves; and above all others the sense of sight. For not only with a view to action, but even when we are not going to do anything, we prefer sight to almost everything else. The reason is that this, most of all the senses, makes us know and brings to light many differences between things.

ARISTOTLE. Book I, 980.a21: Opening paragraph of *Metaphysics*

Acknowledgements

First of all, I would like to thank my advisors Dr. Oriol Pujol and Dr Sergio Escalera for all the support they have giving me during all these years. Without your help this would not happen. Thank you both for your patience and everything else.

I would like to express my gratitude to all my colleagues of University of Barcelona, specifically those of the Department of *Matemàtica Aplicada i Anàlisi*, thanks to them, work and lunch is always a pleasure.

Thanks to my parents Miquel i Rosa, brother Santi and sister Susana for having always been there for me.

Many thanks to David Masip, Carles Noguera, Jordi Campos, Fèlix Bou, Santi Ontañon for all the discussions we had and for the time we spent together. Guys, you really are an inspiration to me.

I would like to mention the members of IIIA-CSIC and Computer Vision Center research centers I had work with, who have shared with me their knowledge and expertise.

I would also like to take this opportunity to thank my lifelong mentors: Josep Maria Fortuny, Eva Armengol, Maria Vanrell, Philippe R. Richard, Markus Hohenwarter, Jordi Vitrià, Francesc Esteve, Ramon López de Mántaras and Carles Sierra. Special thanks goes to Nate Davison for your lessons of life, guitar and english!

Finally, last but not least, I would like to thank all my doctoral fellows in MAIA department: Ari Farrés, Marta Canadell, Dani Pérez, David Martí, Jordi Canela, Carlos Domingo, Ruben Berenguel, Narcís, Marc, Roc, Giulia, Arturo, Nadia, Meri, Maya, Estefania, Miguel Ángel, Toni, Miguel Reyes, Dani, Albert Clapés, Cristina, Carles Riera, Àlex, Adriana, Santi, Laura, Katia, Francesco, Piero, Simone, Carlo, Marina, Elitza, Michal, Xavi Pérez, Òscar Amorós, Javi Morales and Victor Ponce. Each beer with you counts twice!

Per acabar els agraïments, ho faré en la meva llengua mare, el català.

Cada matí quan entro a l'edifici històric de la Universitat de Barcelona, no puc deixar de pensar per un moment que per allà mateix el meu avi Jaume, el meu avi Miguel, que només he conegut en fotografies, i les meves àvies Joana i Adoración deurien passejar-s'hi tot sovint. No puc, doncs, deixar de sentir orgull per tots els meus avis i els meus pares, per haver lluitat, sofert i finalment sortir-se'n endavant durant uns anys tant difícils com els que van haver de viure. El que he pogut gaudir durant tots aquests anys d'estudi, recerca i treball és gràcies a la seva constància i dedicació.

També vull aprofitar l'ocasió per agrair a tota la gent que des del moment en que vaig decidir començar a fer un llarg camí en l'Acadèmia han estat, en algun moment o un altre al meu costat. Els amics de debó sempre seran els millors aliats en els moments d'alegria i el millor refugi en els moments tristos.

Amb el Ferran, l'Àlex, en Jony, la Verònica, el Guillem i el David hem après a viure la Universitat. Amb l'Esteve i la Rosa, el David i l'Òscar hem passat els millors i pitjors moments. Amb el Carles, la Laia, la Su, l'Òscar, el Nèstor, la Marta, el Paco, el Santi, el Jordi i la Camp hem passat els moments més *heavys*. Amb la Cemre, l'Àngela i l'Amanda hem passat moments de tots colors, des dels més divertits al més surrealistes. Amb l'Ivette, l'Anna Bonfill, l'Elisabeth i l'Ariadna Valls, la Núria i el Loki i la Carolina hem constatat que com el Vallès no hi ha res. Amb el Jordi, l'Albert, l'Alfons hem descobert Catalunya des de Salses a Guardamar i de

Fraga a Maó. Amb el Toni Ferrero, Jordi Martínez, els Serres, el Kurto, el Pau, el Martí, el Miquel, el Naves, l'Òscar Bañó, el Robert i el Julià hem fet del futbol més que un esport. Amb la Diamar i l'Albert, el Reixaquet i l'Alba i l'Helena, el Sergi i el Quim hem pogut comprovar que qualsevol nit pot sortir el sol i que casa seva és casa nostra, si és que hi ha cases d'algú. Amb la Sara hem rigut molt. Amb la Marta Palacín hem tingut llargues tertúlies de café sobre la Fe dels Set i la diferència entre pletòric i platònic.

Gràcies a l'Anna Bertran per haver-me donat suport en iniciar aquest llarg camí. Gràcies a l'Anna Lliberia per aguantar-me quan no veia la llum al final del túnel. I sobretot gràcies a la Claire per haver-me acompanyat en aquest últim tram.

Finalment agrair també a tots els estudiants d'Enginyeria Informàtica de la Universitat de Barcelona que he tingut tots aquests anys i que m'han aguantat el rollo i suportat les bronques. Especialment a l'Albert Rosado, Adrian Hermoso, David Trigo, Carles Riera, Albert Clapés, Àlex Pardo, Matilde Gallardo, Albert Huélamo, Pablo Martínez i Xavi Moreno; us asseguro que he aprés més jo de vosaltres que no pas al revés.

Gràcies a tots per ser com sou!

PD: I will never forget you; Marc Esteve and Jordi Masip.

Contents

List of Figures

List of Tables

Input data	
$\mathbf{X}$	Set of input samples
$\mathbf{x}$	An input sample
C_i	The i^{th} class out of a total of N
$y \in \{C_1, C_2, \ldots, C_N\}$	Ground truth labels
Multi-scale SSL	
$H_1(x), H_2(x)$	Two classifiers working on the i.i.d. hypothesis
y'	Predicted label value by $h_1(\mathbf{x})$
$\hat{Y}$	Final MSSL prediction produced by $h_2(\mathbf{x}^{\mathbf{ext}})$
$\hat{F}(\mathbf{x}, \mathbf{c})$	A prediction confidence map
$J(y', \rho, \theta)$	A functional that models the labels context
θ	Neighborhood parameterization
ρ	Set of displacement vectors
M	Cardinality of ρ
$\vec{\rho}_m \in \rho$	A generic displacement vector
$\mathbf{z} \in \mathbb{R}^w$	The contextual feature vector produced by J
$w \in \mathbb{N}$	The length of the contextual feature vector $\mathbf{z}$
$\mathbf{x}^{\mathbf{ext}}$	The extended feature vector combining $\mathbf{x}$ and $\mathbf{z}$
Σ	Set of scales
$s \in \{1, 2, \ldots, S\}$	Index of the Σ scales
$G(\mu, \sigma)$	Multi-dimensional Gaussian distribution
$\Phi(s)$	Multi-resolution decomposition
$\Psi(s)$	Pyramidal decomposition
Multiclass MSSL	
n	Number of dichotomizers
b	A dichotomizer
M	ECOC coding matrix
$\mathcal{Y}$	A class codeword in ECOC framework
$\mathcal{X}$	A sample prediction codeword in ECOC framework
m_x	Margin for a prediction of sample $\mathbf{x}$
β	Constant which governs transition in a sigmoidean function
δ	A soft distance
α	Normalization parameter for soft distance δ
$\mathcal{P}$	A set of partitions of classes
P	A partition of groups of classes
γ	A symbol in a partition codeword
Γ	A partition codeword

Experiments settings

R	The mean ranking for each system configurations
E	The total number of experiments
k	The total number of system configuration
χ_F^2	Friedman statistic value
t	Number of iterations in an ADAboost classifier

1

Introduction

Over the past few decades, machine learning (ML) algorithms have become a very useful tool in tasks where designing and programming explicit, rule-based algorithms are infeasible. Some examples of applications where machine learning has been applied successfully are spam filtering, optical character recognition (OCR), search engines and computer vision. One of the most common tasks in ML is supervised learning, where the goal is to learn a general model able to predict the correct label of unseen examples from a set of known labeled input data. In supervised learning often it is assumed that data is independent and identically distributed (*i.i.d*). This means that each sample in the data set has the same probability distribution as the others and all are mutually independent. However, classification problems in real world databases can break this *i.i.d.* assumption. For example, consider the case of object recognition in image understanding. In this case, if one pixel belongs to a certain object category, it is very likely that neighboring pixels also belong to the same object, with the exception of the borders. Another example is the case of a laughter detection application from voice records. A laugh has a clear pattern alternating voice and non-voice segments. Thus, discriminant information comes from the alternating pattern, and not just by the samples on their own. Another example can be found in the case of signature section recognition in an e-mail. In this case, the signature is usually found at the end of the mail, thus important discriminant information is found in the context. Another case is part-of-speech tagging in which each example describes a word that is categorized as noun, verb, adjective, etc. In this case it is very unlikely that patterns such as [verb, verb, adjective, verb] occur. All these applications present a common feature: the sequence/context of the labels matters.

Sequential learning (25) breaks the *i.i.d.* assumption and assumes that samples are not independently drawn from a joint distribution of the data samples $\mathbf{X}$ and their labels Y. In sequential learning the training data actually consists of sequences of pairs $(\mathbf{x}, y)$, so that neighboring examples exhibit some kind of correlation. Usually sequential learning applications consider one-dimensional relationship support, but these types of relationships appear very frequently in other domains, such as images, or video.

Sequential learning should not be confused with time series prediction. The main difference between both problems lays in the fact that sequential learning has access to the whole data set before any prediction is made and the full set of labels is to be provided at the same time. On the other hand, time series prediction has access to real labels up to the current time t and the goal is to predict the label at $t + 1$. Another related but different problem is sequence classification. In this case, the problem is to predict a single label for an input sequence. If we consider the image domain, the sequential learning goal is to classify the pixels of the image taking into account their context, while sequence classification is equivalent to classify one full image as one class.

Sequential learning has been addressed from different perspectives: from the point of view of meta-learning by means of sliding window techniques, recurrent sliding windows or stacked sequential learning where the method is formulated as a combination of classifiers; or from the point of view of graphical models, using for example Hidden Markov Models or Conditional Random Fields.

In this thesis, we are concerned with meta-learning strategies. Cohen et al. (17) showed that stacked sequential learning (SSL from now on) performed better than CRF and HMM on a subset of problems called "sequential partitioning problems". These problems are characterized by long runs of identical labels. Moreover, SSL is computationally very efficient since it only needs to train two classifiers a constant number of times. Considering these benefits, we decided to explore in depth sequential learning using SSL and generalize the Cohen architecture to deal with a wider variety of problems.

1.1 Overview of Contributions

The contributions of this thesis aim to give solutions to the open problems in sequential learning described in (25) which are: a) how to capture and exploits sequential correlations; b) how to represent and incorporate complex loss functions; c) how to identify long-distance interactions; d) how to make sequential learning computationally efficient.

Our first contribution is a generalization of the SSL framework. We argue that a fundamental and overlooked step in SSL is the way in which the extended set (which is fed into the second classifier) is created. Instead of creating the extended set using a standard window approach, we propose a new aggregation method capable of capturing long-distance interactions efficiently. This method (MSSL) is based on a multi-scale decomposition of the first classifier predictions. In this way, we provide answers to the above open questions obtaining a method that: a) captures and exploit sequential correlations; b) since the method is a meta-learning strategy the loss function dependency is delegated to the second step classifier; c) it efficiently captures long-distance interactions; and d) it is fast, because it relies on training a few general learners.

Starting from this general framework, we propose a range of extensions with the purpose of making our architecture usable in a broader number of applications. By using theses extensions, our framework provides a general way for the classification of objects at different scales as well as for performing multi-class classification in an efficient way.

Our concluding contribution is an application of our framework for human body segmentation.

Summarizing, the main contributions of this thesis are:

- Multiscale Stacked Sequential Learning: A generalization of the SSL framework where the extended set is built by applying a multi-scale decomposition of the first classifier predictions.

- Scale invariant MSSL: An extended architecture of the MSSL framework useful when objects appear at different scales. Using this methodology different sized objects can be classified correctly without retraining.

- Multi-class MSSL: A way to extend MSSL to multi-class classification problems. By applying the ECOC framework in the base classifiers of MSSL and converting predictions to a likelihood measure we propose a general way to use MSSL in multi-class classification

- Memory-efficient multi-class MSSL: A compression approach of multi-class MSSL for reducing the number of features in the extended set depending on the number of classes.

- Application of MSSL for human body segmentation: An application of MSSL framework for human body segmentation. Here results show that our framework gives useful contextual information about joint body parts, helping to improve final classification accuracy.

1.2 Outline

This thesis proceeds as follows:

Chapter 2: Background. Chapter 2 covers some background material on sequential learning from several points of view inside machine learning: meta-learning, hidden markov models and discriminative probabilistic graphical models. Moreover, from the side of computer vision, works related to contextual information are also described. Finally some works specifically related to sequential learning applied to multi-class problems are shown.

Chapter 3: Generalized Stacked Sequential Learning. In chapter 3 we introduce our main contribution to the sequential learning problem. First a generalization of the called stacked sequential learning method is described. Next, an implementation of the proposed multi-scale stacked sequential learning (MSSL) method is presented explained. Finally, experiments and results comparing our methodology with other sequential learning approaches are discussed.

Chapter 4: Extensions to MSSL. Chapter 4 provides several improvements over MSSL framework. First the inclusion of likelihoods measures instead of class labels in the stacked pipeline is proposed. Next, we show the extended architecture of our framework, where objects can be classified at different scales without retraining. In addition, a general methodology for multi-class classification problem is integrated with MSSL framework. Finally, an approach for compressing the number of features in the stacked pipeline is described.

Chapter 5: Application of MSSL for human body segmentation. In chapter 5 an application of MSSL for human body segmentation is described. Here the stacked pipeline is modified to be used along with cutting-edge technologies for body segmentation.

Chapter 6: Conclusions. Chapter 6 concludes this thesis, highlighting the most relevant contributions of this work.

1.3 List of publications

Much of the work presented here has appeared first in other publications. The results of Chapter 3 appeared in (34), though the discussion here is extended. The extension to our MSSL framework *learning objects at multiple scales* described in Chapter 4 appeared in (52). The multi-class and the compression of the extended set appeared in (53).

Finally the application of MSSL for human body segmentation has been published in the ECCV14 workshop *ChaLearn Looking at People: pose recovery, action/interaction, gesture recognition* that will be held in Zurich, Switzerland from September 6th to 12th 2014 (54).

In addition of these publications, preliminary results were presented in high relevant conferences in the area. A comprehensive list of all the contributions is found in the following lines:

- (2009) Multi-modal laughter recognition in video conversations. S Escalera, E Puertas, P Radeva, O Pujol. *Computer Vision and Pattern Recognition Workshops, 2009. CVPR Workshops. IEEE Computer Society Conference on,*
- (2009) Multi-scale stacked sequential learning. O Pujol, E Puertas, C Gatta. *Multiple Classifier Systems*, 262-27.
- (2009) Multi-Scale Multi-Resolution Stacked Sequential Learning. E Puertas, C Gatta, O Pujol. *Proceedings of the 12th International Conference of the Catalan Association for Artificial Intelligence (CCIA).* 112-117.
- (2010) Classifying Objects at Different Sizes with Multi-Scale Stacked Sequential Learning. E Puertas, S Escalera, O Pujol *Proceedings of the 10th International Conference of the Catalan Association for Artificial Intelligence (CCIA)*, 193-200.
- (2011) Multi-scale stacked sequential learning. C Gatta, E Puertas, O Pujol. *Pattern Recognition* 44 (10), 2414-2426
- (2011) Multi-class multi-scale stacked sequential learning. E Puertas, S Escalera, O Pujol. *Multiple Classifier Systems*, 197-206
- (2013) Generalized multi-scale stacked sequential learning for multi-class classification. E Puertas, S Escalera, O Pujol. *Pattern Analysis and Applications*, 1-15

Additionally, in the following lines a list of other coauthored published works related to this PhD is given:

- (2010) Adding Classes Online in Error Correcting Output Codes Framework. S Escalera, D Masip, E Puertas, P Radeva, O Pujol *ICPR 2010*, 2945-2948

- (2011) Online error correcting output codes. S Escalera, D Masip, E Puertas, P Radeva, O Pujol. *Pattern Recognition Letters* 32 (3), 458-467

2

Background

In this chapter we first explain the sequential learning concept. Next, previous works related to sequential learning from different points of view are described. Besides these related works coming from the machine learning field, sequential learning can be applied in computer vision problems as a tool for contextual information retrieval. Therefore, relevant works in this area are also commented. To conclude this chapter, we point out some works related to sequential learning but explicitly in the case of multi-class problems.

2.1 Sequential Learning

The classical supervised learning problem consists in constructign a classifier that can correctly predict the classes of new objects given training examples of already known objects (48). This task is typically formalized as follows:

Let assume the problem domain of classifying a pixel of an image to the class which it belongs to. Let $\mathbf{X}$ denote an image of an object of interest and $Y \in \{C_1, C_2, ..., C_N\}$ denote the corresponding ground truth label image. A training example is a pair $(\mathbf{x}, \mathbf{y})$ consisting of a pixel of the image and its associated class label. We assume that the training examples are drawn independently and identically from the joint distribution $P(\mathbf{x}, \mathbf{y})$, and we will refer to a set of n such examples as the training data. A classifier is a function H that maps from images to classes. The goal of the learning process is to find an H that correctly predicts the class $y = H(\mathbf{x})$ for each pixel $\mathbf{x}$ from a new image. This is accomplished by searching some space $\mathcal{H}$ of possible classifiers for a classifier that produces good results on the training data without overfitting. One thing that is apparent in this and other applications is that they do not quite fit the supervised learning framework. Rather than being drawn independently and identically (*i.i.d.*) from some joint distribution $P(\mathbf{x}, \mathbf{y})$, the training data actually consist of sequences of $(\mathbf{x}, \mathbf{y})$ pairs. These sequences exhibit significant sequential correlation. That is, nearby x and y values are likely to be related to each other. Sequential patterns are important because they can be exploited to improve the prediction accuracy of our classifiers, as in the case of image segmentation, where surrounding pixels belong to the same class, except for the ones on the edges.

Sequential learning (25) breaks the independent and identically distributed (**i.i.d.**) assumption and assumes that samples are not independently drawn from a joint distribution of the data samples $\mathbf{X}$ and their labels Y. In sequential learning the training data consists of sequences of pairs $(\mathbf{x}, \mathbf{y})$, and the goal is to construct a classifier H that can correctly predict a new label sequence $Y = h(\mathbf{X})$ given an input sequence $\mathbf{X}$.

Sequential learning is often confused with two other, closely-related tasks. The first of these is the time-series prediction problem. The main difference between both problems lays in the fact that sequential learning has access to the whole data set before any prediction is made and the full set of labels is to be provided at the same time. On the other hand, time series prediction has access to real labels up to the current time t and the goal is to predict the label at $t+1$. The second closely-related task is sequence classification. In this task, the problem is to predict a single label y that applies to an entire input sequence $\mathbf{X}$. For example, in the case of images, instead of classifying each pixel of the image, simply to say whether the whole image belongs to a class or another.

In literature, sequential learning has been addressed from different perspectives. We split them into three big families: a) from the point of view of meta-learning techniques, b) from the point of view of hidden markov models and c) from the point of view of various probabilistic graphical models.

2.1.1 Meta-Learning sequential learning

Meta-learning techniques (71) use a combination of different classifiers in order to predict a test example. The idea is to extend the classical supervised learning problem in a recursive fashion, where each step is aimed to obtain better results than the previous, but without overfitting. Recurrent sliding windows and stacked learning are well-known meta-learning strategies. In next subsections they are explained whitin the context of sequential learning,

2.1.1.1 Sliding and recurrent sliding window

The sliding window method converts the sequential supervised learning problem into the classical supervised learning problem. It constructs a classifier H that maps an input window of width w into an single output value y. Specifically, let $d = (w-1)/2$ be the half-width of the window. Then H predicts y_i using the window $[x_{t-d}, x_{t-d+1}, \ldots, x_t, \ldots, x_{t+d-1}, x_{t+d}]$. The window classifier H is trained by converting each sequential training example $(\mathbf{x_i}, \mathbf{y_i})$ into windows and then applying a standard supervised learning algorithm. A new sequence $\mathbf{x}$ is classified by converting it to windows, applying H to predict each y to form the predicted sequence Y. The obvious advantage of this sliding window method is that it permits any classical supervised learning algorithm to be applied. Although the sliding window method gives adequate performance in many applications(29, 55, 63), it does not take advantage of correlations between nearby y_t values. To be more precise, the only relationships between nearby y_t values that are captured are those that are predictable from nearby $\mathbf{x_t}$ values. If there are correlations among the y_t values that are independent of the $\mathbf{x_t}$ values, then these are not captured. One way that sliding window methods can be improved is to make them recurrent. In a recurrent sliding window method, the predicted value y_t is fed as an input to help make the prediction for y_{t+1}. Specifically, with a window of half-width d, the most recent d predictions, $y_{t-d}, yt - d + 1, \ldots, y_{t-1}$, are used as inputs (along with the sliding window $[\mathbf{x_{t-d}}, \mathbf{x_{t-d+1}}, \ldots, \mathbf{x_t}, \ldots, \mathbf{x_{t+d-1}}, \mathbf{x_{t+d}}]$) to predict y_t. Clearly, the recurrent method captures predictive information that was not being captured by the simple sliding window. The values used for the y_t inputs when training the classifier can be achieved by means of meta-learning; by training a first non-recurrent classifier, and then use its y_t predictions as the inputs. This process can be iterated, so that the predicted outputs from each iteration are employed as inputs in the next iteration. Another approach is to use the correct labels y_t as the inputs. The advantage of using the correct labels is that training can be performed with the standard supervised learning algorithms, since each training example can be constructed independently. On the other hand, when correct labels are used instead of predicted labels, the window classifier can overfit, thus the features used during the training will be much more accurate than the ones used during testing, leading the classifier to a higher testing error by relying on not trustworthy features. By using a first non-recurrent classifier we can know the *a priory* accuracy of the predictions features that will be used during the testing phase, resulting in a more reliable testing error.

2.1.1.2 Stacked sequential learning

Stacked sequential learning is a meta-learning (71) method, in which an arbitrary base learner is augmented, in this case, by making the learner aware of the labels of nearby examples. Basically, the stacked sequential learning (SSL) scheme is a two layers classifier where, firstly, a base classifier $H_1(x)$ is trained and tested with the original data $\mathbf{X}$. Then, an extended data set is created which joins the original training data features $\mathbf{X}$ with the predicted labels Y' produced by the base classifier considering a fixed-size window around the example. Finally, a second classifier $H_2(x)$ is trained with this new feature set. Then the inference algorithm takes part. Using the trained model of H_1 on new instances $\mathbf{x}$, a set of predictions $\hat{y}$ are obtained. With these predictions, a new extended set instance $\mathbf{x^{ext}}$ is constructed as above. Finally, using the trained model of H_2 on this extended set, a final set of predictions $\hat{Y}$ are obtained. Figure 2.1 describes the SSL algorithm. The main drawback of the SSL approach is that the width of the window around the sample determines the maximum length of interaction among samples. Therefore, the longer the window, the further the interaction is considered, but also the extended data set is increased in terms of features. This makes this approach not suitable for problems that present long range sequential relationships. Furthermore, if we consider more than one relationship dimension, the size of the extended set increases exponentially, making it not feasible for sequential type of datasets like images.

2.1.2 Hidden Markov Models

The hidden Markov Model (HMM (1, 56)) is a statistical Markov model in which the system being modeled is assumed to be a Markov process with unobserved (*hidden*) states. A HMM can be presented as the simplest dynamic Bayesian network. HMM describes the joint probability $P(\mathbf{x}, \mathbf{y})$ of a collection of hidden and observed discrete random variables. It is defined by two probability distributions: the transition distribution $P(y_t|y_{t-1})$, which tells how adjacent y values are related, and the observation distribution $P(\mathbf{x}|\mathbf{y})$, which tells how the observed x values are related to the hidden y values. It relies on the assumption that the t^{th} hidden variable given the $(t-1)^{th}$ hidden variable is independent of previous hidden variables, and the current observation variables depend only on the current hidden state. These distributions are assumed to be stationary (i.e., the same for all times t). In most learning problems, $\mathbf{x}$ is a vector of features $(x_1, \ldots, x_n)$, which makes the observation distribution difficult to handle without further assumptions. A common assumption is that each feature is generated

```
**Parameters:** a neighborhood window of size W, a cross-validation parameter K, two base classifiers $H_1$ and $H_2$
**Result:** prediction $\hat{y} = H_2 x$

*Learning algorithm*: Given a data set $\mathbf{X} = \{(\mathbf{x_t}, \mathbf{y_t})\}$
// Construct a sample of predictions $Y_t'$ for each $\mathbf{x_t} \in \mathbf{X}$ as follows:
1. Split $\mathbf{X}$ into $K$ equal-sized disjoint subsets $X_1, \dots, X_k$
for $i \leftarrow 1$ to $K$ do
  2. $f_j \leftarrow H_1(\mathbf{X} - \mathbf{X_j})$
end for
3. $Y' \leftarrow \{(\mathbf{x_t}, \mathbf{y_t'}) : \mathbf{y_t'} \leftarrow \mathbf{f_j}(\mathbf{x_t}); \mathbf{x} \in \mathbf{X_j}\}$
// Construct an extended set $\mathbf{x^{ext}}$
4. $\mathbf{x^{ext}} \leftarrow (\mathbf{x_t}', \mathbf{y_t}) : \mathbf{x_t}' \leftarrow [\mathbf{x_1'}, \dots, \mathbf{x_t'}]$ where $x_i' \leftarrow (x_i, y_i' - W, \dots, y_i' + W)$ and $y_i'$ is the $i$-th component of $y_t'$, the label vector paired with $\mathbf{x_t} \in \mathbf{Y}'$
return $\{f \leftarrow H_1(\mathbf{X}), \mathbf{f}' \leftarrow \mathbf{H_2}(\mathbf{x^{ext}})\}$

*Inference algorithm*: Given an instance vector $\mathbf{x}$
1. $\hat{y} \leftarrow f(\mathbf{x})$
2. Construct an extended set instance $\mathbf{x^{ext}}$, as above (using $\hat{y}$ instead of $y_t'$)
return $\hat{Y} \leftarrow f'(\mathbf{x^{ext}})$
```

Figure 2.1: Stacked sequential learning algorithm.

independently (conditioned on y). This means that $P(\mathbf{x}|\mathbf{y})$ can be replaced by the product of n separate distributions $P(x_j|y), j = 1, \ldots, n$.

In a sequential supervised learning problem, it is straightforward to determine the transition and observation distributions. $P(y_t|y_{t-1})$ can be computed by looking at all pairs of adjacent y labels Similarly, $P(x_j|y)$ can be computed by looking at all pairs of x_j and y. The most complex computation is to predict a value $\hat{y}$ given an observed sequence $\mathbf{x}$. Because the HMM is a representation of the joint probability distribution $P(\mathbf{x}, \mathbf{y})$, it can be applied to compute the probability of any particular y given any particular $\mathbf{x} : P(\mathbf{y}|x)$. Hence, for an arbitrary loss function $L(\hat{y}, y)$, the optimal prediction is:

$$\hat{y} = \arg\min_z \sum_y P(y|\mathbf{x}) L(z, y).$$

In the case where the loss function decomposes into separate decisions for each y_t, the Forward-Backward algorithm (56) can be applied. Rather, where the loss function depends on the entire observed sequence, the goal is usually to find the y with the highest probability: $y = \arg\max_y P(y|\mathbf{x})$. This can be solved by the dynamic programming algorithm known as the Viterbi algorithm (56), that computes, for each class label c and each time step t, the probability of the most likely path starting at time 0 end ending at time t with class u. When the algorithm reaches the end of the sequence, it has computed the most likely path from time 0 to time t_i and its probability.

Although HMMs provide an elegant and sound methodology, they suffer from one principal drawback: any relationship relying on long-range interactions (this is, involving not only two consecutive y values) cannot be captured by a first-order Markov model (i.e., where $P(y_t)$ only depends on y_{t-1}). A second problem with the HMM model is that it generates each $\mathbf{x_t}$ only from the corresponding y_t. This makes it difficult to use an input window, moreover if the input window is not just of one dimension, but two, like in the case of images, where there exists a spatial relationship.

2.1.3 Discriminative Probabilisitic Graphical Models

Several directions have been explored to try to overcome the limitations of the HMM. The introduction of probabilistic graphical models that represent discriminative model $P(\mathbf{y}|\mathbf{x})$ rather than the generative model $P(\mathbf{x}, \mathbf{y})$ is one of these directions. These models do not try to explain how the $\mathbf{x}$'s are generated. Instead, they just try to predict the y values given the $\mathbf{x}$'s. In a generative model, one expends efforts to model the joint distribution $P(\mathbf{x}, \mathbf{y})$, which involves implicit modeling of the observations $\mathbf{x}$. This means that the generative approach may spend a lot of resources on modeling the generative

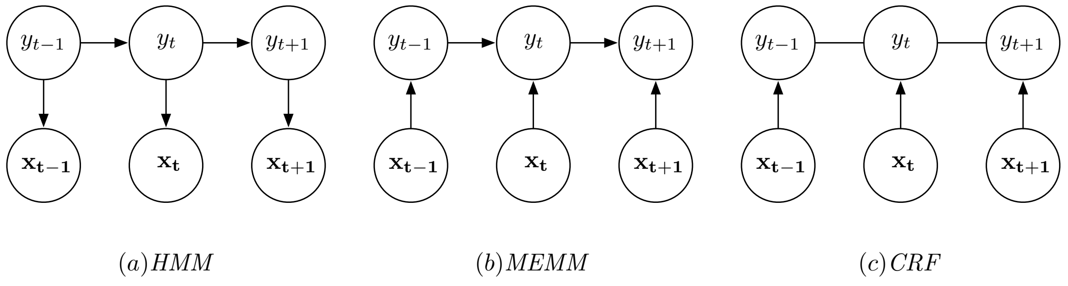

Figure 2.2: Graphical structures of HMM, MEMM and CRF for sequencial learning.

models which are not particularly relevant to the task of inferring the class labels. This permits them to use arbitrary features of the $\mathbf{x}$'s including global features, features describing non-local interactions, and sliding windows. Moreover, discriminative approaches can be particularly beneficial in cases where the domain of $\mathbf{x}$ is very large or even infinite. Some examples of discriminative graphical models are: Maximum Entropy Markov models (MEMM (47)), Input-Output HMM (IOHMM (5)), Conditional random fields (CRF (44)). Figure 2.2 shows the graphical structures of HMM which is a purely generative model, MEMM which is a discriminative model, hence it represents a conditional distribution $P(y|\mathbf{x})$ and CRF which is also discriminative model but here the interactions between the labels y are modeled as undirected edges.

2.1.3.1 Maximum Entropy Markov model (MEMM)

A maximum-entropy Markov model (MEMM), or conditional Markov model (CMM), is a probabilistic graphical model that combines features of hidden Markov models (HMMs) and maximum entropy (MaxEnt) models. An MEMM is a discriminative model that extends a standard maximum entropy classifier by assuming that the unknown values to be learnt are connected in a Markov chain rather than being conditionally independent of each other, i.e. it learns $P(y_t|y_{t-1}, \mathbf{x_t})$. It is trained via a maximum entropy method that attempts to maximize the conditional likelihood of the data: $\prod_{i=1}^{n} P(y_i|y_{i-1}, \mathbf{x_t})$. The maximum entropy approach represents $P(y_t|y_{t-1}, \mathbf{x_t})$ as a log-linear model:

$$P(y_t|y_{t-1}, \mathbf{x}) = \frac{1}{Z(\mathbf{x}, y_{t-1})} \exp\left(\sum_a \lambda_a f_a(\mathbf{x}, y_t)\right),$$

where, the $f_a(\mathbf{x}, \mathbf{y_t})$ are real-valued or categorical feature-functions that can depend on y_t and on any properties of the input sequence x, and $Z(\mathbf{x}, \mathbf{y_{t-1}})$ is a normalization term ensuring that the distribution sums to one. This form for the distribution corresponds to the maximum entropy probability distribution satisfying the constraint that the empirical expectation for the feature is equal to the expectation given the model:

$$\mathrm{E}_e\left[f_a(\mathbf{x},\mathbf{y})\right] = \mathrm{E}_p\left[f_a(\mathbf{x},\mathbf{y})\right] \quad \forall a.$$

The parameters λ_a can be estimated using generalized iterative scaling (21). The optimal state sequence $y_1, \ldots, y_n$ can be found using a very similar Viterbi algorithm to the one used for HMMs.

Bengio and Frasconi (5) introduced a variation of MEMM called Input-Output HMM (IOHMM). It is similar to the MEMM except that it introduces hidden state variables s_t in addition to the output labels y_t. Sequential interactions are modeled by the s_t variables. To handle these hidden variables during training, the Expectation-Maximization (EM (22)) algorithm is applied.

One drawback of MEMMs and IOHMM models is that they potentially suffer from the "label bias problem". Notice that in MEMM model:

$$\begin{aligned}\sum_{y_t} P(y_t|y_{t-1}, \mathbf{x}_1, \ldots, \mathbf{x}_t) &= \sum_{y_t} P(y_t|yt-1, \mathbf{x}_t) \cdot P(y_{t-1}|\mathbf{x}_1, \ldots, \mathbf{x}_{t-1}) \\ &= 1 \cdot P(y_t|y_{t-1}, \mathbf{x}_1, \ldots, \mathbf{x_{t-1}}) \\ &= P(y_t|y_{t-1}, \mathbf{x_1}, \ldots, \mathbf{x_{t-1}})\end{aligned}$$

This says that the total probability mass "received" by y_{t-1} (based on $x_1, \ldots, x_{t-1}$) must be "transmitted" to labels y_t at time t regardless of the value of x_t. The only role of x_t is to influence which of the labels receive more of the probability at time t. In particular, all of the probability mass must be passed on to some y_t even if x_t is completely incompatible with y_t. Thus, observations $\mathbf{x_t}$ from later in the sequence has absolutely no effect on the posterior probability of the current state; or, in other words, the model does not allow for any smoothing.

Conditional random fields (CRF) (44) were designed to overcome this weakness, which had already been recognized in the context of neural network-based Markov models in the early 1990s. Another source of label bias is that training is always done with respect to known previous predictions, so the model struggles at test time when there is uncertainty in the previous prediction.

2.1.3.2 Conditional Random Fields (CRF)

Conditional random fields (44) are a type of discriminative undirected probabilistic graphical model. In the CRF, the relationship among adjacent pairs y_{t-1} and y_t is modeled as an Markov Random Field (13) conditioned on the $\mathbf{x}$ inputs. In other words, the way in which the adjacent y values influence each other is determined by the input features. It is used to encode known relationships between examples and construct consistent interpretations. The CRF is represented by a set of potentials $M_t(y_{t-1}, y_t|\mathbf{x})$, for each position in t in the sample sequence x, it is defined as:

$$\begin{aligned} M_t(y_{t-1}, y_t|\mathbf{x}) &= \exp(\Lambda_t(y_{t-1}, y_t|\mathbf{x})) \\ \Lambda_t(y_{t-1}, y_t|\mathbf{x}) &= \sum_k \lambda_k f_k(y_{t-1}, y_t, \mathbf{x}) + \sum_k \mu_k g_k(y_t, \mathbf{x}), \end{aligned}$$

where the f_k are features that encode some information about y_{t-1}, y_t, and arbitrary information about $\mathbf{x}$, and the g_k are features that encode some information about y_t and $\mathbf{x}$. It is assumed that both f_k and g_k are given and fixed. In this way, it is possible to incorporate arbitrarily long-distance information about $\mathbf{x}$. The conditional probability $P(y|\mathbf{x})$ is written as:

$$P(y|\mathbf{x}) = \frac{\prod_{t=1}^{n+1} M_t(y_{t-1}, y_t|\mathbf{x})}{\left[\prod_{t=1}^{n+1} M_t(\mathbf{x})\right]_{\text{start,stop}}},$$

where $y_0 = \text{start}$ and $y_{n+1} = \text{stop}$. The normalizer in the denominator is needed because the potentials M_t are unnormalized "scores".

The training of CRFs is expensive, because it requires a global adjustment of the λ values. This global training is what allows the CRF to overcome the label bias problem by allowing the x_t values to modulate the relationships between adjacent y_{t-1} and y_t values. Algorithms based on iterative scaling and gradient descent have been developed for optimizing both $P(y|\mathbf{x})$ and also for separately optimizing $P(y_t|\mathbf{x})$ for loss functions that depend only on the individual label. Whereas in HMMs or MEEMs case, each gradient step required only a single execution of inference, when training a CRF, we must execute inference for every single data case, conditioning on variables $\mathbf{x}$. This makes the training phase considerably more expensive than HMMs or MEMMs. For example, in image classification task, inference step using a generative method involves summation over the space of all possible images; if we have $N \times N$ image where each pixel can take 256 values, the resulting space has 256^{N^2} values, giving rise to a highly intractable inference problem (even using approximate inference methods). The next section shows other methods and approaches that particularly exploit contextual information in image classification tasks.

2.2 Contextual information in image classification tasks

While the contribution of this thesis can appear limited into the machine learning area, it is also of interest for the computer vision community. A large part of the computer vision community is recently devoting efforts to exploit contextual information to improve classification performance in object/class recognition and segmentation. For these reasons, relevant state of the art comes from machine learning as well as from computer vision communities.

The use of contextual information is potentially able to cope with ambiguous cases in classification. Moreover, the contextual information can increase a machine learning system performance both in terms of accuracy and precision, thus helping to reduce both false positive and false negatives. However, the methods presented in the previous section suffer from different disadvantages.

Although CRFs are a general and powerful framework for combining features and contextual information, its application to image classification tasks can be very expensive. This is because the computational cost of both training and inference are very high and both proportional to the exponential of the clique cardinality. Since we assume that all the variables are observed in the training set, we can find the global optimum of the objective function, so long as we can compute the gradient exactly. Unfortunately for CRF involving large clique cardinality it is not tractable to compute the exact gradient. Several approximate inference methods have been used, like mean field, loopy belief propagation (69) or graph cuts (11). Even though approximate inference methods will be used, if the clique is not reduced to a few nodes (usually the 4-neighborhood, i.e. the pixels at north, west, south and east of the center pixel), it is infeasible to compute the inference step. In fact, successful CRF models (43, 68) have been applied to groups of pixels using a clique of size 2 on a 4-neighborhood.

Other methods of the literature exploit contextual information by identifying super-pixels using segmentation algorithms tuned to perform over-segmentation (18, 36, 37). In (37), for example, the set of super-pixels is clustered forming a vocabulary of possible local contexts. Finally, the super-pixels are considered as the context for classification by considering the spatial relationship between the pixel (or area) being classified and the neighborhood super-pixels. In (18, 36) the super-pixels are used to form the puzzle that better fits the object, using also contextual information, and geometric coherence, among different puzzles. All these methods assume that an over-segmentation is possible, and hopefully, different super-pixels can cluster together in a semantically meaningful way.

Other contextual methods extract a global representation of the context, and use it to influence the classification step. In (65), the context is modeled globally. Thus, the method does not locally compute the context and can not relate labels (or objects) spatially (or temporally) by means of the local context.

2.3 Sequential learning in multi-class problems

Usually, the applications considered need classifiers that are able to deal with multiple classes. However, in the case of sequential learning, few of the previous approaches are able to deal with the multi-class case. One case of multi-class extension is the CRF using graph-cut with alpha-expansion (11). Another approach is to decompose the multi-class problem into a set of binary-class problems and combine them in some way. In this sense, the Error-Correct Output Codes (ECOC) (24) framework is a well-studied methodology that is used to transform multi-class problems to an ensemble of binary classifiers. The fundamental issues here are: how this decomposition can be done in an efficient way, and how a final classification can be obtained from the different binary predictions. In the ECOC framework, these two issues are defined as coding and decoding phases in a communication problem. During the coding phase a codeword is assigned to each label in the multi-class problem. Each bit in the codeword identifies the membership of such class for a given binary classifier. The most used coding strategies are the *one-versus-all* (50), where each class is discriminated against the rest and *one-versus-one* (3), which splits each possible pairs of classes. The decoding phase of the ECOC framework is based on error-correcting principles, where distances measurements between the output code and the target codeword are the strategies most frequently applied. Among these, Hamming and Euclidean measures are the most used (27).

2.4 Conclusions

Independently of the specific method, there are still fundamental issues in sequential supervised learning that require the attention of the community. In (25) the authors acknowledge the following issues: a) how to capture and exploit sequential correlations; b) how to represent and incorporate complex loss functions; c) how to identify long-distance interactions; d) how to make sequential learning computationally efficient.

In the next chapter we propose our contribution to the sequential learning research. Our framework, called Generalized SSL (GSSL), is a generalization of the standard stacked sequential learning stated in the stacked sequential learning section 2.1.1.2. Our method aims to give an answer to these previous questions. Particularly, we are interested in how to capture and exploit sequential correlations and how to identify long-distance interactions, focusing on image classification tasks. Our secondary goal is to do it as generally (i.e. setting the minimum number of parameter) as possible, while being computationally efficient and accurate compared to general probabilisitics models, as CRFs.

3

Generalized Stacked Sequential Learning

In this chapter, first (Section 3.1) we propose a Generalized Stacked Sequential Learning (GSSL) schema for classification tasks. As mentioned in the previous chapter, our contribution is centered on sequential learning problems. Sequential learning assumes that samples are not independently drawn from a joint distribution of the data samples $\mathbf{X}$ and their labels Y. Therefore, here the training data is considered as a sequence of pairs: example and its label $(\mathbf{x}, y)$, such that neighboring examples exhibit some kind of relationship.

Cohen *et al* (17) presents an approach of sequential learning based on a meta-learning framework (71) . Basically, the Stacked Sequential Learning (SSL) scheme is a two layers classifier where, firstly, a base classifier $H_1(x)$ is trained and tested with the original data $\mathbf{X}$. Then, an extended data set is created which joins the original training data features $\mathbf{X}$ with the predicted labels Y' produced by the base classifier considering a fixed-size window around the example. Finally, second classifier $H_2(x)$ is trained with this new feature set. The final result is a set of predictions $\hat{Y}$. Figure 3.1 shows a scheme of the SSL framework. As said before, the main drawback of this SSL approach is that the width of the window around the sample determines the maximum length of interaction among samples. Therefore, the longer the window, the further the interaction is considered, but also the extended data set is increased in terms of features. This makes this approach not suitable for problems that present long range sequential relationships. Furthermore, if we consider more than one relationship dimension, the size of the extended set increases exponentially, making it not feasible for sequential types of datasets like images, videos, or time series. Our method aims to give an answer to these drawbacks. Particularly, we are interested in how to capture and exploit sequential correlations and how to identify long-distance interactions, focusing on image classification tasks. Our secondary goal is to do it as generally (i.e. setting the minimum number of parameter) as possible, while being computationally efficient and accurate compared with general probabilisitics models, as CRFs.

Next, section 3.2 describes our implementation of Generalized Stacked Sequential Learning, called Multi-scale Stacked Sequential Learning (MSSL), which gives response to these questions. Finally this chapter ends (Section 3.3) with some experiments using our approach and a discussion of the results obtained.

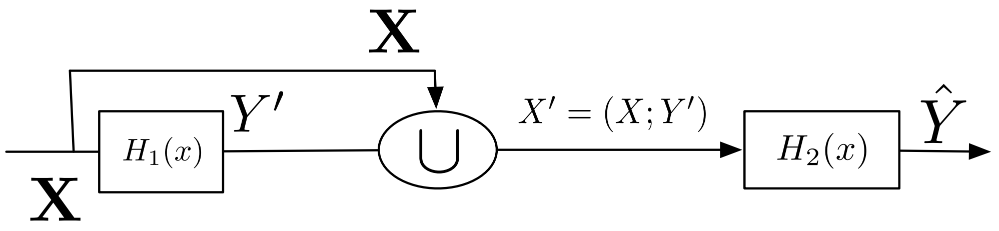

Figure 3.1: Block diagram for the stacked sequential learning.

3.1 Generalized Stacked Sequential Learning

The framework for generalizing the stacked sequential learning includes a new block, called J, in the pipeline of the basic SSL. Figure 3.2 shows the Generalized Stacked Sequential Learning process.

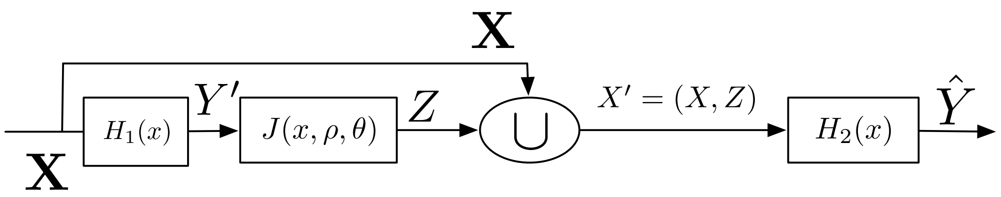

Figure 3.2: Block diagram for the generalized stacked sequential learning.

As before, a classifier $H_1(x)$ is trained with the input data set $\mathbf{X} \in (\mathbf{x}, \mathbf{y})$ and the predicted labels Y' are obtained. Now, but, the next block defines the policy for creating the neighborhood model of the predicted labels, where $z = J(y', \rho, \theta) : \mathcal{R} \to \mathcal{R}^w$ is a function that captures the data interaction with a model parameterized by θ in a neighborhood ρ. The result of this function is a w-dimensional value, where w is the number of elements in the support lattice of the neighborhood ρ. In the case of defining

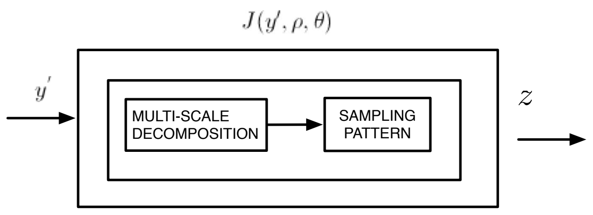

Figure 3.3: Design of $J(y', \rho, \theta)$ in two stages: a multi-scale decomposition followed by a sampling pattern.

the neighborhood by means of a window, w is the number of elements in the window. Then, the output $z = J(y', \rho, \theta)$ is joined with the original training data creating the extended training set $\mathbf{X}' \in (\mathbf{x}', \mathbf{z})$. This new set is used to train a second classifier $H_2(\mathbf{x}')$ with the goal of producing the final prediction $\hat{Y}$. Observe, that the system will be able to deal with neighboring relations depending on how well $J(y', \rho, \theta)$ characterize them. In next section we propose a way for defining neighboring relationships based on multi-scale decomposition.

3.2 Multi-Scale Stacked Sequential Learning (MSSL)

In our approach called Multi-Scale Stacked Sequential Learning (MSSL), we propose to design $J(y', \rho, \theta)$ function in a two stage way: (1) first the output of the classifier $H_1(x)$ is represented according to a multi-scale decomposition in a similar way of Laplacian-pyramid code by Burt and Andelson(12) and (2) a grid sampling of the resulting decomposition to create the extended set $\mathbf{x}^{\mathbf{ext}}$. The first stage answers how to model the relationship among neighboring locations, and the second stage answers how to define the support lattice given by the extended set. Figure 3.3 shows the two stages composing J.

In the next subsections we will explain how to obtain a *multi-resolution decomposition* and a *pyramidal decomposition.* Then, an appropriate sampling pattern is presented for the two types of multi-scale decompositions. Finally, we discuss advantages and disadvantages of each decomposition method. A discussion on how the sampling schema influences the long-range interaction ends the section.

3.2.1 Multi-scale decomposition

We propose two ways to decompose the initial label field that outputs the first classifier $H_1(x)$. A standard multi-resolution (MR-MSSL) decomposition and a pyramidal decomposition (Pyr-MSSL). To clarify the method, figure 3.4 shows an example in which a label field, resulting from an image classification algorithm, is decomposed and sampled.

s	Multi-resolution	Pyramidal
1	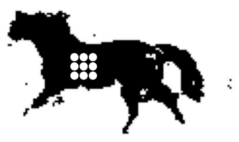	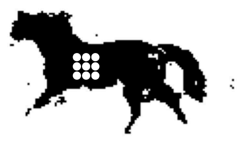
2	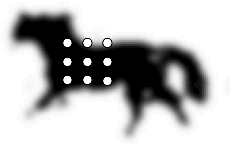	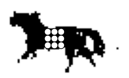
3	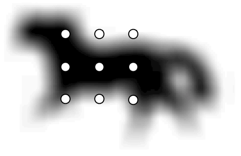	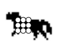

Figure 3.4: Two examples of multi-scale decomposition and a possible sampling pattern for both. White and black crosses denote the sampling positions.

3.2.1.1 Multi-resolution Decomposition

The Multi-resolution decomposition directly derives from classical multi-resolution theory in image processing and analysis. Given $y'_{C_i}(\vec{q})$, the probability, the marginal, or the likelihood of the class C_i at position $\vec{q}$; we define the multi-resolution decomposition Φ, as following:

$$\Phi_{C_i}(\vec{q}; s) = y'_{C_i}(\vec{q}) * G(0, \gamma^{s-1}) \qquad (3.1)$$

where $s \in \{1, 2, \ldots, S\}$ represents the scale; '$*$' is the convolution operator, G is a multidimensional Gaussian distribution with zero mean and $\sigma = \gamma^s$. Here γ is the "step" of the multi-resolution decomposition (typically $\gamma = 2$). As it can be seen in figure 3.4, this methodology, applied on label fields coming from image pixel classification, is mimicking exactly the well known multi-scale methodology used in image processing and analysis techniques. However here the images represent the probability, the marginal or the likelihood of a certain class. As a result, the Multi-resolution decomposition provides information regarding the spatial homogeneity and regularity of the label field at different scale. It is easy to understand that, for example, a noisy classification at scale 1 does not influences importantly the results of scale 3. In this way, the highest scale robustly represents the label field in presence of noisy classification (reaching the limit of an almost homogeneous label field) and, at the same time, intermediate scales give different levels of details in the initial label field.

3.2.1.2 Pyramidal Decomposition

An alternative is provided by the pyramidal decomposition (2). The pyramidal decomposition is substantially similar to the multi-resolution decomposition with the exception that actually, the resulting pyramid codify more efficiently the multi-scale information. However, it has an important drawback that will be discussed in next subsections.

Starting from the above mentioned Multi-resolution decomposition, the Pyramidal decomposition Ψ can be obtained as follows:

$$\Psi_{C_i}(\vec{q}; s) = \Phi_{C_i}(\lfloor k_s s \vec{q} \rceil; s) \tag{3.2}$$

where $\lfloor \cdot \rceil$ is the floor function, $\vec{q} \in \mathbb{N}^N$, N is the dimensionality of the data. Here $\vec{q_j} \in \left[1 \;\; \frac{X_j}{\gamma^{s-1}}\right]$, where X_j is the integer size of every dimension j (for an image, $N = 2$, X_1 and X_2 are respectively the width and height of the image). Here k_s is the sampling step and depends on γ, $k_s = \gamma^s/2$. Actually, the pyramidal decomposition samples the Multi-resolution theoretically without loss of information, since at higher scales, the high frequency content have been progressively filtered out.

3.2.1.3 Pros and cons of multi-resolution and pyramidal decompositions

The multi-resolution approach is the most appropriate in terms of signal processing theory. However, the pyramidal decomposition actually contains the same information as the multi-resolution while coding it in a more compact way. Unfortunately, as it can be noticed in formula (3.5), the sampling at large scales is prone to produce blocking artifacts. This is due to the fact that during the pyramidal decomposition process, each scale summarizes the information of the above area in a block that is γ^N times smaller (here N is the dimensionality of the data, for images $N = 2$). Obviously, at large scales this reflects a sharp transition form a value to another in the feature vector. This does not happen using the multi-resolution decomposition, where the Gaussian filtering assures smooth transitions at every scale.

Summarizing, if the input data is sufficiently small, the use of the multi-resolution decomposition is highly recommended, while if the input data is inherently large, the pyramidal decomposition can help to save memory at the cost of possible blocking artifacts. To avoid blocking artifacts, an interpolation technique could be used. However, after the next step, sampling pattern, the resulting output will be the same size, therefore pyramidal decomposition compactness is not a big advantage. For sake of simplicity, our MSSL framework will use the multi-resolution approach as a standard multi-scale decomposition method.

3.2.2 Sampling pattern

Once the desired multi-scale representation has been computed, an appropriate sampling pattern should be applied. This pattern can be represented by a set of displacement vectors that defines the neighborhood $\rho = \bigcup_{m=1}^{M} \vec{\delta_m}$. Once the displacement vectors are defined, the feature vector for the multi-resolution decomposition is obtained by the following formula:

$$\begin{aligned}
z(\vec{p}) = \quad & \{\underbrace{\Phi(\vec{p}+\vec{\delta_1};1), \Phi(\vec{p}+\vec{\delta_2};1), \dots, \Phi(\vec{p}+\vec{\delta_M};1),}_{scale\, s=1} \\
& \underbrace{\Phi(\vec{p}+\gamma\vec{\delta_1};2), \Phi(\vec{p}+\gamma\vec{\delta_2};2), \dots, \Phi(\vec{p}+\gamma\vec{\delta_M};2),}_{scale\, s=2} \\
& \vdots \\
& \underbrace{\Phi(\vec{p}+\gamma^{(S-1)}\vec{\delta_1};S), \Phi(\vec{p}+\gamma^{(S-1)}\vec{\delta_2};S), \dots, \Phi(\vec{p}+\gamma^{(S-1)}\vec{\delta_M};S)}_{scale\, s=S}\}
\end{aligned} \tag{3.3}$$

This formula shows that the sampling is performed following the displacement vectors at each scale s. However, the displacement at different scales are multiplied by a factor $\gamma^{(s-1)}$ so that, higher scales correspond to larger displacement. For the sake of clarity, the sampling in figure 3.4 (left) is obtained with $S = 3$, $\gamma = 2$, $M = 9$ and the following set of displacements:

$$\begin{aligned}
\rho = \{ \quad & \vec{\delta_1} = (-1,-1), \quad \vec{\delta_2} = (-1,0), \quad \vec{\delta_3} = (-1,1), \\
& \vec{\delta_4} = (0,-1), \quad \vec{\delta_5} = (0,0), \quad \vec{\delta_6} = (0,1), \\
& \vec{\delta_7} = (1,-1), \quad \vec{\delta_8} = (1,0), \quad \vec{\delta_9} = (1,1)\}.
\end{aligned} \tag{3.4}$$

This displacement set can be represented graphically as in figure 3.5.

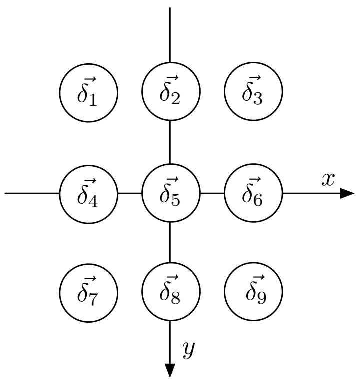

Figure 3.5: A graphical representation of the displacements set ρ as defined in formula (3.4)

The feature vector for the pyramidal decomposition can be obtained by the following formula:

$$
\begin{aligned}
z(\vec{p}) = \quad & \{\underbrace{\Psi(\vec{p}+\vec{\delta_1};1),\ldots,\Psi(\vec{p}+\vec{\delta_M};1),}_{scale\,s=1} \\
& \underbrace{\Psi(\lfloor\vec{p}/\gamma\rfloor+\vec{\delta_1};2),\ldots,\Psi(\lfloor\vec{p}/\gamma\rfloor+\vec{\delta_M};2),}_{scale\,s=2} \\
& \vdots \\
& \underbrace{\Psi(\lfloor\vec{p}/\gamma^{(S-1)}\rfloor+\vec{\delta_1};S),\ldots,\Psi(\lfloor\vec{p}/\gamma^{(S-1)}\rfloor+\vec{\delta_M};S)}_{scale\,s=S}\}
\end{aligned}
\tag{3.5}
$$

where $\lfloor\cdot\rfloor$ is the floor function. As in the previous case, the sampling is performed over all the displacements and scales. On the other hand, the position vector $\vec{p}$ is divided by the quantity $\gamma^{(s-1)}$ to adequately re-scale the coordinates to the resized images at higher scales. The floor function is needed to obtain an integer vector that lays in the image lattice. The displacement pattern ρ is not modified as the images are progressively smaller at a higher scale. Figure 3.4 (right) shows an example of this sampling with $S = 3$, $\gamma = 2$, $M = 9$ and the same displacement set ρ as in formula (3.4).

3.2.3 The coverage-resolution trade-off

If we look carefully at the design of J, we can observe that for a fixed size of the extended set, the sampling policy defines whether we focus on nearby or far away samples. Notice that the higher the number of scales is, the longer the range of interaction is considered. This feature allows us to capture long distance interactions with a very small set of features while keeping a relatively good short distance resolution. In order to quantify this effect we define the coverage of the method as the maximum effective range in which two samples affect each other. Similarly we can define the detail as the average detail size considering all the scales in the multi-resolution sampling scheme. If we restrict to

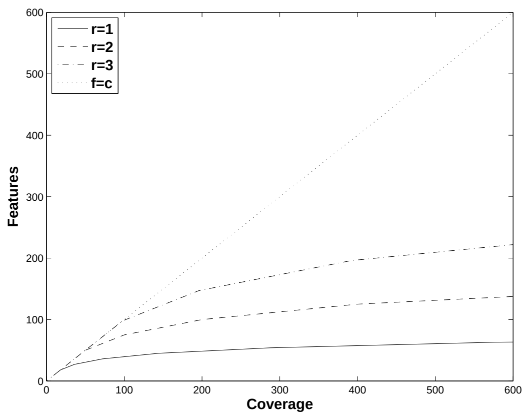

(a)

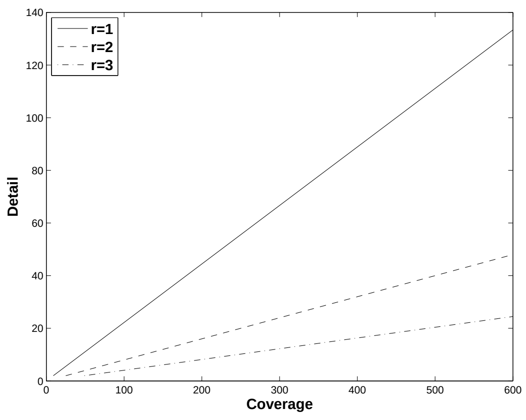

(b)

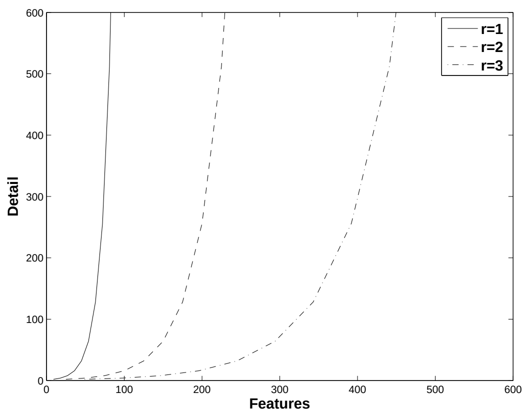

(c)

Figure 3.6: (a) number of features needed for covering a certain number of predicted values for different window sizes r, (b) detail with respect to the coverage, (c) number of features needed to consider a certain detail value

grid square samplings, the sampling scheme can be expressed as a set of displacements obtained by $\vec{\delta} = (k \cdot i, k \cdot j)$ where $i, j \in \{1, 0, -1\}$ and $k = 1, 2, \ldots, r$. This defines a square grid of size $2r + 1$ centered at the sample of interest as the one shown in figure 3.5. The value of r plays an important role in the scheme since it allows to govern the average detail of the approximation. In this setup the *coverage* can be computed as $c = \gamma^{(S-1)}(2r + 1)^d$, the number of features generated by the proposed approach is $f = S(2r + 1)^d$ and detail is computed as the average value of the relative distance between adjacent points at scale i, given by γ^{i-1}. Thus, $d = \frac{1}{S}\sum_{i=0}^{S-1} \gamma^i = \frac{\gamma^S - 1}{\gamma - 1}$.

Figure 3.6 shows the relationship among detail, coverage and number of features. Figure 3.6(a) plots the number of features needed for observing a certain number of predicted labels (coverage). Different curves show the effect of altering the size of the support window r. Thus, in a 2-dimensional sequential domain if the support window has a size of 3, $r = 1$, we need 7 scales and a total of 63 features to capture information from about 600 labels. The parameter r governs the trade-off between resolution and coverage. Observe in Figure 3.6(b) that average detail is coarser as the coverage increases. Thus, small patterns in long distance label interactions are lost. As r increases, the number of features also increase (Figure 3.6(c)), but more complex and detailed label patterns can be captured. On the contrary, maximum interaction details are observed at the cost of using the same number of features as the coverage value. This trade-off allows the practitioner to consider different strategies according to the degree of sequential correlation expected in the sequence.

3.3 Experiments and Results

In order to validate the proposed techniques, MR-SSL and Pyr-SSL are applied and compared to state-of-the-art strategies in two different scenarios. The first scenario considers one dimensional correlations in the label field in a text categorization task. The second experiment concerns the image domain, where correlations are found on a two dimensional support lattice.

3.3.1 Categorization of FAQ documents

- **Dataset** The FAQ categorization task has been frequently used in literature as a benchmark for sequential learners (17) (26). In this data set, three different computer science FAQ groups pages are used (ai-neural-nets, ai-general, aix). Each FAQ group consists of 5 to 7 long sequences of lines; each sequence corresponds to a single FAQ document. Each line is characterized using McCallun et al features

(47), with 24 attributes that describe line characteristics with the respective class label. In total, each FAQ group contains between 8965 and 12757 labeled lines. This data set is multi-class, with 4 possible classes; in our experiments, for each of the three groups we split the multi-class problem into two binary problems considering the following labels “answer” vs “not answer”, and “tail” vs “not tail”, yielding a total of 6 different problems.

- **Methods** We compared the pyramidal and multiresolution approaches with standard Adaboost with decision stumps, Conditional Random Fields, and the original stacked sequential learning strategy.
- **Experimental and parameters settings** The base classifier for SSL, Pyr-SSL and MR-SSL is Adaboost with a maximum of 100 decision stumps. All stacked learning techniques use an inner 5-fold cross validation on the training set for the first step of the sequential learning schema.
- **Evaluation metrics** Due to the fact that each sequence must be evaluated as a whole set, and that there is a small amount of sequences per problem, one of the fairest ways for comparing the results is to average the accuracy using a leave-one-sequence-out cross-validation scheme – one sequence is used as testing and the rest of the sequences are joined into one training sequence – for each problem. Different configurations according to the (γ, S, ρ) parameterization are compared. The average rank for each method is also provided[1].
- **Statistical analysis** In order to guarantee that the results convey statistically relevant information, a statistical analysis was performed for each experiment. First, an Iman’s and Davenport correction of the Friedman’s test was performed to ensure that the differences in the results are not due randomness with respect to the average performance rank. The statistic for this test is distributed according to a F-distribution with $k-1$ and $(N-1)(k-1)$ degrees of freedom, where k is the number of methods compared and N the number of data sets. The statistic is computed as follows,

$$F_F = \frac{(N-1)\chi_F^2}{N(k-1)-\chi_F^2}$$

where χ_F^2 is the Friedman’s statistic given by

$$\chi_F^2 = \frac{12N}{k(k+1)}\left[\sum_j R_j - \frac{k(k+1)^2}{4}\right]$$

[1]The average rank accounts for the sum of the ranking position of each method for each database.

where R_j is the average rank of each method.

If the null hypothesis is rejected we can ensure that the resulting ranks convey significantly relevant information. Then, a post-hoc test using Nemenyi's test can be performed in order to single out methods or groups of methods. Using this statistical test, two sets are statistically different if the difference of ranks is higher than a given critical value computed as follows,

$$CD = q_\alpha \sqrt{\frac{k(k+1)}{6N}}$$

where, q_α is based on the studentized base statistic divided by $\sqrt{2}$.

	AdaBoost	CRF	SSL		Pyr-SSL		MR-SSL	
(γ, S)	-	-	$(-,1)$	$(-,1)$	$(2,2)$	$(4,4)$	$(2,2)$	$(4,4)$
ρ	-	-	ρ_3	ρ_6	ρ_1	ρ_1	ρ_1	ρ_1
Features	-	-	7	13	6	12	6	12
Coverage	-	-	7	13	12	192	12	192
neural-netsA	7.0675	7.5812	5.9855	5.8103	6.1495	4.5257	5.4504	**3.4667**
neural-netsT	1.8067	2.0831	1.4826	0.7825	1.3146	0.5199	**0.2834**	0.4065
Ai-GeneralA	**8.2764**	9.3902	9.2944	10.3183	9.2636	10.3834	9.8923	9.1097
Ai-GeneralT	1.8916	2.4267	1.6275	0.9392	1.7031	1.1964	1.4219	**0.0001**
Ai-AixA	9.7971	12.5310	9.3519	9.9028	9.3307	9.5689	**8.9304**	9.7452
Ai-AixT	1.2553	1.5741	0.8966	0.7493	0.9233	0.2662	0.4257	**0.0001**
Rank	5.67	7.34	4.67	4.67	4.34	3.67	3	2

Table 3.1: Average percentage error and methods ranking for different FAQ datasets, different methods; and different parameterization of SSL, Pyr-SSL and MR-SSL. For the sake of table compactness, the following definitions should be considered: $\rho_3 = \{-3, -2, \ldots, 2, 3\}$, $\rho_6 = \{-6, -5, \ldots, 5, 6\}$, $\rho_1 = \{-1, 0, 1\}$.

Table 3.1 shows the results obtained for the FAQ experiments comparing the base algorithm Adaboost with decision stumps, conditional random fields, two configurations of SSL, two configurations of Pyr-SSL and two of MR-SSL. In order to ensure a fair comparison, the configurations have similar number of features in the extended training set. The average performance rank of each method is displayed in the last row of the table. The best performance for each data set is highlighted in bold font.

Observe that sequential learning approaches generally reduce the error rate percentage except for the AI-GeneralA data set. Moreover, as the number of features increases the accuracy improves. Comparing SSL with Pyr-SSL and MR-SSL approaches, it

	Pyr-SSL				MR-SSL			
(γ, S)	$(2,2)$	$(2,3)$	$(2,4)$	$(4,4)$	$(2,2)$	$(2,3)$	$(2,4)$	$(4,4)$
ρ	ρ_1	ρ_1	ρ_1	ρ_1	ρ_1	ρ_1	ρ_1	ρ_1
Features	6	9	12	12	6	9	12	12
Coverage	12	24	48	192	12	24	48	192
neural-netsA	6.1495	5.624	4.9195	4.5257	5.4504	4.6303	4.0018	**3.4667**
neural-netsT	1.3146	0.7159	0.5257	0.5199	0.2834	0.2499	**0.2210**	0.4065
Ai-GeneralA	9.2636	9.1998	9.0374	10.3834	9.8923	9.3698	**8.8874**	9.1097
Ai-GeneralT	1.7031	1.2716	0.6582	1.1964	1.4219	0.7136	0.6407	**0.0001**
Ai-AixA	9.3307	9.3412	9.1311	9.5689	**8.9304**	9.1276	9.2907	9.7452
Ai-AixT	0.9233	0.4754	0.2888	0.2662	0.4257	**0.0001**	0.0806	**0.0001**
Rank	7	6.17	4	5.33	5	3.25	2.16	3.08
Avg rank	5.63				3.37			

Table 3.2: Average percentage error for different configurations of Pyr-SSL and MR-SSL. The last two rows show the average rank for each parameterization as well as the average rank for each of the multi-scale families.

is worth noting that using a similar number of features, the multi-scale counterparts achieve much better results. This seems to suggest that the data sets include some structure information that can only be captured at large scales. This idea is reinforced by the fact that for some of the data sets, the larger the coverage, the lower the error rate achieved. Finally, when the multi-scale step γ is doubled – thus quadrupling the coverage by sacrificing resolution in the data sequence – we can see that applying Pyr-SSL accuracy improves on half of the data sets. On the other hand, when applying MR-SSL accuracy improves in all except for one data set.

Observing the ranks for all proposed methods, it can be noticed that Pyr-SSL and MR-SSL strategies perform better than Adaboost, CRF and SSL. Considering the different configurations of the MSSL technique, Pyr-SSL performs poorer than MR-SSL. A detailed analysis of this effect is shown in Table 3.2.

A statistical analysis of the results shows that, in our case, Iman's and Davenport correction of the Friedman's test yields $F_F = 2.9329$ and the critical value for this test is $F(7, 35) = 2.249$, so we reject the null hypothesis that the results may be due to randomness with respect to the average rank. Thus we can safely say that the analysis of ranks convey statistically relevant information.

A post-hoc analysis of the data using Nemenyi's test[1] singles out MR-SSL $(4, 4)$ from SSL, CRF and AdaBoost with a 95% confidence. Additionally, all proposed strategies

[1]Critical difference using Nemenyi's test at 0.05 is 2.44, and at 0.10 is 2.05.

are statistically different than CRF and Adaboost at 90% confidence. On the other hand, SSL shows statistically significant differences with respect to CRF, as reported in the original SSL paper but fails to display any statistically significative difference with respect to Adaboost.

Table 3.2 shows a detailed comparison between Pyr-SSL and MR-SSL using different parameter configurations. Average ranks for each configuration are provided. Additionally, a single average rank for Pyr-MSSL and MR-SSL is given. The parameters are chosen such that the number of features and coverages are comparable.

Using Iman's and Davenport statistic $F_F = 6.0689$, with a critical value for $F(7, 35) = 2.249$, so we reject the null hypothesis that the results may be due to randomness with respect to the average rank. A post-hoc test using Nemenyi's test critical difference with 95% of confidence shows that MR-SSL always statistically outperforms Pyr-SSL when we compare the same parameter configurations.

3.3.2 Weizmann horse database

- **Dataset** The Weizmann horse database is composed of 328 side-view color images of horses and their respective manual segmentations. This database has been proposed to evaluate the performance of a segmentation algorithm (7). In the database, the horses exhibit a sufficiently regular structure; i.e. all are standing and face towards the left. They vary significantly in color and size.

- **Methods** We compared the proposed methods against AdaBoost, CRF and standard SSL (using a window of size 7×7). For the following experiments, the CRF implementation is a modified version of the one in (68). We incorporated AdaBoost to generate the unary potential. In this way, the base classifier for all the SSL strategies is the same as the one used by CRF. For the learning phase we used the stochastic gradient descent as it proved to be one of the fastest ways to train a CRF (68). Finally, inference is performed by means of the belief propagation method.

- **Experimental and parameters settings**

  Two different experiments are performed using this dataset:

  - First, in order to perform a fair comparison to the method in (7), we resize all the images to 40x30 pixel size. This problem will also serve to establish proper comparisons with computationally intensive methods such as CRF.

A good way to show the capabilities of the proposed method, is to reduce the number of features that the first classifier can use to discriminate the horse class. In this way, the behavior of the proposed method will be easier to describe. We actually reduce the feature vector to pixel-wise color. The images are transformed from sRGB to CIELAB color space to highlight lightness and chromatic components. The first classifier ($h_1(\mathbf{x})$) only has access to the three CIELAB color coordinates for each pixel in the image. Observe that this classification can be prone to several errors due to the similarity between horses color and background color. Moreover, since the classification is performed pixel-wise, the first classifier is prone to isolated misclassifications.

As in the previous experiment, the base classifier is an AdaBoost with decision stumps reaching a maximum of 100 iterations. Regarding the MR-SSL, to have an effective long-range label interaction, we set the number of scales $S = 5$, $\gamma = 2$ and ρ as in formula (3.4), so that the maximum displacement during sampling is of $\pm\gamma^{(S-1)} = \pm 2^4 = \pm 16$ pixel, thus covering great part of the image size.

– In order to show that the proposed method also works well with bigger images, the other experiment uses full size images. In this case results are compared with segmentation state-of-the-art methods.

  To deal with full size images, we use the SIFT descriptor for the first classifier (using the CIELAB color space) because texture is an important feature when the images have a sufficient resolution. Moreover, we set the number of scales $S = 7$, $\gamma = 2$ and ρ as in formula (3.4), obtaining a coverage value of ± 64 pixels.

- **Evaluation metrics**

  Due to the significant amount of data a 5-fold cross-validation technique is used for obtaining the average evaluation metrics. As done in (7), we used the Jaccard index (40) as a quality measure of the overlapping o between the automatic segmentation and the labeled ground-truth; being A and M respectively the automatic and manual (ground-truth) segmentations, the overlapping is defined as $o = \frac{|A \cap M|}{|A \cup M|}$. This measure is equivalent to the ratio of the true positive over the sum of true positive, false positive and false negatives.

- **Statistical analysis** The amount of data in these experiments enable the possibility of using powerful statistical tests that were not available in the former experiment. In this case, we tested for statistical significance of the results using the Wilcoxon signed rank test and comparing the p-values obtained across the different methods, as suggested in (23).

3.3.2.1 Results on the resized Weizmann horse database

Figure 3.7 shows comparisons in terms of accuracy, precision and the overlapping measure o. In the first row, the plots represent respectively the accuracy, precision and overlapping of AdaBoost and the proposed MR-SSL method. Each dot in the plot represents the performance obtained on a specific image for both algorithms. In the plot, a distribution that is mainly above the diagonal means that MR-SSL performs better than AdaBoost. The same applies for the second row, where MR-SSL is compared to CRF. It is clear that MR-SSL outperforms both AdaBoost and CRF. Last row shows a comparison between MR-SSL and Pyr-SSL, confirming that the former performs better than the latter. Table 3.3 shows the average accuracy, precision and overlapping values for all the tested configurations, with the respective standard deviation. Observe that both Pyr-SSL and MR-SSL achieve much better results than standard SSL, CRF and AdaBoost. Moreover, MR-SSL shows improvements over Pyr-SSL.

	Accuracy	Precision	Overlapping o
AdaBoost	0.7322 (0.1808)	0.5555 (0.2398)	0.6112 (0.2064)
CRF	0.7195 (0.1946)	0.5174 (0.3257)	0.5137 (0.2641)
SSL 7×7	0.7915 (0.1285)	0.6327 (0.2308)	0.5584 (0.2264)
Pyr-SSL	0.8196 (0.1158)	0.6664 (0.2250)	0.6030 (0.2195)
MR-SSL	**0.8592** (0.0903)	**0.7191** (0.2091)	**0.6819** (0.2109)

Table 3.3: The average performance of AdaBoost, SSL (7×7 window size), MR-SSL, CRF and Pyr-SSL in terms of Accuracy, Precision and Overlapping. Standard deviations are in brackets.

Tables 3.4 and 3.5 show the p-values applying the Wilcoxon signed rank test on the values of accuracy and overlapping for all the images of the horse data set. Values followed by ∘ display those results that are not statistically significant. Values followed by • are statistically significant at 10%. In Table 3.4 we observe that the proposed methodologies as well as the standard SSL show results statistically significant with respect to Adaboost and CRF in terms of accuracy. Furthermore, the multi-scale strategies proposed statistically differ from SSL. And, in particular, MR-SSL is the most statistically different from all the techniques studied. In Table 3.5 we see that

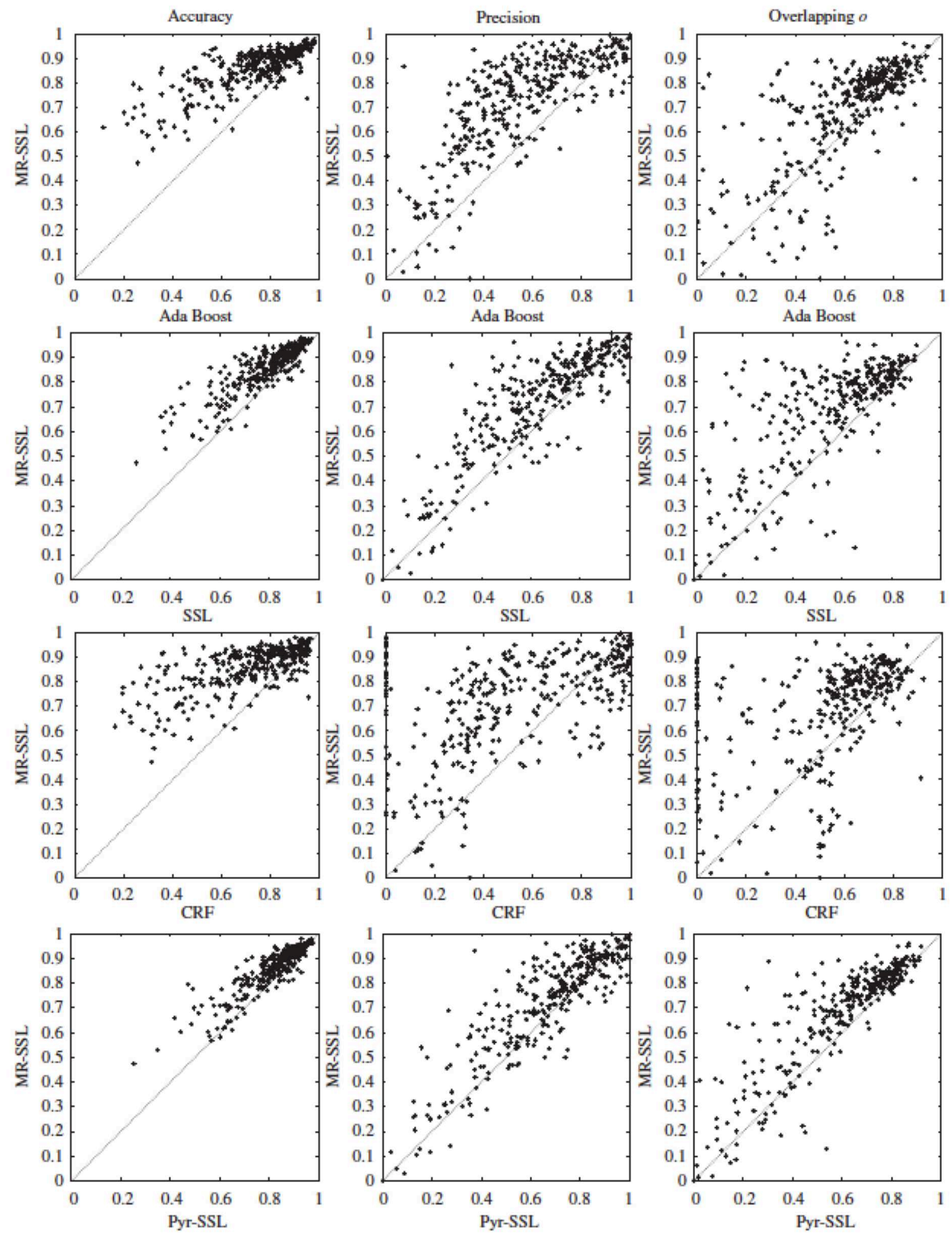

Figure 3.7: Comparison of the proposed MR-SSL method to AdaBoost (first row), SSL using a window of size 7×7 (second row), CRF (third row) and Pyr-SSL (last row) on the resized Weizmann horse database.

MR-SSL is again the most statistically different from the rest in terms of overlapping. In general, the conclusions are very similar to those obtained in the accuracy table. It is worth noting that SSL and Pyr-SSL are not statistically significant. And, Pyr-SSL only achieve statistically significant results at 10% when compared with Adaboost.

Accuracy p-val	ADA	SSL	Pyr-SSL	MRSSL	CRF
ADA	-	0.0001	0.0000	0.0000	0.6847○
SSL	0.0001	-	0.0032	0.0000	0.0001
PyrSSL	0.0000	0.0032	-	0.0000	0.0000
MRSSL	0.0000	0.0000	0.0000	-	0.0000
CRF	0.6847○	0.0001	0.0000	0.0000	-

Table 3.4: Wilcoxon paired signed rank test p-values for the results of the accuracy measure.

Overlapping p-val	ADA	SSL	Pyr-SSL	MRSSL	CRF
ADA	-	0.0048	0.0691●	0.0000	0.0000
SSL	0.0048	-	0.3082○	0.0000	0.0426
PyrSSL	0.0691●	0.3082○	-	0.0000	0.0031
MRSSL	0.0000	0.0000	0.0000	-	0.0000
CRF	0.0000	0.0426	0.0031	0.0000	-

Table 3.5: Wilcoxon paired signed rank test p-values for the results of the overlapping measure.

It is also interesting to compare the training and inference time of both MR-SSL and CRF. The CRF implementation used in this work is the one in (68), written in Matlab but with many optimized functions in C. The MR-SSL has been implemented in Matlab without specific optimization. To train one fold (using about 260 images), the CRF requires 52' 6" while the MR-SSL only 1' 10". Regarding inference, for each image CRF requires and average time of 0.4846 seconds, while the MR-SSL just 0.0882 seconds. We also tested the training time of the MR-SSL with full size images (using $S = 7$), resulting in a training time of 14' 35" for one fold. The same test performed with CRF is unfeasible since training the method on each fold requires several days.

Finally, it is interesting to note that in reference (7) they achieve an average $o = 0.71$ using a sophisticated segmentation algorithm on 40x30 image size, requiring about 40 sec per image to perform the segmentation, using a leave-one-out testing. Using the proposed MR-SSL, and just with color features, we achieved an average $o = 0.682$.

	Accuracy	Precision	Overlapping o
AdaBoost-Haar-27	0.7651 (0.1468)	0.5727 (0.1960)	0.6451 (0.1699)
MR-SSL-Haar-27	0.8716 (0.0745)	0.7379 (0.1659)	0.7147 (0.1846)

Table 3.6: The average performance of AdaBoost and MR-SSL in terms of Accuracy, Precision and Overlapping; adding 27 Haar-like features to the first feature vector $\mathbf{x}$. Standard deviations are in brackets.

However, one can argue that the advantage of the proposed method is relevant only if the first classifier performs poorly. To controvert this hypothesis, we performed another test, in which the feature vector $\mathbf{x}$ is augmented with 27 Haar-like features. As it can be seen in table 3.6, the performance of the base AdaBoost classifier is increased (+0.033 accuracy, +0.017 precision, +0.034 overlapping); but at the same time the MR-SSL performs better (+0.012 accuracy, +0.018 precision, +0.033 overlapping). The Haar-like features helped the first classifier and this improvement has reflected entirely on the MR-SSL performance; this shows that the improvement due to the MR-SSL schema over the base classifier is still significant (+0.11 accuracy, +0.16 precision, +0.07 overlapping). Finally, it is worth noting that the proposed MR-SSL in this case achieves an average overlap of ($o = 0.7147$) that is comparable with the one reported in (7).

3.3.2.2 Results on the full size Weizmann horse database

Finally, to compare our method to state-of-the-art *segmentation* methods, we used the MR-SSL together with the SIFT descriptor as detailed above. Table 3.7 shows the results in terms of accuracy, precision and overlapping of the Adaboost-SIFT and the MR-SSL-SIFT on full size images of the Weizmann dataset. Several segmentation methods have used the Weizmann dataset to evaluate their performances: in (36) the authors report an average accuracy of 91.47%, the method in (6) reports 93%, method in (70) reports 93% on 200 horse images, the method in (46) reports an accuracy of 95%, finally the method in (42) reports an accuracy of 96% and precision of 89%. As depicted in Table 3.7 our method shows an average accuracy of 92.1% and an average precision of 82.1% using all the images of the dataset. Figure 3.8 shows the best 30 segmentations on full size images, which overlap ranges from 0.92 to 0.85; first column shows the input image, second column the ground truth, third column the classification result and the last column shows a color coded image with true positives (blue), true negatives (white), false positives (cyan) and false negatives (red).

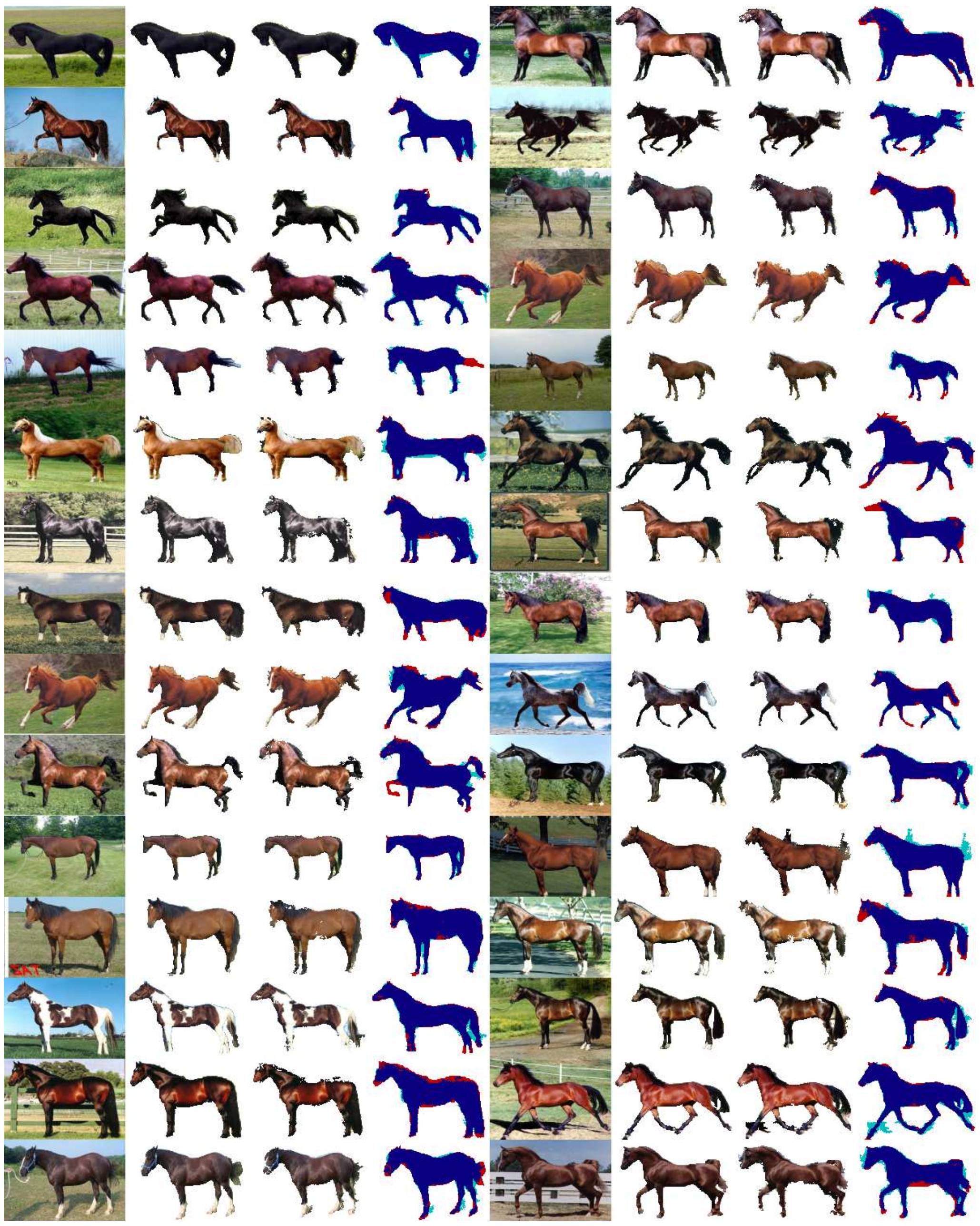

Figure 3.8: The best 30 segmentations on full size images. First column shows the input image, second column shows the ground truth, third column shows the classification result and the last column shows a color coded image with true positives (blue), true negatives (white), false positives (cyan) and false negatives (red).

	Accuracy	Precision	Overlapping o
AdaBoost-SIFT	0.8123 (0.1122)	0.6286 (0.1818)	0.7041 (0.1302)
MR-SSL-SIFT	0.9209 (0.03)	0.821 (0.13)	0.7466 (0.16)

Table 3.7: The average performance of AdaBoost and MR-SSL in terms of Accuracy, Precision and Overlapping using the color plus SIFT descriptor as the first feature vector $\mathbf{x}$. Standard deviations are in brackets.

To clearly show the contribution of the extended set to the final classification performance, in Figure 3.9 we show the weights Adaboost assigned respectively to the (a) pixel-wise color features, (b) textural SIFT descriptor and (c) contextual features. The total weight of the pixel-wise color feature is 1.06 (10.2%), the total weight of SIFT features is 2.4 (23.2%) and the total weight of contextual features is 6.89 (66.6%). This experiment confirms two important facts: (1) the original feature vector $\mathbf{x}$, in this case the color and SIFT features, contributes to the final classification, giving the second classifier the possibility to exploit correlations between appearance features and contextual features; (2) the contextual features are providing relevant information, as confirmed by the fact that Adaboost assigns the 66.6% of the weights to these features. Further comments must be devoted to the plot in Figure 3.9(c). The second classifier gives a large weight (23.5%) to the central location at the second scale and a very low weight (0.024%) at the central location at the first scale. This means that the second classifier does not "trust" pixel-wise classifications of the first stage classifier (first scale), but it is much more prone to "trust" the classification if averaged in a small neighborhood (second scale). Moreover, the central locations at scales 6 and 7 have respectively the 7% and 4.6%; this means that, to a certain extent, the classifier consider the information over large areas useful, probably due to the fact that the horses' bodies tend to cover quite a large area. Finally, at central scales, from $3th$ to $5th$, central locations have very low weights while neighborhoods at almost all directions have more consistent weights. This means that the second classifier correctly uses the mid-range interaction between horse and background classes.

3.4 Results Discussion

In this section, we discuss in depth some of the results obtained in the experiments. Without loss of generality, we focus this discussion on the Weizmann database because of the ease of illustrating classification results in the form of images. However, the same conclusions and observations can be drawn for the FAQ data sets.

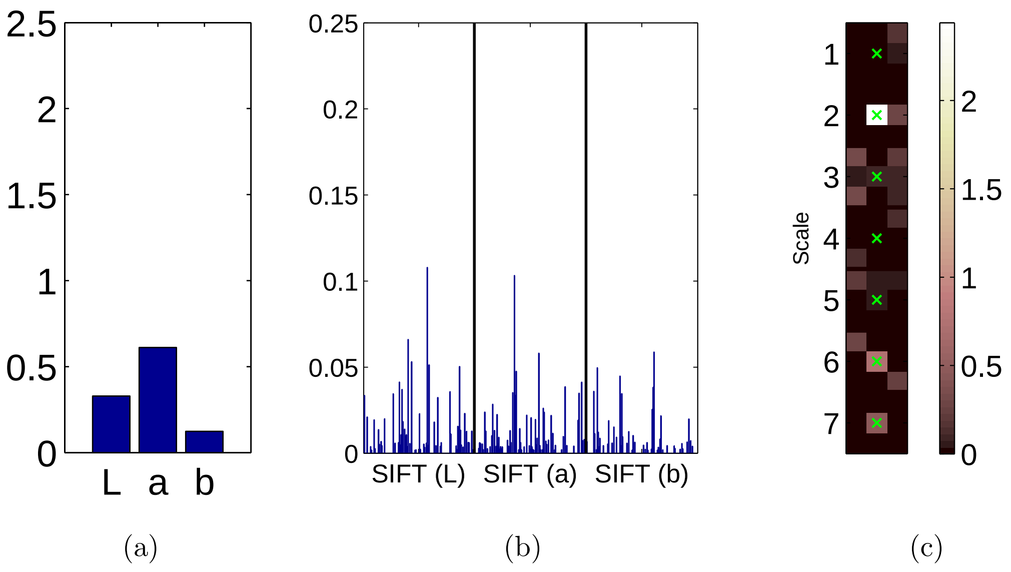

Figure 3.9: The weights Adaboost assigned to the (a) pixel-wise color features, (b) textural SIFT descriptor and (c) contextual features. The total weight of the pixel-wise color feature is 1.06 (10.2%), the total weight of SIFT features is 2.4 (23.2%) and the total weight of contextual features is 6.89 (66.6%).

First of all, it is interesting to note that CRF works especially well when the base classifier is able to perform a quite good classification. In these cases, CRF is able to distinguish and remove isolated misclassifications. Figure 3.10 shows one example in which CRF slightly outperforms the proposed MR-SSL method. It is easy to notice that AdaBoost performed well, and the only contribution of the CRF is to remove some isolated misclassification and refine the silhouette of the horse.

Input	Ground truth	h_1 (x)	SSL 7×7	CRF	MR-SSL
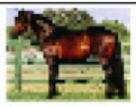	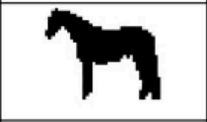	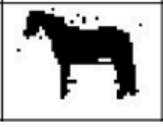	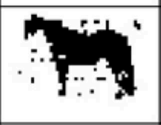	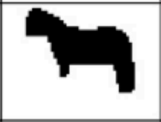	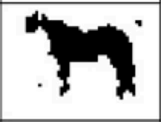

Figure 3.10: Input, ground truth and results of different methods on the test image number 142.

When the classification performance of the base classifier is poorer, CRF is usually not able to improve the classification. On the contrary, the proposed MR-SSL method, thanks to its multi-scale approach, is able to improve the classification helping in discriminating ambiguous cases exploiting the contextual information. Figure 3.11 shows several cases in which the base classifier performs poorly.

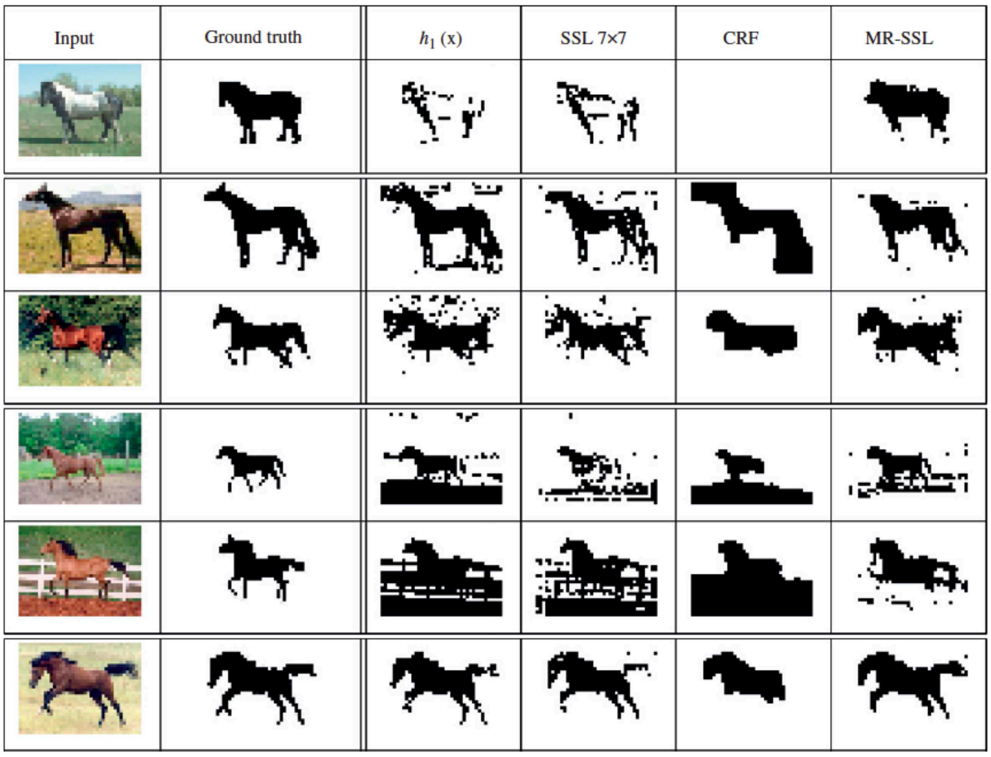

Figure 3.11: Input, ground truth and results of different methods on the test image numbers: 84, 22, 71, 88, 108 and 109 respectively.

The first row shows an example in which the CRF interprets the base classification result (the unary potential) as if it represents a sparse set of misclassifications. Within this interpretation, the best behavior CRF can exhibit is to remove the misclassifications, thus classifying no horse in the picture. Thanks to the multi-scale approach, the label field probability that results from the base classifier is interpreted within the multi-scale paradigm, so that at coarser scales the horse is roughly classified correctly. Figure 3.12 shows the multi-resolution decomposition $\Phi_{C_i}(\vec{q}; s)$ obtained from the base classifier output, for the scales $s = \{1, 2, 3, 4\}$, when classifying the horse in the first row of figure 3.11).

As it can be noticed, at scale 1, the body of the horse has less probability to be classified correctly than the horse legs and head. However, at coarser scales, the

s	1	2	3	4
		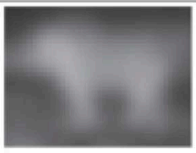		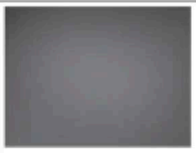

Figure 3.12: Label field multi-resolution decomposition classifying image number 84.

horse outline is roughly visible and the discrepancy in these probabilities is lower. This "blurred" information gives the necessary contextual information to the second classifier that is consequently able to correctly classify a great part of the horse. Obviously, the quality of the classification is not perfect, but compared with the AdaBoost and CRF, the achieved result is clearly superior.

In figure 3.11, the second and third rows show two cases in which the AdaBoost classification is noisy. Here, the CRF removes all the one pixel size false positives. Unfortunately, close to the horse silhouette, it tends to fuse some false classifications (see row 2) or remove thin structures such as the horse legs (see row 3). On the other hand, MR-SSL removes many of the noisy false positives, but not all of them, while preserving small structures in both examples.

Rows 4 and 5 show two examples in which the color of the ground and the fence easily cheats the first AdaBoost classifier, that incorrectly classifies all the ground and the fence as 'horse'. Here, SSL tries to reduce the false positives with limited results. CRF cannot represent the structure of the context and thus converges to blocks that fuse the ground and the horse. Finally, the MR-SSL outperforms the previous methods, removing great part of the false positives, thus segmenting the horse sufficiently well.

The last row of figure 3.11 shows an example in which the result of AdaBoost is already very good; in this case, the proposed method slightly refines the segmentation while the CRF removes the legs of the horse, as they are small structures.

In some of the examples we also found that the contextual information is able to almost invert the classification performed by the first classifier. Figure 3.13 shows one of this cases. While the final result is surely not excellent, the ability of the proposed method to understand the context is evident.

Finally, Figure 3.14 shows an example in which the MR-SSL algorithm is able to remove an important quantity of misclassifications while, at the same time, increasing the precision. As it can be noticed, the upper part of the picture background is very

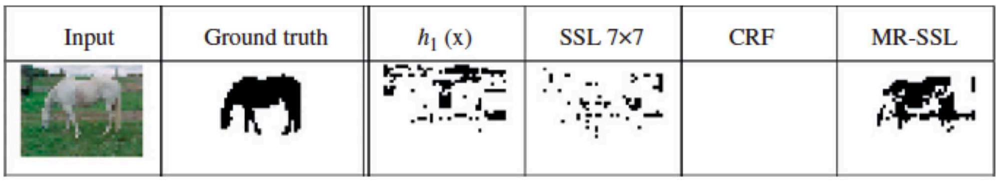

Figure 3.13: Input, ground truth and results of different methods on the test image number 41.

similar to the horse. For this picture, the overlapping o for AdaBoost is 0.3534 while for the MR-SSL is 0.7298. The precision is 0.4023 for AdaBoost, and 0.6811 for MR-SSL. This tremendous increase in the performance parameters clearly show the potential ability of the MR-SSL method to solve ambiguous classification cases. However, this behavior is not occasional, but it is evident as a general trend in the plots of Figure 3.7.

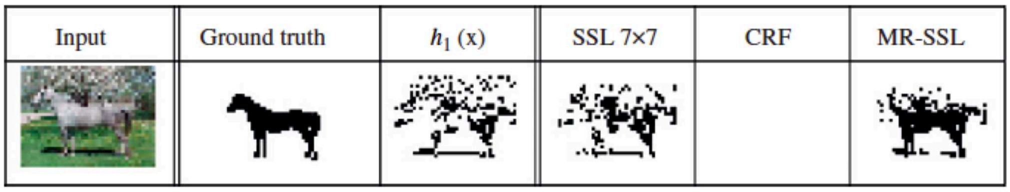

Figure 3.14: Input, ground truth and results of different methods on the test image number 153.

3.4.1 Blocking effect using the pyramidal decomposition

For the sake of completeness we now show some examples of the blocking effect that can appear if using the pyramidal decomposition without any interpolation method. This effect is hard to note in small images, thus in this subsection we show two examples in figure 3.15, where the image size is 100×150 pixels. In the figure, it is clear that a blocking effect is visible for the Pyr-SSL method. Moreover, the performance of the Pyr-SSL is visibly inferior than the one of the MR-SSL, as confirmed by the plots in figure 3.7.

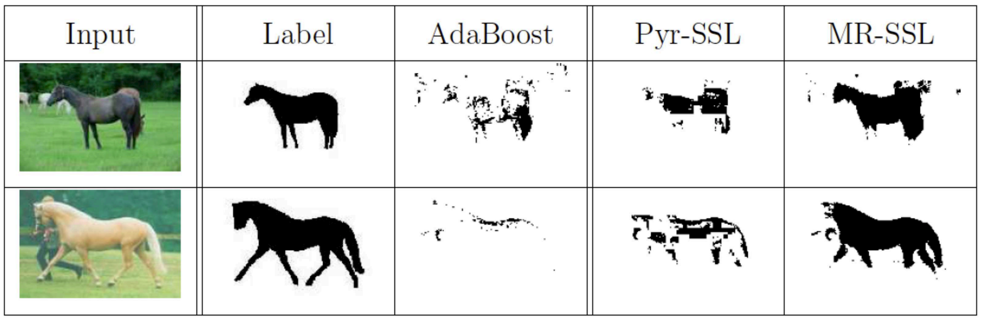

Figure 3.15: Visual comparison of the Pyr-SSL and the MR-SSL on images number 68 and 144.

3.5 Conclusions

In this chapter we generalized the Stacked Sequential Learning framework. We proposed a multi-scale decomposition of the predicted label field, followed by an appropriate sampling schema to form a extended feature vector. The proposed method is able to capture long range interactions in the label field efficiently, as well as, it is highly modular, thus any base classifier can be applied. In addition, a clear and detailed explanation on how to define the sampling schema with respect to the desired coverage/resolution trade-off is provided.

The proposed method has been tested on two different data sets, the first on a 1D correlation lattice and the second on a 2D correlation lattice. For the 1D case, the proposed method outperformed the CRF on 5 data-sets over 6. In the only case in which CRF outperforms the proposed MR-SSL, the best performance is given by the base AdaBoost classifier. For the 2D case, the proposed method outperformed both the base AdaBoost classifier and the CRF in terms of Accuracy, Precision and Overlapping.

The next chapter covers several extensions to the MSSL framework explained so far. We will show how to use likelihoods instead of label predictions; how to learn objects that appear at different scales; how to cope with multi-class problems and finally how to efficiently reduce the number of features in the extended set for large multi-class problems.

4

Extensions to MSSL

In this chapter we introduce four extensions to our MSSL framework. First extension is using likelihoods instead of predictions labels as inputs of J function. Second extension is learn to classify objects which are present in different scales by doing several test phases where the extended set is shifted. Third extension is upgrade MSSL for binary classification problem to a multi-class classification problem. We present a general framework suitable for any binary classifier thanks to the ECOC framework used. Finally our fourth extension is provide a compression approach for reducing the amount of features in the extended set. This is particularly useful in multi-class problems where the number of features in the extended set increase geometrically.

4.1 Extending the basic model: using likelihoods

In the MSSL model we use the predicted labels as the input of $J(y', \rho, \theta)$. An extension of this idea is to use a likelihood-based measure for each label instead of label prediction. The use of likelihoods gives more precise information about the decisions of the first classifier than just its predictions. In the bi-class case, where the set of possible labels is $\mathcal{L} = \{\lambda_1, \lambda_2\}$, we have two membership likelihoods: $z = J(\{F(y = \lambda_1|x), F(y = \lambda_2|x)\}, \rho, \theta)$. The multi-scale decomposition and the sampling phases are the same, but now, each step is applied for each label, resulting in as many decomposition sequences as labels, and thus, the number of features in the extended set becomes $(2r+1)^d \times |\Sigma| \times |\mathcal{L}|$. In the case of binary classification, the second term is not needed, because it is complementary of the first. Therefore in this case the number of features are the same as using labels. This information can be taken into account by the second classifier, and then a more accurate prediction can be given, specifically in those cases that the first classifier has limited support for deciding the predicted label.

In order to obtain these values we need the base classifier $H_1(x)$ to generate not only a class prediction, but also its likelihood. Unfortunately, not all kind of classifiers can give a likelihood for their predictions. However, classifiers that work with margins, such as Adaboost or SVM, can be used (32). In these cases, it is necessary to convert the margins used by these classifiers to a measure of likelihood. In case of using Adaboost, we apply a sigmoid function that normalizes Adaboost margins from the interval $[-\infty, \infty]$ to $[-1, 1]$ by means of the following equation,

$$f(x) = \frac{1 - e^{-\beta m_x}}{1 + e^{-\beta m_x}}, \tag{4.1}$$

where m_x is the margin given by Adaboost algorithm for the example x, and a constant that governs the transition: $\beta = \frac{-\ln(0.5\epsilon)}{0.25t}$. It depends on the number of iterations t that Adaboost performs, and an arbitrary small constant ϵ. Now, we use a soft distance to convert the normalized values to a likelihood in the range $[0, 1]$ for each label λ as follows:

$$\begin{aligned} f(x|y = \lambda_1) &= e^{-\alpha d(-1, f(x))}, \\ f(x|y = \lambda_2) &= e^{-\alpha d(1, f(x))}, \end{aligned}$$

where $\alpha = -\ln(\epsilon)/2$, and ϵ is an arbitrarily small constant (i.e $\epsilon = 10^{-3}$).

4.2 Learning objects at multiple scales

In MSSL the choice of the scales is critical. The more scales are selected, the better performance is obtained. This is because different patterns at different scales can be detected. Nonetheless, if we learn a pattern with a concrete size, then when a new sequence at different size (smaller for example) is classified, the prediction would not be correct using such scales. This is because the ranges of interactions displayed in the test sequence are not comparable with the ones displayed in the training phase, due to the fact that MSSL learns absolute interaction ranges. In order to effectively learn interactions in the pattern of interest we must ensure that the training set display these interactions at the same range. We call this particular training set a *template*. However, during the testing phase, objects can be found at different sizes displaying different interaction ranges that the ones learned.

For example, let suppose we have a set of template images $\mathbf{X}$ of size D and we train the model using a set of scales $\Sigma_0 = \{2, 4, 8\}$. During the testing phase, let it be a set of test images X of size $D/2$ and the same set of scales $\Sigma_0 = \{2, 4, 8\}$, then we

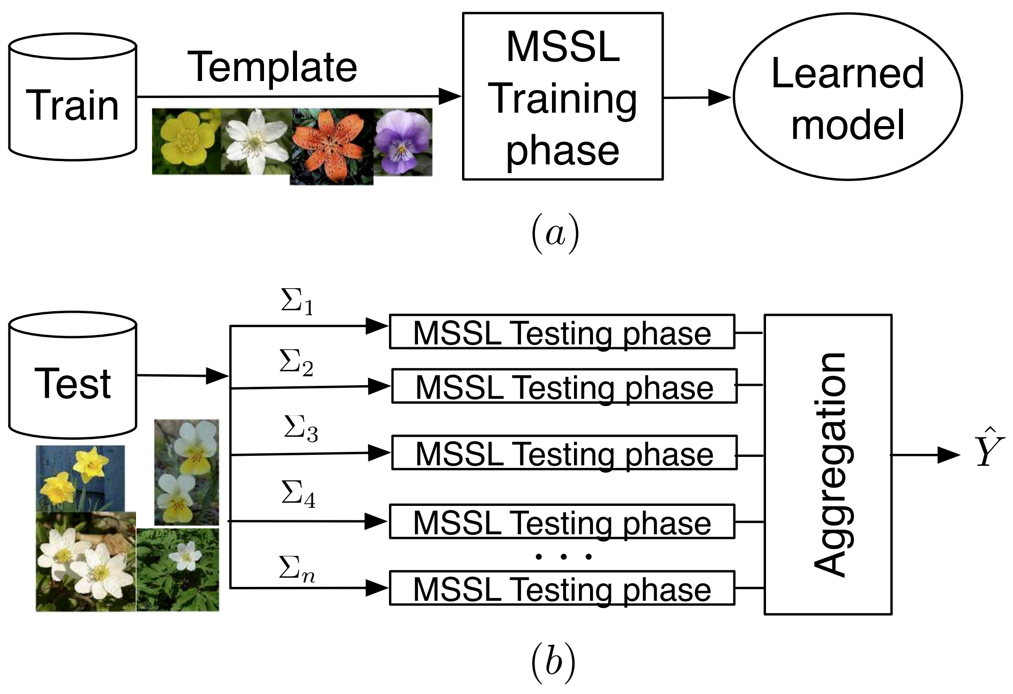

Figure 4.1: Architecture of the *shifting* technique.

can observe that the features in both extended sets (training and testing) do not fit, relationships between them are now halved.

In order to successfully cope with this problem we propose an ensemble architecture at testing time. Figure 4.1(a) shows an example of training phase using selected *templates*. A learned model is produced and then used in testing phase. Figure 4.1(b) show a scheme of this phase. It is based on the aggregation of the responses of the trained system considering different relative range of interactions. Since the interaction range set Σ defined in MSSL follows a geometric progression such that $\sigma_i = k\sigma_{i-1}$; therefore testing at different ranges can be simply regarded as a shifting process of the extended features set. Following the previous example, if we use a different set of scales $\Sigma_1 = \{1, 2, 4\}$, i.e. $\Sigma_0/2$ during the testing phase, now the resulting test features z have been shifted and their interaction relationships fit with those learned. Finally all results are combined with an aggregation function, for example taking the maximum value among all the likelihood responses for each sample. In section 4.5 we present several experiments where this shifting technique is used.

4.3 MMSSL: Multi-class Multi-scale Stacked Sequential Learning

In order to extend the Generalized Stacked Sequential Learning scheme to the multi-class case,it is necessary that base classifiers $H_1(x)$ and $H_2(x)$ can deal with data belonging to N classes instead of just two (binary case). This can be achieved using inherent multi-class base classifiers such as Random Forests, Naive Bayes, Decision Trees, Nearest Neighbors, Linear Discriminant Analysis etc. However in those cases where the base classifiers are not inherently multi class, such as Super Vector Machines or Regularized Lesat-Squares, a multi-class scheme is needed. The two basics schemes are: *One vs. All* and *All vs. All.* The former consists in building N different binary classifiers, where for the ith classifier, all the points in class i are the positive examples, and all the points not in class i are the negative examples. Therefore, let f_x be the ith classifier, the result of classification is to pick the class of the most confident classifier (Equation 4.2). While the later consists in building $N(N-1)$ classifiers, one classifier to distinguish each pair of classes i and j. Let f_{ij} be the classifier where class i were positive examples and class j were negative. Note that exists symmetry between classifiers of the same pair of classes, i.e. $f_{ji} = -f_{ij}$. Therefore the result of classification can be expressed as in Equation 4.3.

$$f(x) = \arg\max_i f_i(x). \tag{4.2}$$

One vs. All

$$f(x) = \arg\max_i \left(\sum_j f_{ij}(x) \right). \tag{4.3}$$

One vs. One

An other approach is using the ECOC framework. Error-Correcting Output Codes (ECOC) are a general framework to combine binary problems to address the mutli-class problem (24, 27). ECOC framework consists of two phases: a coding phase, where a codeword is assigned to each class of a multi-class problem, and a decoding phase, where, given a test sample, it looks for the most similar class codeword. Originaly (24), a codeword was a sequence of bits represented by $\{-1, +1\}$, where each bit identifies the membership of the class for a given binary classifier (dichotomizer). Afterwards (3), a third symbol (the zero symbol) was introduced, which means that a particular class is not considered by a given classifier. Given a set of N classes to be learned in an ECOC design, n different bipartitions (groups of classes) are formed, and n dichotomizers over the partitions are trained. As a result, a codeword $\mathcal{Y}_c, c \in [1, \ldots, N]$ of length n is obtained for each class c. Arranging the codewords as rows, a coding matrix $M \in \{-1, 0, +1\}^{N \times n}$ is defined. The most used coding strategy is the *one-versus-all* (50), where each class is discriminated against the rest, obtaining a codeword of length equal to the number of classes. In Figure 4.2 we show an example of *one-versus-one* coding matrix, which considers all possible pairs of classes, with a codeword length of $\frac{N(N-1)}{2}$. The matrix is coded using ten dichotomizers $\{b_1, \ldots, b_{10}\}$ for a 5-class problem. The white regions are coded by 1 (considered as one class by the respective dichotomizer b_j, the dark regions by -1 (considered as the other class), and the gray regions correspond to the zero symbol (classes that are not considered by the respective dichotomizer b_j).

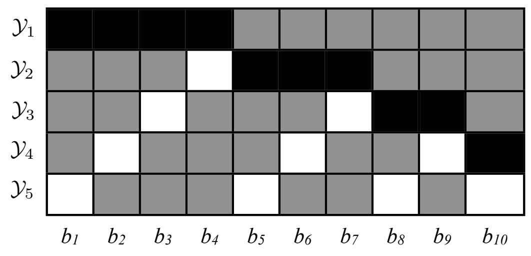

Figure 4.2: ECOC *one-versus-one* coding matrix.

During the decoding process, applying the n binary classifiers, a code $\mathcal{X}$ is obtained for each data sample in the test set. This code is compared to the base codewords ($\mathcal{Y}_c, c \in [1, \ldots, N]$) of each class defined in the matrix M. The data sample is then assigned to the class with the closest codeword. In order to find the closest codeword, the decoding strategies most frequently used are Hamming and Euclidean measures (28). those based on distances measurements between the output code and the target codeword. Among these, the most applied(27) are defined as: $HD(x, y_i) = \sum_{j=1}^{n}(1 - sign(x^j \cdot y_i^j))/2$; defined as: $ED(x, y_i) = \sqrt{\sum_{j=1}^{n}(x^j - y_i^j)^2}$.

Apart from the extension of the base classifiers, the neighborhood function $J(y', \rho, \theta)$ has also to be modified. Figure 4.3 shows the Multi-class Multi-scale Stacked Sequential Learning (MMSSL) scheme presented in this work. Given an input sample $\mathbf{x}$, the first classifier produces not only a prediction, but a measure of confidence $\hat{F}(\mathbf{x}, c)$ for belonging to each class defined in $c \in [1, \ldots, N]$. These confidence maps are the input of the neighborhood function $J(\hat{F}(\mathbf{x}, c), \rho, \Sigma)$. This function performs a multi-class decomposition over the confidence maps into s scales defined by Σ. Over this decomposition, a sampling ρ around each input example is returned, producing the z vector. The extended data set is built up using the original samples as well as the set of features in z. Finally, having the extended data set $\mathbf{x^{ext}}$ as input, the second classifier will predict to which class the input sample $\mathbf{x}$ belongs to. In the next two subsections we explain in detail this process. In the last subsection, we propose a compression approach for encoding the resulting confidence maps in order to reduce them to $\log_2 N$ without degrading the performance of the second classifier. Figure 4.3 shows the detail of function J once added the compression step between multi-scale decomposition and sampling.

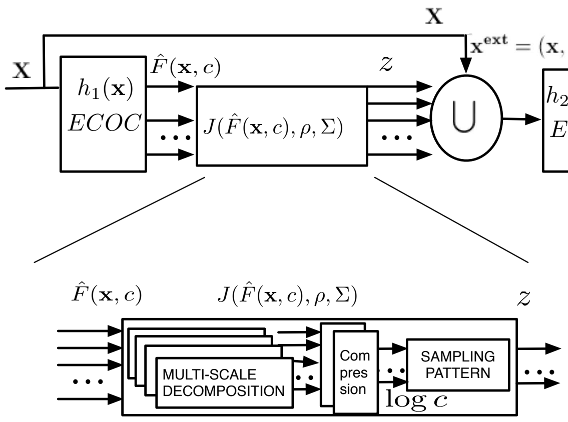

Figure 4.3: Multi-class multi-scale stacked sequential learning and detail of function $J(\hat{F}(\mathbf{x}, c), \rho, \Sigma)$ with the compression step between multi-scale decomposition and sampling.

4.3.1 Extending the base classifiers

For training the first base classifier $h_1(\mathbf{x})$, where $\mathbf{x}$ is a sample of N possible classes, an ECOC coding strategy is defined. Based on this strategy, we obtain a codeword $\mathcal{Y}_c$, $c \in [1, 2, \ldots, N]$ of length n for each class. The symbols in the codeword $\{-1, 1, 0\}$ indicate whether this class belongs to one partition or another or if it should not be considered at all. The length of the codeword determines the number of dichotomizers (binary classifiers) that has to be trained. The matrix M defines for each dichotomizer which binary partition has to be performed on the training set. Given a test sample $\mathbf{x}$, each dichotomizer produces a prediction $[1, -1]$, forming a new codeword $\mathcal{X}$ of length n. The final predicted class is the closest codeword $\mathcal{Y}_c$ to codeword $\mathcal{X}$. A distance measure between codewords can be used for determining the closest class.

If the dichotomizers only produce binary predictions, all the predictions within

$\mathcal{X}$ have the same importance. Instead, if the dichotomizers can produce a measure of confidence on its predictions, a more fine-grained distance between codewords can be obtained. By applying equation 4.1 we can convert the margins used by those classifiers to a measure of confidence with values between the codeword interval $[-1, 1]$. Applying this for each dichotomizer, a new codeword $\mathcal{X}$ of length n is formed, where all the symbols $\in \mathbb{R}$. Once we have a normalized codeword, we use a soft distance δ for decoding, i.e. we compare the codeword $\mathcal{X}$ with each codeword $Y_c, c \in [1, \dots, N]$ defined in the matrix M. These distance measures can be seen as a prediction confidence measure for each class, once we normalize them to the range $[0, 1]$. Therefore, given a set of possible labels $c_i, i \in [1, \dots, N]$, we define the membership confidences as follows:

$$\hat{F}(y = c_i|\mathbf{x}) = e^{-\alpha\delta(\mathcal{Y}_1, \mathcal{X})}, \forall i \in [1, .., N], \tag{4.4}$$

where δ is a soft distance such the Euclidean one, and α depends on δ. By applying this to the all data samples in $\mathbf{X}$ we define the confidence map for each class as expressed in Equation 4.5:

$$\hat{F}(\mathbf{x}, c) = \{\hat{F}(y = c_1|\mathbf{x}), \dots, \hat{F}(y = c_N|\mathbf{x})\}, \forall \mathbf{x} \in \mathbf{X}. \tag{4.5}$$

4.3.2 Extending the neighborhood function J

We define the neighborhood function J in two stages: 1) a multi-scale decomposition over the confidence maps $\hat{F}(\mathbf{x}, c)$ and 2) a sampling performed over the multi-scale representation. This function is extended in order to deal with multiple classes. Now it is formulated as follows:

$$z = J(\hat{F}(\mathbf{x}, c), \rho, \Sigma).$$

Starting from the confidence maps, we apply a multi-scale decomposition upon them, resulting in as many decomposition sequences as classes. For the decomposition we use the multi-resolution Gaussian approach (3.2.1.1). Each level of the decomposition (scale) is generated by the convolution of the confidence map by a Gaussian mask with standard deviation σ. In this way, the bigger σ is, the longer interactions are considered. Therefore, at each level of decomposition all the points have information from the rest accordingly to the sigma parameter. Given a set of $\Sigma = \{\sigma_1, \dots, \sigma_s\} \in \mathbb{R}^+$ and all the predicted confidence maps $\hat{F}(\mathbf{x}, c)$, each level of the decomposition $s_i, i \in [1, \dots, s]$ is computed as follows:

$$\hat{F}^{s_i}(\mathbf{x}, c) = g^{\sigma_i}(\mathbf{x}) * \hat{F}(\mathbf{x}, c), \forall i \in [1, .., s],$$

where $g^{\sigma_i}(\mathbf{x})$ is defined as a multidimensional isotropic gaussian filter with zero mean:

$$g^{\sigma_i}(\mathbf{x}) = \frac{1}{(2\pi)^{d/2}\sigma_i^{1/2}} e^{-\frac{1}{2}\mathbf{x}^T\sigma_i^{-1}\mathbf{x}}.$$

Once the multi-scale decomposition is performed, we define the support lattice z. This is, the sampling over the multi-scale representation which forms the extended data. Our choice is to use a scale-space sliding window over each label multi-scale decomposition. The selected window has a fixed radius with length defined by ρ in each dimension d and with origin in the current prediction example. Thus, the elements covered by the window is $w = (2\rho + 1)^d$ around the origin. Then, for each scale s_i considered in the previous decomposition the window is stretched in each direction using a displacement proportional to the scale we are analyzing. This displacement at each scale forces that each point considered around the current prediction has very small influence from previous neighbor points. In this way, the number of features of z appended to the input data set is equal to $(2\rho + 1)^d \cdot s \cdot c$. According to this, we can see that the extended data set increases with the number of classes. This can produce a scalability problem, since the second classifier has to deal with large feature sets.

4.4 Extended data set grouping: a compression approach

The goal of grouping the extended data set is to compress its number of features without losing significant performance. Using our MMSSL approach, we can see that the size of the extended set depends on the number of classes, the number of scales, and the number of samples around each example. We can choose the number of samples and scales, but the number of classes is problem dependent. Therefore, for reducing the number of confidence maps, we add a compression process between the multi-scale decomposition and the sampling process as shown in Figure 4.3. This compression is done following information theory by means of partitions.

Let $\mathcal{P}$ be a set $\{\{P_1^1, P_1^2\}, \ldots, \{P_\kappa^1, P_\kappa^2\}\}$ of partitions groups of classes and $c = \{c_1, \ldots, c_N\}$ the set of all the classes, so that for any j, $P_j^1 \subseteq c$, $P_j^2 \subseteq c \mid P_j^1 \cup P_j^2 = c$, and $P_j^1 \cap P_j^2 = \emptyset$. The confidence maps are grouped using the elements on $\mathcal{P}$. We have defined two different ways of combining the partitions: using *binary compression* or using *ternary compression*. Let the confidence map $\hat{F}^{s_k}$ of a certain scale s_k, $k \in [1, \ldots, s]$ be expressed as follows,

$$\hat{F}^{s_k}(\mathbf{x}, P_j) = \sum_{i}^{N} \gamma_{ij} \hat{F}^{s_k}(\mathbf{x}, c_i), \tag{4.6}$$

Binary compression

	c_1	c_2	c_3	c_4	c_5
Γ_1	1	0	0	1	1
Γ_2	0	1	1	0	1
Γ_3	1	0	1	0	1

Table 1.

Ternary compression

	c_1	c_2	c_3	c_4	c_5
Γ_1	1	-1	-1	1	1
Γ_2	-1	1	1	-1	1
Γ_3	1	-1	1	-1	1

Table 2.

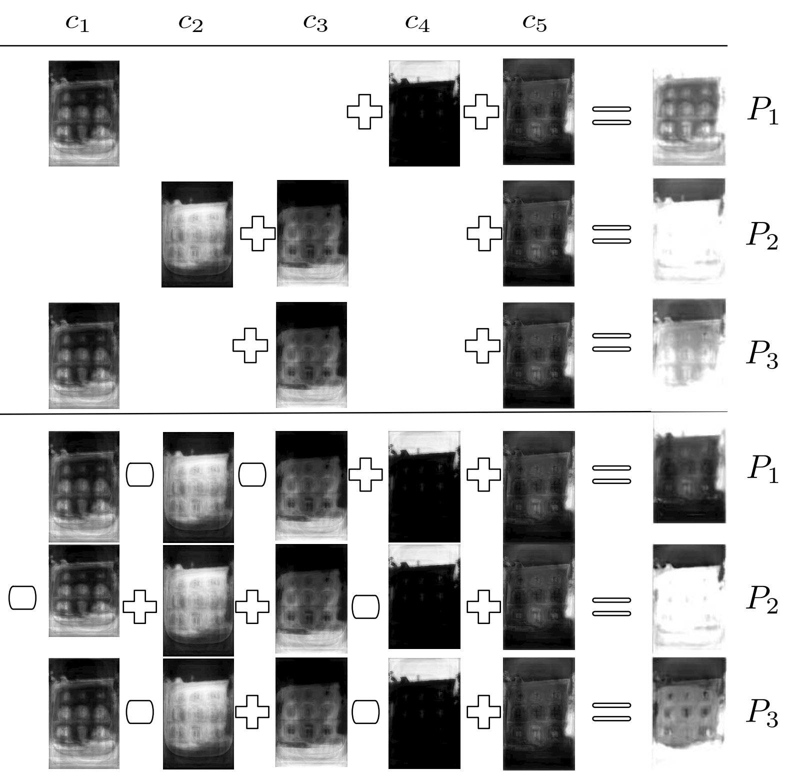

Figure 4.4: 5-class likelihood maps compressed to three, using partitions. Binary approach is represented by Table 1. The symbols used are 0 and 1. Ternary approach is represented by Table 2. The symbols used are -1 and 1. Applying Equation. 4.6 we obtain the aggregated likelihood maps $P_1, P_2, P_3 \in \mathcal{P}$. In the case of binary compression, any class marked with zero in a codeword Γ is not considered, while in the case of ternary compression, all classes are aggregated according to each of the codewords Γ.

where

$$\gamma_{ij} = \begin{cases} a & \text{if } c_i \in P_j^1 \\ b & \text{if } c_i \in P_j^2 \end{cases}$$

for all the sets of partitions $P_j, j \in [1, \ldots, \kappa]$ in $\mathcal{P}$, being $a = 0$ and $b = 1$ in the case of binary compression and $a = -1$ and $b = 1$ in the case of ternary compression (we choose only $\{-1, 1\}$ values from the ternary set $\{-1, 0, 1\}$).

We use a partition strategy for $\mathcal{P}$ which produces a minimum set of partitions $\mathcal{P} = \{\{P_1^1, P_1^2\} \ldots, \{P_\kappa^1, P_\kappa^2\}\}$, where $\kappa = \lceil \log_2 |c| \rceil$, being $\lceil x \rceil = \min\{n \in \mathbb{Z} \mid n \geq x\}$. Our strategy builds the partitions assigning an unique binary code of length equals to number of partitions in $\mathcal{P}$ for each class. For example in Figure 4.4 a 5-class problem $c = \{c_1, c_2, c_3, c_4, c_5\}$ is illustrated. We can reduce the problem to a set of three partitions $\mathcal{P} = \{\{P_1^1 = \{c2, c3\}, P_1^2 = \{c1, c4, c5\}\}, \{\{P_2^1 = \{c1, c4\}, P_2^2 = \{c2, c3, c5\}\}, \{\{P_3^1 =$

$\{c2, c4\}, P_3^2 = \{c1, c3, c5\}\}$. Therefore, in the binary case, the assigned codes for each partition are $\Gamma_1 = \{1, 0, 0, 1, 1\}$, $\Gamma_2 = \{0, 1, 1, 0, 1\}$, and $\Gamma_3 = \{1, 0, 1, 0, 1\}$, and in the ternary case, the assigned codes are $\Gamma_1 = \{1, -1, -1, 1, 1\}$, $\Gamma_2 = \{-1, 1, 1, -1, 1\}$, and $\Gamma_3 = \{1, -1, 1, -1, 1\}$. Thus, applying Equation 4.6, we obtain the likelihood maps for each partition, P_1, P_2, P_3. As it is shown in Figure 4.4, in the case of binary compression, the classes in P_i^1 for any partition i are not considered, while in the case of ternary compression, the classes in P_i^1 and P_i^2 for any partition i are combined.

Following this compression approach, now the support lattice z is defined over $\hat{F}^{\Sigma}(\mathbf{x}, \mathcal{P})$. This is, applying Equation 4.6 over all the scales defined by $\Sigma = \{\sigma_1, \ldots, \sigma_s\}$. Therefore, the number of features in z is reduced from $(2\rho + 1)^d \cdot s \cdot c$ to $(2\rho + 1)^d \cdot s \cdot \lceil \log_2 c \rceil$.

4.5 Experiments and Results

In this section we present different experiments for validating our extensions on the MSSL framework. First the shifting technique explained in 4.2 is tested in two domains, horse image classification and flowers classification. Second we performed experiments in several multi-class classification problems where different approaches of compression are used as well.

4.5.1 Horse image classification using shifting

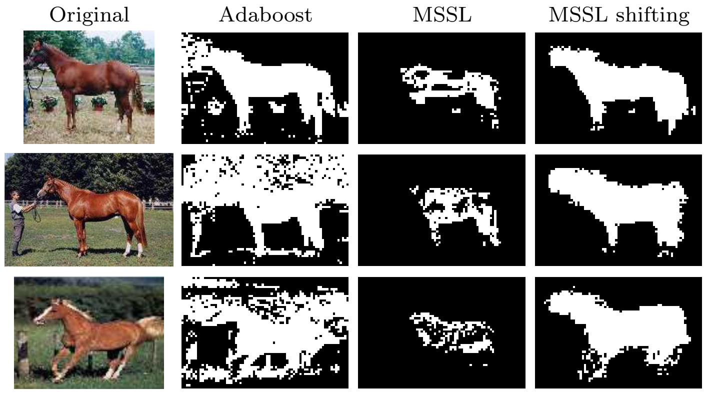

Figure 4.5: Examples of horse classification. Second column shows Adaboost prediction. Third and forth uses MSSL over the images with and without shifting.

In order to validate the shifting technique, we define a toy problem using the Weizmann horse database (8), which consist in classify RGB horse images but rescaled to half size with respect to the ones used during the training phase. Each image is labelled according to the horse silhouette. We selected 100 images of horses from the database. Then, we define 5 random partitions of samples, each one consisting of the half of images for training and the remaining for testing. As a pre-processing step, we rescale all the horses images to the same resolution 150×100. The feature vector is composed of RGB attributes. All configurations use Adaboost with 100 iterations of decision stumps. For each image in the training set we perform a stratified sampling of 7500 pixels per image. This data is classified by the first base classifier applying leave-one-image-out. Using the generated predicted labels we perform a multi-scale decomposition with $\Sigma = \{2, 4, 8, 16\}$. The extended data set is created choosing the 8-neighbors of each pixel on each level of decomposition. Finally, both classifiers are trained using the same feature samples without and with the extended set, respectively. Table 4.1 shows results of predictions whether shifting is applied or not. For assessing the validity of the results we use the *Overlapping*, defined as $\frac{TP}{FN+FP+TP}$. First row shows the metrics using Adaboost. As sensitivity and specificity show up, the classification of the horses (*MSSL*) fails, because the system have learned the relative distance with respect to the size of the training horses. Now, we use the shifting approach by sliding the scales that are used in the testing phase to $\Sigma = \{1, 2, 4, 8\}$. As we can observe in Figure 4.5, applying this scale decomposition the model we trained before is able to classify the small horses appropriately without the need of retraining the system. Table 4.1 shows the improvement of the results classifying the small horses with the shifting approach.

Table 4.1: Results of prediction using Adaboost and MSSL with and without shifting technique.

	Acc	Over	Sens	Spec	Prec	NPV
Adatboost	0.7789	0.4417	0.8237	0.6559	0.8681	0.5749
MSSL	0.7465	0.0588	**0.9963**	0.0594	0.7444	**0.8561**
MSSL shift	**0.8734**	**0.6448**	0.8777	**0.8617**	**0.9458**	0.7193

4.5.2 Flowers classification using shifting

In this experiment we test the shifting technique in a free environment where flowers can be found in different number and size. (49). As training set, we define a flower template consisting of a set of similar flowers in size and shape, but having different types and colors. Each image is labeled according to the flower silhouette whether it is flower class or background class. For the testing set we choose flowers related to the

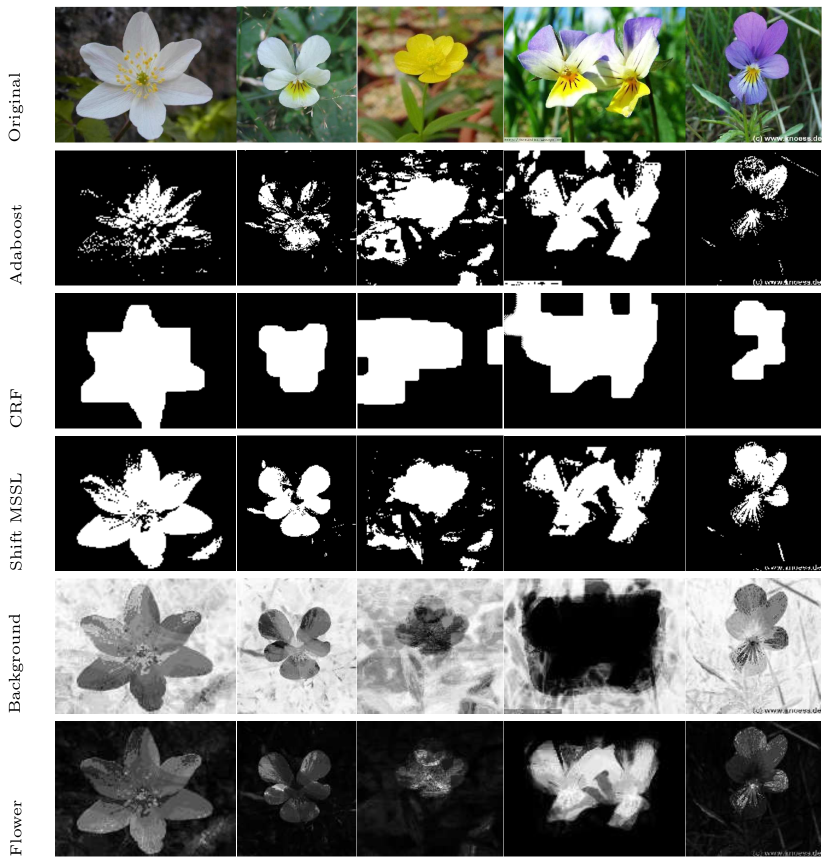

Figure 4.6: Predictions using Adaboost and MSSL.

defined template but at different size and color. We use 16 images for training and 25 for test. As a pre-processing step, we rescale all the images to the same resolution on the x-axis, maintaining the same proportion in the y-axis. The feature vector is only composed of RGB attributes. All configurations use Adaboost with 100 iterations of decision stumps.

Table 4.2: Results using Adaboost and MSSL.

	Acc	Over	Sens	Spec	Prec	NPV
ADABoost	0,8773	0,5621	0,9207	0,7217	0,9222	0,7176
CRF	0,8568	0,5840	0,8430	**0,9052**	**0,9689**	0,6220
Shift MSSL	**0,9012**	**0,6243**	**0,9427**	0,7524	0,9317	**0,7858**

For each image in the training set we perform a stratified sampling of 3000 pixels per image. This data is classified by the first base classifier applying leave-one-image-out. Using the generated predicted labels we perform a multi-scale decomposition with $\Sigma = \{18, 27, 41\}$. The extended data set is created choosing the 8-neighbors of each pixel on each level of decomposition. Finally, both classifiers are trained using the same feature samples with and without the extended set, respectively. We have performed several testing phases using always the same trained model. For each testing phase, we use a three scale decomposition from the range $\Sigma = \{0.5, 3, 5, 8, 12, 18, 27, 41\}$. This makes a total of 6 test rounds per image. At the end of each test round we take the measures of the likelihood of each image. Examples of background and flower likelihoods images at different rounds are shown in Figure 4.6. We calculate the maximum for all rounds, resulting in two images. The row *Shift MSSL* shows the result of joining both images using the greater than operation. The figure also shows the original image and its resulting classification using Adaboost and CRF (45). Table 4.2 shows the metrics for these methods. Shift MSSL approach beats the non-sequential Adaboost approach for each metric and it also beats CRF in accuracy and overlapping. The rest of metrics point out that our method is better defining the flower class than the CRF method.

4.5.3 MSSL for multi-class classification problems

In the next subsection data, methods and validation protocol for each experiment are presented. Afterwards, the results are presented in two aspects, a) statistical results, where different measures are computed and significance tests are performed on different datasets, and b) qualitative results, where concrete results are particularly analyzed for a more intuitive understanding of the behavior of each method.

4.5.3.1 Experimental Settings

- **Data**: we test our multi-class methodology performing 9 different experiments out from four databases:

    1. Sensor Motion data database: The sensor motion database (14) is a data set of accelerometer sensor runs from 15 different people performing certain activities. Each accelerometer sample is labeled as one of 5 different activities, namely walking, climbing stairs, standing idle, interacting and working. The spatial relationship in label space is 1D. There are two different scenarios. Sequential scenario is where all the people is doing the activities in the same order (*motion sequential scenario*). Random scenario is where all the people is performing the activities in random order (*motion random scenario*)). We

also performed a third experiment for benchmark purposes in which there are only activities from one person (*motion one person*).

2. FAQ database (17, 26): The FAQ database is a set of frequented asked questions pages from Usenet. There are 48 annotated pages from several topics. Each line in a page is labeled as (0) header, (1) question, (2) answer, or (3) tailing. There are 24 boolean features characterizing each line. The spatial relationship in label space is 1D.
3. IVUS image database (16): It contains images from Intravascular Ultrasound (IVUS). They are a set of IVUS frames manually labelled. 8 classes are considered: (1) blood, (2) plaque, (3) media, (4) media adventitia, (5) guide-wire, (6) shadowing, (7) external tissue, and (8) calcium. The spatial relationship in label space is 2D. There are 29 textural features in total extracted from IVUS data.
4. e-trims database (41): The e-trims database is comprised of two image datasets, *e-trims 4-class* with four annotated object classes and *e-trims 8-class* with eight annotated object classes. There are 60 annotated images in each of the dataset. The object classes considered in 4-class dataset are: (1) building, (2) pavement/road, (3) sky, and (4) vegetation. In 8-class dataset the object classes considered are: (1) building, (2) car, (3) door, (4) pavement, (5) road, (6) sky, (7) vegetation, and (8) window. Additionally, for each database we have a background class (0) for any other object. All images are resized proportionally to 150 pixels height. Train images are stratified sampled, taking 3000 pixels. We have performed experiments with two different set of features: **RGB** representation of each pixel, and RGB plus **HOG** (Histogram of oriented gradient (19)) with 9 bins, ending up with 12 features for sample. The spatial relationship in label space is 2D.

- **Methods**: We test all the databases with four different configurations of our MMSSL methodology. Also, we test with Real Adaboost (31) and CRF Multi-label optimization through Graph Cut α-expansion (10) as baseline experiments. The settings for all the MMSSL configurations are the same, the only difference is the way the extended data set is generated. We have used as base classifier a Real Adaboost ensemble of 100 decision stumps. The coding strategy for the ECOC framework in each classifier is *one-versus-one* and the decoding measure is Euclidean distance. The neighborhood function performs a Gaussian multi-resolution decomposition in 4 scales, using $\Sigma = \{1, 2, 4, 8\}$, except in IVUS database where we used 6 scales $\Sigma = \{1, 2, 4, 8, 16, 32\}$ due to the images dimensions. In 1D databases, we used $w = 7$ elements in both directions of the neighborhood, while in 2D databases we used just the surrounding points, i.e. $w = 1$. Summarizing, the different experiments we have performed are:

1. MMSSL using labels. It uses the MMSSL framework using only the predicted labels from the first classifier as input for neighborhood function.
2. MMSSL using confidences. It uses the MMSSL framework using the confidence maps for all the classes as input for neighborhood function.
3. MMSSL using compression approach with binary matrix: It uses the MMSSL framework using a compression over the confidence map. The compression matrix uses binary values $\{0, 1\}$.
4. MMSSL using compression approach with ternary matrix. It uses the MMSSL framework using a compression over the confidence map. The compression matrix uses ternary values $\{-1, 1\}$.
5. Adaboost. Uses only one Adaboost classifier, without taking into account the neighborhood relationship. Used as baseline experiment.
6. Multi-label optimization. It uses multi-label optimization via α-expansion. We have applied the α-expansion optimization, using the confidence maps for each class obtained from the first classifier. For the neighborhood term, we use the intensity between the point and its neighbors for each direction defined in the database.

- **Validation**: For the different experiments we use 5-fold cross-validation or one-leave-out for final prediction. For each fold, the base classifier $h_1(x)$ uses ten-fold cross-validation for predicting the labels of the training set, which produces the confidence maps used later for the second classifier $h_2(x)$. We measure the results in terms of the accuracy, and the mean of overlapping, recall, and precision from a $N \times N$ confusion matrix , computed as follow: $accuracy = \frac{\sum_i^N TP_i}{\sum_i^N (TP+FP+FN)_i}$, $overlapping_i = \frac{TP_i}{(TP+FN+FP)_i}$, $recall_i = \frac{TP_i}{(TP+FN)_i}$, and $precision_i = \frac{TP_i}{(FP+TP)_i}$, where TP_i means the predictions correctly classified in the class i, FP_i means the predictions misclassified as class i and FN_i means the actual class i predictions misclassified as any other class. For comparing the results obtained from the different experiments we have used statistic tests: the Friedman test for checking the non-randomness of the results and the Nemenyi test for checking if one of the configurations can be statistically singled out (23).

4.5.3.2 Numerical Results

Tables 4.3 to 4.9 show accuracy, overlapping, recall, and precision averaged for each experiment. Best results are marked in bold. The tables show similar tendency of the different classifiers results for different databases. Non sequential methods such Adaboost give the poorest accuracies. Multi-label optimization using Graph cut achieves better results, specially in 2D databases. Finally, all methods based in MMSSL give the best results. Usually, using just predictions it leads to worse results than using confidence maps. It is also remarkable that by using compression techniques (binary and ternary coding) the global accuracy is not significantly degraded. In order to compare the performances provided for each of theses strategies, Table 4.10 shown in the mean rank of each strategy considering the accuracy terms of the 9 different experiments. The rankings are obtained estimating each particular ranking r_i^j for each data sequence i and each system configuration j, and computing the mean ranking R for each configuration as $R_j = \frac{1}{E}\sum_i r_i^j$, where E is the total number of experiments.

	Accuracy	Overlapping	Recall	Precision
ADABoost	0.5771	0.3142	0.4419	0.4504
GraphCut	0.5766	0.3129	0.4404	0.4489
Labels	0.6403	0.4766	0.6079	0.6516
Standard	0.7069	0.5905	0.7048	**0.8098**
SublinealBinary	**0.7361**	**0.6021**	**0.7427**	0.7914
SublinealTernary	0.7026	0.5648	0.6843	0.7638

Table 4.3: Result figures for database motion sequential scenario.

	Accuracy	Overlapping	Recall	Precision
ADABoost	0.5771	0.3142	0.4419	0.4504
GraphCut	0.5766	0.3129	0.4404	0.4489
Labels	0.5951	0.3833	0.5292	0.5375
Standard	0.7109	0.4365	0.552	0.5867
SublinealBinay	**0.7305**	**0.4677**	**0.5912**	**0.6266**
SublinealTernary	0.6937	0.4392	0.5748	0.6159

Table 4.4: Result figures for database motion random scenario.

	Accuracy	Overlapping	Recall	Precision
ADABoost	0.7607	0.553	0.6805	0.715
GraphCut	0.7888	0.5865	0.7043	0.7654
Labels	0.879	0.7489	0.8372	0.8736
Standard	**0.902**	**0.793**	**0.8792**	**0.8824**
SublinealBinary	0.8571	0.7133	0.8125	0.8458
SublinealTernary	0.8796	0.7477	0.8395	0.8652

Table 4.5: Result figures for database motion one person.

	Accuracy	Overlapping	Recall	Precision
ADABoost	0.8552	0.2392	0.2781	0.3906
GraphCut	0.858	0.2355	0.2718	0.4427
Labels	0.8906	0.4346	0.4961	0.6675
Standard	0.8866	0.5125	0.5627	**0.8122**
SublinealBinary	0.8786	0.4809	0.5275	0.7649
SublinealTernary	**0.8998**	**0.5628**	**0.6277**	0.8067

Table 4.6: Result figures for database FAQ.

	Accuracy	Overlapping	Recall	Precision
ADABoost	0.6605	0.3127	0.422	0.4978
GraphCuts	0.6748	0.3102	0.4175	0.4654
Labels	0.6789	0.3359	0.4435	0.5098
Standard	**0.7199**	**0.3764**	**0.4842**	**0.5555**
SublinealBinary	0.684	0.3379	0.4457	0.5205
SublinealTernary	0.7006	0.3544	0.4618	0.5345

Table 4.7: Result figures for database IVUS, using 6 scales.

In order to reject the null hypothesis that the measured ranks differ from the mean rank, and that the ranks are affected by randomness in the results, we use the Friedman test. The Friedman statistic value is computed as follows:

$$\chi_F^2 = \frac{12E}{k(k+1)} \left[\sum_j R_j^2 - \frac{k(k+1)^2}{4} \right].$$

		Accuracy	Overlapping	Recall	Precision
RGB	ADABoost	0.7274	0.3612	0.4351	0.5334
	GraphCuts	0.7283	0.3435	0.4113	0.4688
	Labels	0.7612	0.4232	0.5004	0.6716
	Standard	0.8074	**0.5189**	**0.6137**	0.6922
	SublinealBinary	0.7987	0.4957	0.5806	0.6924
	SublinealTernary	**0.8078**	0.5172	0.6085	**0.7028**
HOG	ADABoost	0.8067	0.5115	0.608	0.6648
	GraphCuts	0.8317	0.53	0.6108	0.6962
	Labels	0.8305	0.5447	0.6385	0.6878
	Standard	**0.8686**	**0.599**	**0.6912**	**0.7373**
	SublinealBinary	0.8514	0.5767	0.678	0.7151
	SublinealTernary	0.8599	0.5852	0.6752	0.7333

Table 4.8: Result figures for database ETRIMS 4 classes RGB and HOG.

		Accuracy	Overlapping	Recall	Precision
RGB	ADABoost	0.606	0.1991	0.2591	0.3003
	GraphCuts	0.6039	0.1859	0.2405	0.2719
	Labels	0.6549	0.2526	0.3193	0.4297
	Standard	**0.703**	**0.3133**	**0.3891**	**0.4752**
	SublinealBinary	0.6616	0.267	0.3389	0.4439
	SublinealTernary	0.6742	0.2768	0.346	0.4361
HOG	ADABoost	0.6723	0.2868	0.3618	0.4623
	GraphCuts	0.6812	0.2618	0.3255	0.3678
	Labels	0.6885	0.3031	0.3797	0.4706
	Standard	**0.7312**	**0.3479**	**0.4338**	**0.5103**
	SublinealBinary	0.6895	0.3038	0.3837	0.4765
	SublinealTernary	0.7164	0.3348	0.4222	0.4986

Table 4.9: Result figures for database ETRIMS 8 classes RGB and HOG.

In our case, with $k = 6$ system configurations to compare, $\chi^2_F = 35.79$. Since this value

	ADAboost	GraphCut	Labels	Standard	Sub.Binary	Sub.Ternary
Rank	5.7	5.1	3.9	1.7	2.8	1.9

Table 4.10: Mean rank of each strategy considering the accuracy terms of the different experiments.

is undesirable conservative, Iman and Davenport (23) proposed a corrected statistic:

$$F_F = \frac{(N-1)\chi_F^2}{E(k-1)-\chi_F^2}.$$

Applying this correction we obtain $F_F = 31.11$. With 6 methods and 9 experiments, F_F is distributed according to the F distribution with 5 and 40 degrees of freedom. The critical value of $F(5,40)$ for 0.05 is 2.44. As the value of $F_F = 31.11$ is higher than 2.44 we can reject the null hypothesis. Once we have checked for the non-randomness of the results, we can perform an a post-hoc test to check if one of the configurations can be statistically singled out. For this purpose we use the Nemenyi test. The Nemenyi statistic is obtained as follows:

$$CD = q_\alpha \sqrt{\frac{k(k+1)}{6E}}.$$

In our case with $k = 6$ system configurations to compare and $E = 9$ experiments (data configurations) the critical value for a 90% of confidence is $CD = 1.27$. In Figure 4.7 we can see a graphical representation of this post-hoc test. As the ranking of the MMSSL Standard method intersects with both sub-lineal approaches ranks for that value of the CD, we can state that MMSSL using confidences outperforms the rest of the methods in the presented experiments. Moreover, it reveals that among compressed and non compressed MMSSL strategies statistically significant differences do not exist. This fact reinforce our idea of grouping features without losing performance is feasible. The main advantage for using the compression approach is that by reducing the number of features in the extended dataset, the time of the learning phase for the second classifier is reduced. Therefore, the MMSSL framework scales sublinearly in feature space with the number of classes without a loss in generalization.

4.5.3.3 Qualitative Results

In this section we highlight general observations comparing ADAboost, multi-label optimization gaph cut and our MMSSL approach. Figure 4.8 shows results in 1D motion database. The rest of figures shows results in 2D databases, Figure 4.11 shows

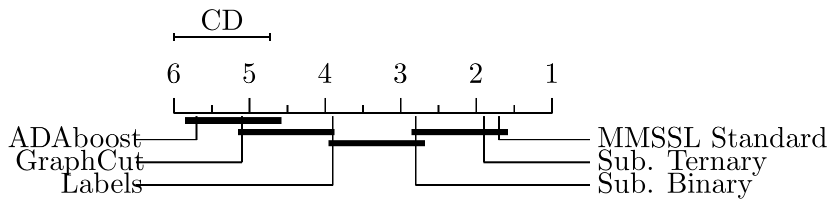

Figure 4.7: Comparison of all methods against each other with the Nemenyi test. Groups of classifiers that are not significantly different are connected.

results in IVUS database, Figure 4.9, and Figure 4.10 show results in e-trims database 4 and 8 classes, respectively.

The images resulting from *ADAboost* classification show how this method is not capable to capture sequential relationship among labels. For example, in 1D database results shown in Figure 4.8, we can see how contiguous points inside a long class interval are classified as belonging to another class. In 2D database results show spurious classified pixels appearing inside big objects. For example, in the first row of Figure 4.9 in the upper side of the building appears few pixels labelled as tree. In the second row of the same image clouds in the middle of sky are marked as building and in the third row of the same figure a wire crossing the sky is misclassified. In the last two rows shadows on the top of the buildings are classified as road. In Figure 4.10 as many other classes exist, the effect of spurious artifacts on Adaboost results are more notorious, for example int he last row dark clouds are misclassified as belonging to the building. In Figure 4.11 we can see that Adaboost fails, producing results far from the real classification, like in the first and second row. All artifacts observed appear due to specific pixel values which lead the classifier to a misclassification.

On the contrary, the multi-label optimization technique by means of *Graph Cut* captures sequential relationships between labels, erasing such interclass artifacts. In 1D database results shown in Figure 4.8, we can see how the number of bad classified contiguous points decreases respect ADAboost, but it still fails in classify correctly short intervals of contiguous points of certain classes. In 2D databases, the drawbacks of this method are a) the tendency to crop the contours of the objects producing sharp shapes resembling blobs, as is reflected in the first, third and fourth rows of Figure 4.9 where trees lose all its shape, even the building in the third row is rounded, and b) the elimination of entire overlapped objects, as is shown in the three first rows of Figure 4.10, where trees, windows and doors are completely removed, only prevailing the building class. Even though, long objects are still misclassified, as the shadows in the top part of the buildings in the last two rows in Figure 4.9, or worst, the dark clouds in the last row of Figure 4.10 are completely joined with the building forming a huge building. In Figure 4.11 we can see a fairly improvement respect Adaboost, but it still fails in the classification of the three first rows. This method fails mainly because it is not considering the relationship among objects at different scales.

The last method considered is our approach, *MMSSL* using confidences without compression.The results of this method are qualitatively better than the rest. The results are a trade-off between spacial coherence and shape permanence. This is because the relationship among classes is considered at different scales. In 1D database results shown in Figure 4.8, we can see how the MMSSL is the only method that achieves good performance as well in long sequences as in short sequences of points of the same class and does not matter whether the activities are carried on in the same order as trained or not. In 2D databases, we can see in Figure 4.9 how MMSSL is able to keep the shape of buildings and trees in all the images and how it removes interclass artifacts that previous method were not able to, for example the shadows on the top of the building in the last two rows. In Figure 4.10 we can see in all the images that windows, trees and doors are fairly kept, even the dark clouds in the last row are practically removed, appearing only spurious pixels in the border of the image. Moreover, in Figure 4.11, we can see how MMSSL is able to close big areas of the same class like in the three firsts rows, where the rest of methods fail. Also is remarkable in the fourth and fifth row how narrower classes between wider classes are preserved, where the other methods fail. The points where the method fails the most are the junctions between classes where does not exist a clear distinction, for example in the second row in Figure 4.10 where cars are classified altogether as one, mixing with the grass and the road.

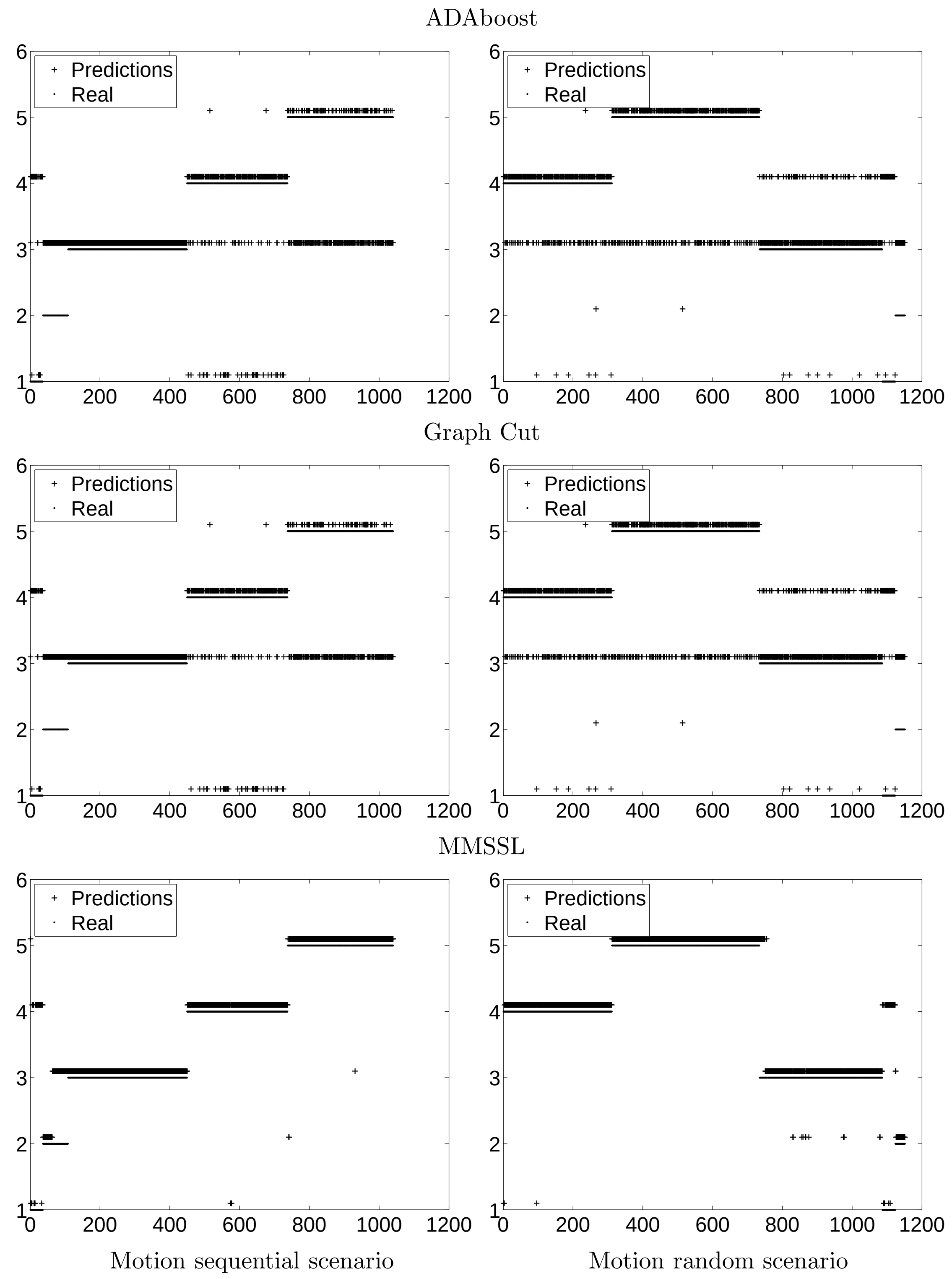

Figure 4.8: Figures of final classification in motion sequential scenario and motion random scenario for ADAboost, multi-label optimization Graph cut, and our proposal MMSSL. Y-axe shows the labels for each class and X-axe is the time interval. Predictions values are marked with + and real values are marked just below with dots.

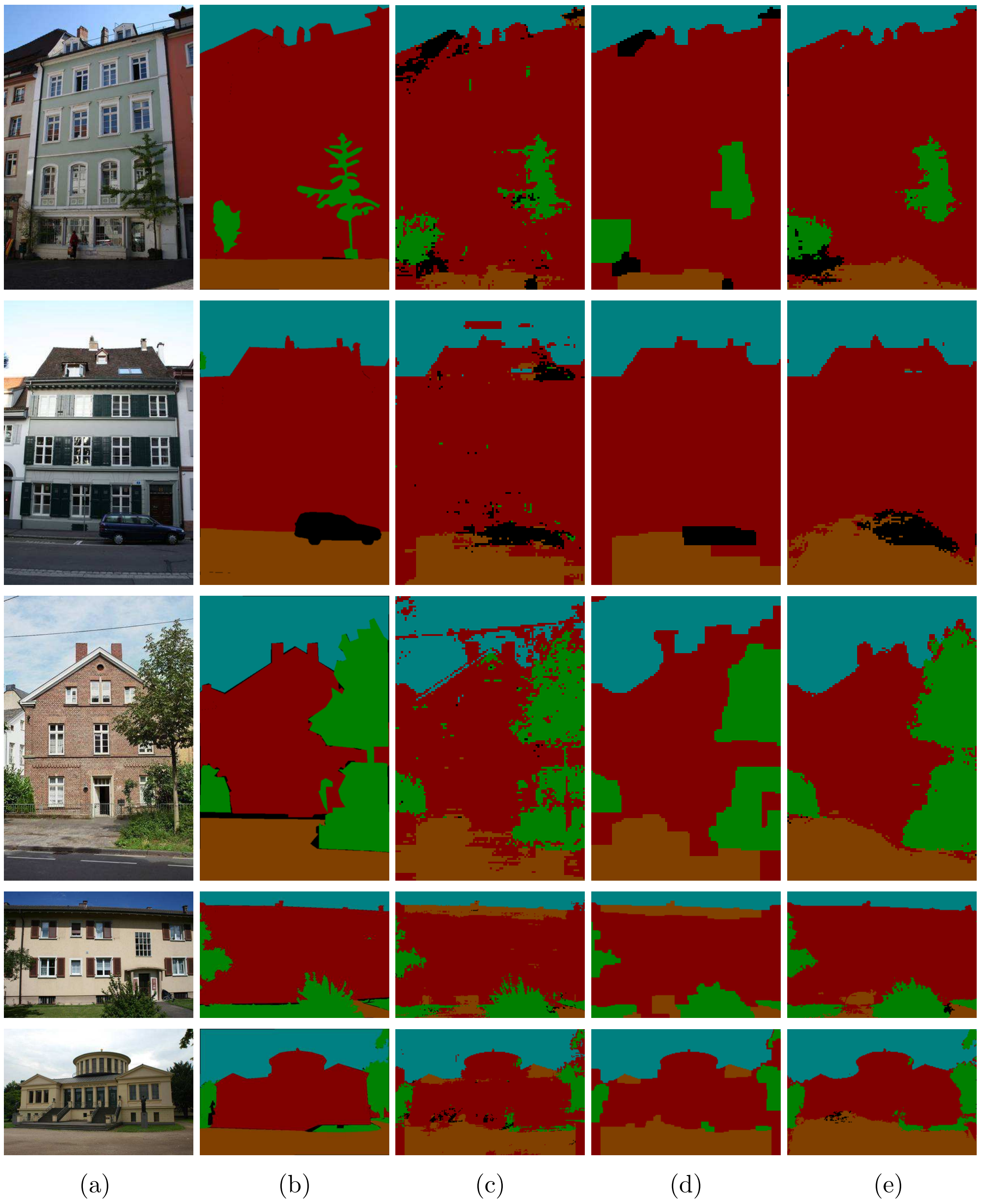

Figure 4.9: Figures of final classification in ETRIMS 4 Classes HOG database. (a) Shows the original image, (b) the groundtruth image, and (c),(d), and (e) show ADAboost, GraphCut, and MMSSL without compression, respectively.

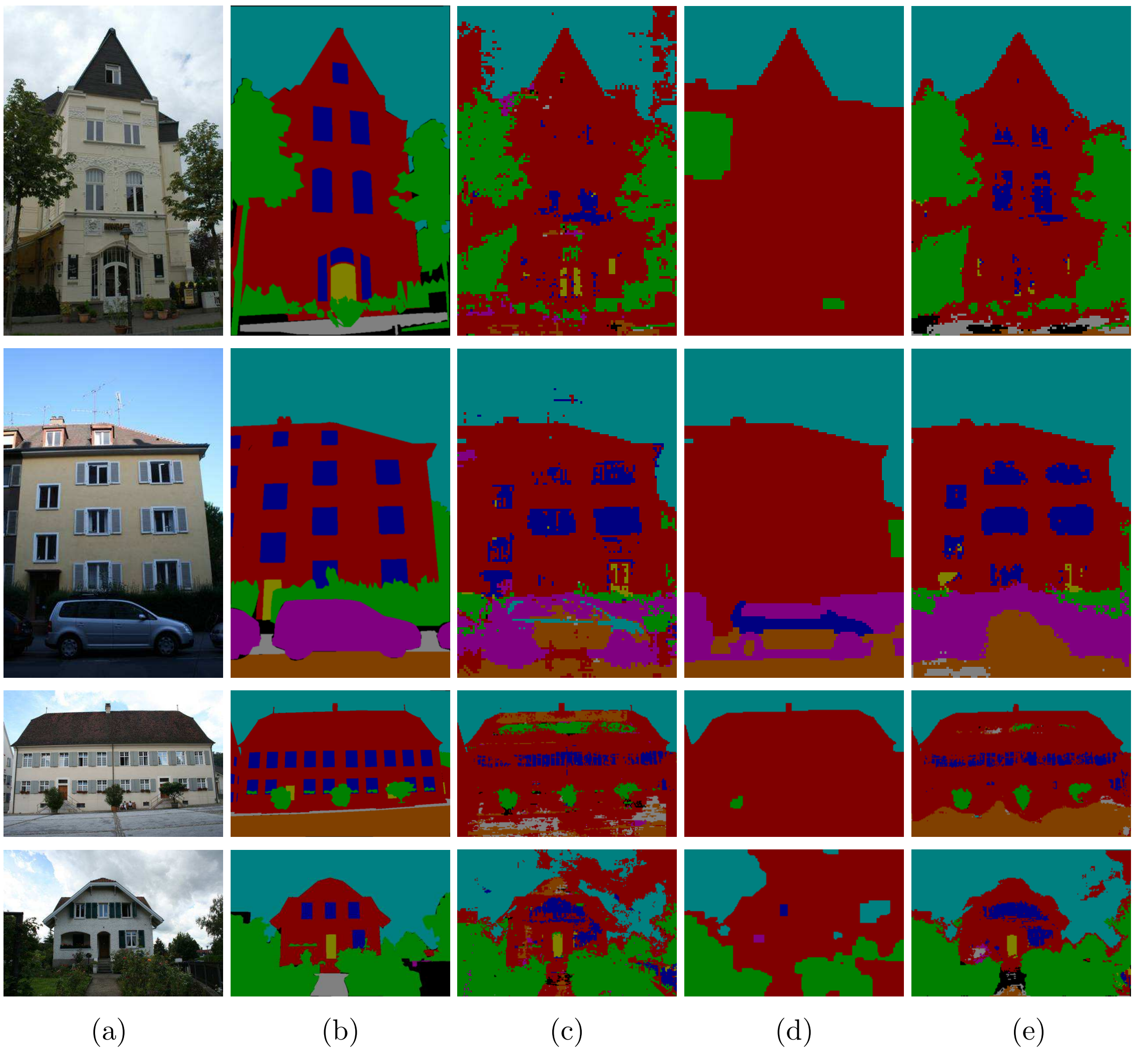

Figure 4.10: Figures of final classification in ETRIMS 8 Classes HOG database. (a) Shows the original image, (b) the groundtruth image, and (c),(d), and (e) show ADAboost, GraphCut, and MMSSL without compression, respectively.

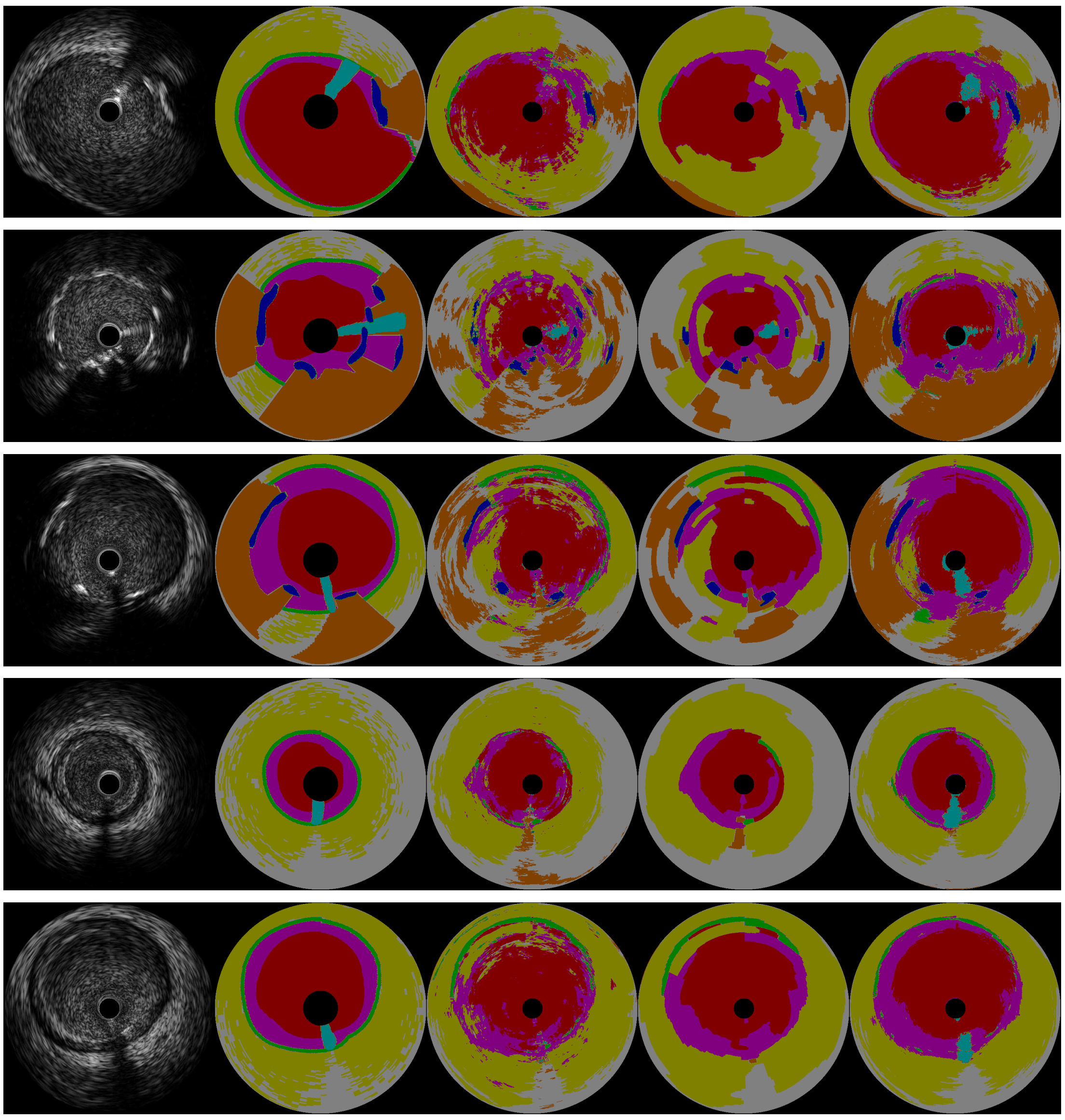

Figure 4.11: Figures of final classification in IVUS using 6 scales. (a) Shows the original image, (b) the groundtruth image, and (c),(d), and (e) show ADAboost, GraphCut, and MMSSL without compression, respectively.

4.5.3.4 Comparing among proposed multi-class MSSL techniques

Finally, Figures 4.12 and 4.13 show the difference among MMSSL approaches. It is appreciable how MMSSL using labels fails classifying long areas of contiguous pixels, while the rest of methods predict them correctly. This is because using confidences for each sample instead of the most probable label makes possible to break ties of equiprobable classes. Differences between compressed and non compressed methods are not so straightforward to see, but while in Figure 4.12 there are few differences in Figure 4.13 we can see how non compressed methods leads to smoother results than compressed methods. Compressed methods tend to fail in closing some classes, appearing spurious pixels inside them. Sometimes this behavior can lead to a better classification if it was misclassified, as it happens in the last row of Figure 4.12. The second row of Figure 4.13 shows the learning capacity of the likelihood maps. In column (d), MMSSL without compression, we can see a boundary marked as unknown object (class 0, black label) in front of the building. Inside this region, it is marked as car label. In the original image, column (a), it is appreciable a woman riding a bicycle in those area. Although in the groundtruth image, column (b), these elements are omitted, our method using likelihood maps is capable of detecting them as an element different to road or building, and assigning the inner region to car label, given its visual appearance and position.

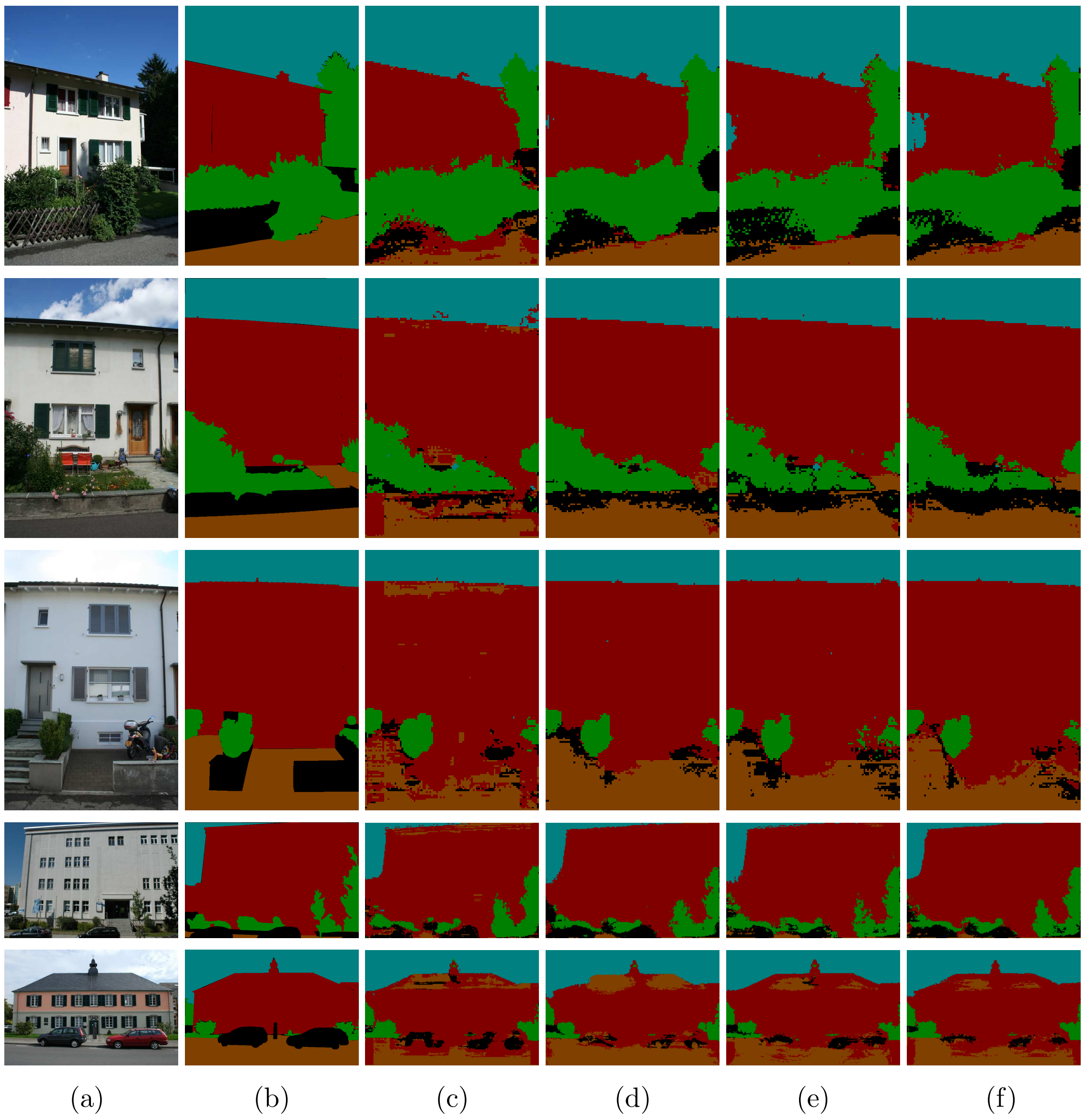

Figure 4.12: Comparative between multi-class multi-scale stacked sequential learning approaches in ETRIMS 4 Classes HOG database. (a) Shows the original image, (b) the groundtruth image, and (c), (d), (e), and (f) shows the different MMSSL schemes: (c) MMSSL using only label predictions, (d) MMSSL using confidences, (e) MMSSL using binary compression, and (f) MMSSL using ternary compression

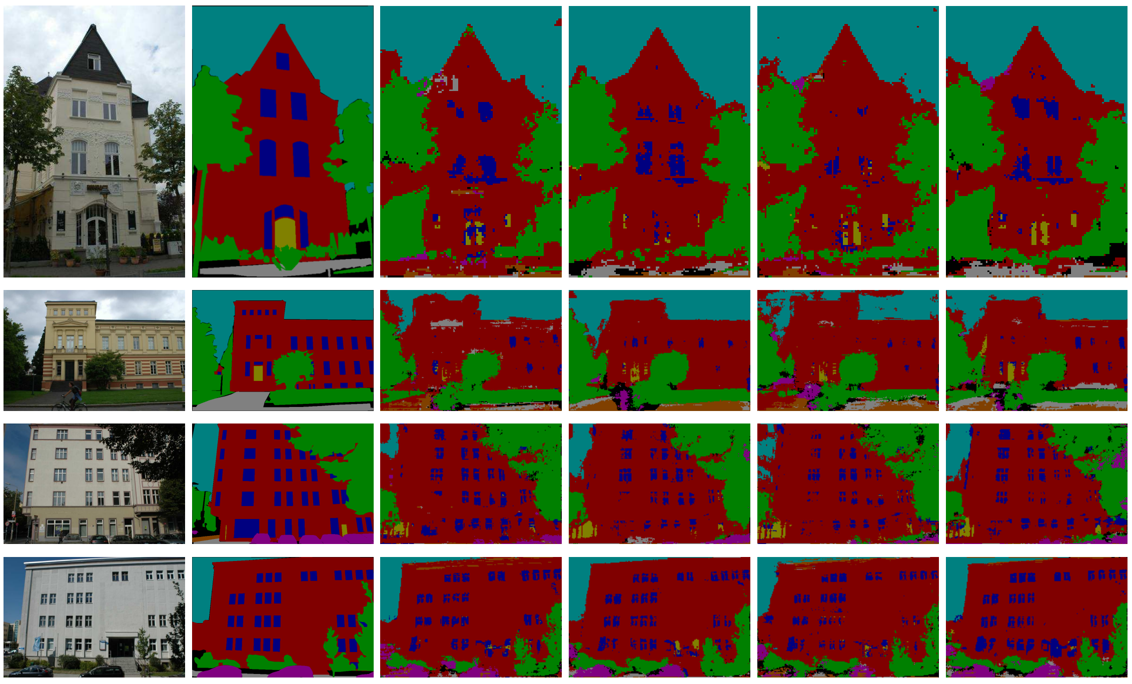

Figure 4.13: Comparative between multi-class multi-scale stacked sequential learning approaches in ETRIMS 8 Classes HOG database. (a) Shows the original image, (b) the groundtruth image, and (c), (d), (e), and (f) shows the different MMSSL schemes: (c) MMSSL using only label predictions, (d) MMSSL using confidences, (e) MMSSL using binary compression, and (f) MMSSL using ternary compression.

4.6 Conclusions

In this chapter we extended the Multi-scale stacked sequential learning framework in different ways. First we adapt the J for working with likelihood values instead of prediction labels when the first classifier is able to produce them. Secondly we adjust the MSSL framework for classifying objects at different sizes. In order to do this, we proposed the *shifting* technique at testing time. This allows to correctly classify objects at different sizes than the learned ones. Thirdly, we adapt the multi-scale sequential learning (MSSL) to the multi-class case (MMSSL). In order to do this, we put the ECOC framework into the base classifiers and show how to compute the confidence maps using the normalized margins obtained from the ECOC base classifiers. Finally we define a compression approach for reducing the number of features in the extended data set. The results show that, on the one hand, MMSSL achieves accurate classification performance in multi-class classification problems taking benefit of sequential learning. On the other hand, the compression process is feasible, since in terms of accuracy the loss of information is negligible.

In next chapter we present an example application of MSSL for human body segmentation, where exists sequential dependences between instances. In this scenario MSSL is used with great success, improving results with respect state-of-the-art methodologies.

5

Application of MSSL for human body segmentation

Human segmentation in RGB images is a challenging task due to the high variability of the human body, which includes a wide range of human poses, lighting conditions, cluttering, clothes, appearance, background, point of view, number of human body limbs, etc. In this particular problem, the goal is to provide a complete segmentation of the person/people appearing in an image. In literature, human body segmentation is usually treated in a two-stage fashion. First, a human body part detection step is performed, obtaining a large set of candidate body parts. These parts are used as prior knowledge by segmentation/inference optimization algorithms in order to obtain the final human body segmentation.

In the first stage, that is the detection of body parts, weak classifiers are trained in order to obtain a soft prior of body parts (which are often noisy and unreliable). Most works in literature have used edge detectors, convolutions with filters, linear SVM classifiers, Adaboost or Cascading classifiers (67). For example, (58) used a tubular edge template as a detector, and convolved it with an image defining locally maximal responses above a threshold as detections. In (57), the authors used quadratic logistic regression on RGB features as the part detectors. Other works, have applied more robust part detectors such as SVM classifiers (15, 35) or AdaBoost (51) trained on HOG features (19). More recently, Dantone et. al used Random Forest as classifiers to learn body parts (20). Although recently robust classifiers have been used, part detectors still involve false-positive and false-negatives problems given the similarity nature among body parts and the presence of background artifacts. Therefore, a second stage is usually required in order to provide an accurate segmentation.

In the second stage, soft part detections are jointly optimized taking into account the nature of the human body. However, standard segmentation techniques (i.e. region-growing, thresholding, edge detection, etc.) are not applicable in this context due to the huge variability of environmental factors (i.e lightning, clothing, cluttering, etc.) and the changing nature of body textures. In this sense, the most known models for the optimization/inference of soft part priors are Poselets (9, 51) of Bourdev et. al. and Pictorial Structures (4, 30, 62) by Felzenszwalb et. al., both of which optimize the initial soft body part priors to obtain a more accurate estimation of the human pose, and provide with a multi-limb detection. In addition, there are some works in literature that tackle the problem of human body segmentation (segmenting the full body as one class) obtaining satisfying results. For instance, Vinet et al. (66) proposed to use Conditional Random Fields (CRF) based on body part detectors to obtain a complete person/background segmentation. Belief propagation, branch and bound or Graph Cut optimization are common approaches used to perform inference of the graphical models defined by human body (38, 39, 59). Finally, methods like structured SVM or mixture of parts (72, 73) can be use in order to take profit of the contextual relations of body parts.

In this chapter, we present a novel two-stage human body segmentation method based on the Multi-Scale Stacked Sequential Learning (MSSL) framework. In the first stage of our method for human segmentation, a multi-class Error-Correcting Output Codes classifier (ECOC) is trained to detect body parts and to produce a soft likelihood map for each body part. In the second stage, a multi-scale decomposition of these maps and a neighborhood sampling is performed, resulting in a new set of features. The extended set of features encodes spatial, contextual and relational information among body parts. This extended set is then fed to the second classifier of MSSL, in this case a Random Forest binary classifier, which maps a multi-limb classification to a binary human classification problem. Finally, in order to obtain the resulting binary human segmentation, a post-processing step is performed by means of Graph Cuts optimization, which is applied to the output of the binary classifier.

5.1 Stage One: Body Parts Soft Detection

In this work, the first stage detector $H_1(x)$ in the MSSL pipeline is based on the soft body parts detectors defined in (60). The work of Bautista *et al* (60) is based on an ECOC ensemble of cascades of Adaboost classifiers. Each of the cascades focuses on a subset of body parts described using Haar-like features where regions have been previously rotated towards main orientation to make the recognition rotation invariant. Although any other part detector technique could be used in the first stage of our process, we also choose the same methodology. As a case study, although any classifier can be included in the ECOC framework, here we considerer as base learner also the same ensemble of cascades given its fast computization.

Because of its properties, cascades of classifiers are usually trained to split one visual object from the rest of possible objects of an image. This means that the cascade of classifiers learns to detect a certain object (body part in our case), ignoring all other objects (all other body parts). However, some body parts have similar appearance, i.e. legs and arms, and thus, it makes sense to group them in the same visual category. Because of this, we learn a set of cascades of classifiers where a subset of limbs are included in the positive set of one cascade, and the remaining limbs are included as negative instances together with background images in the negative set of the cascade. In this sense, classifier H_1 is learned by grouping different cascades of classifiers in a tree-structure way and combining them in an Error-Correcting Output Codes (ECOC) framework (28). Then, H_1 outputs correspond to a multi-limb classification prediction.

An example of the body part tree-structure defined taking into account the nature of human body parts is shown in Fig. 5.2(a). Notice that classes with similar visual appearance (e.g. upper-arm and lower-arm) are grouped in the same meta-class in most dichotomies. In addition, dichotomies that deal with difficult problems (e.g. d^5) are focused only in the difficult classes, without taking into account all other body parts. In this case, class c^7 denotes the background.

We use the problem dependent coding matrix defined in (60) in order to allow the inclusion of cascade of classifiers and learn the body parts. In particular, each dichotomy is obtained from the body part tree-structure. Fig. 5.2(b) shows the coding matrix codification of the tree-structure in Fig. 5.2(a).

In the ECOC *decoding* step an image is processed using a sliding windowing approach. Each image patch x, is described and tested. In our case, each patch is first rotated by main gradient orientation and tested using the ECOC ensemble with Haar-like features and cascade of classifier. In this sense, each classifier d outputs a prediction whether x belongs to one of the two previously learnt meta-classes. Once the set of predictions $c \in \{+1, -1\}^{1\times n}$ is obtained, it is compared to the set of codewords of the classes y^i from M, using a decoding function $\delta(c, y^i)$ and the final prediction is the class with the codeword with minimum decoding, i.e. $\arg\min_i \delta(c, y^i)$. As a decoding function we use the Loss-Weighted approach with linear loss function defined in (28). Then, a body-like probability map is built. This map contains, at each position the

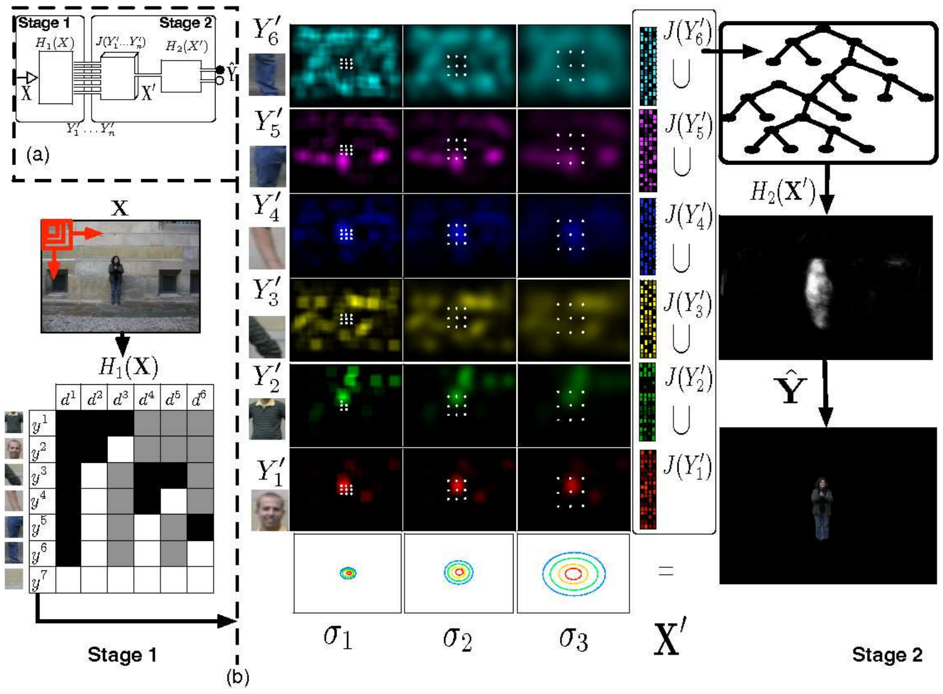

Figure 5.1: Method overview. (a) Abstract pipeline of the proposed MSSL method where the outputs Y'_i of the first multi-class classifier $H_1(x)$ are fed to the multi-scale decomposition and sampling function $J(x)$ and then used to train the second stacked classifier $H_2(x)$ which provides a binary output $\hat{\mathbf{Y}}$. (b) Detailed pipeline for the MSSL approach used in the human segmentation context where $H_1(x)$ is a multi-class classifier that takes a vector $\mathbf{X}$ of images from a dataset. As a result, a set of likelihood maps $Y'_1 \dots Y'_n$ for each part is produced. Then a multi-scale decomposition with a neighborhood sampling function $J(x)$ is applied. The output $\mathbf{X}'$ produced is taken as the input of the second classifier $H_2(x)$, which produces the final likelihood map $\hat{\mathbf{Y}}$, showing for each point the confidence of belonging to human body class.

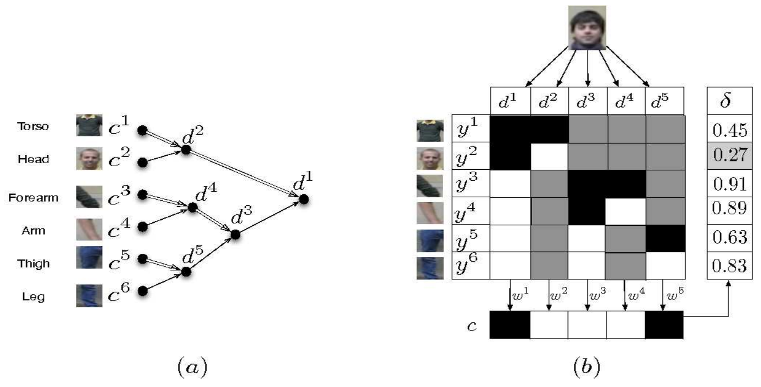
Torso
Head
Forearm
Arm
Thigh
Leg
c^1 c^2 c^3 c^4 c^5 c^6
d^1 d^2 d^3 d^4 d^5
y^1 y^2 y^3 y^4 y^5 y^6
δ
0.45
0.27
0.91
0.89
0.63
0.83
w^1 w^2 w^3 w^4 w^5
c
(a)
(b)

Figure 5.2: (a) Tree-structure classifier of body parts, where nodes represent the defined dichotomies. Notice that the single or double lines indicate the meta-class defined. (b) ECOC decoding step, in which a head sample is classified. The coding matrix codifies the tree-structure of (a), where black and white positions are codified as $+1$ and -1, respectively. c, d, y, w, X, and δ correspond to a class category, a dichotomy, a class codeword, a dichotomy weight, a test codeword, and a decoding function, respectively.

proportion of body part detections for each pixel over the total number of detections for the whole image. In other words, pixels belonging to the human body will show a higher body-like probability than the pixels belonging to the background. Additionally, we also construct a set of limb-like probability maps. Each map contains at each position (i, j) the probability of pixel at the entry (i, j) of belonging to the body part class. This probability is computed as the proportion of detections at point (i, j) over all detection for that class. Examples of probability maps obtained from ECOC outputs are shown in Fig. 5.3, which represents the $H_1(x)$ outputs $Y_1' \dots Y_n'$ defined in Fig. 5.1 (a).

5.2 Stage Two: Fusing Limb Likelihood Maps Using MSSL

The goal of this stage is to fuse all partial body parts into a full human body likelihood map (see Fig. 5.1 (b) second stage). The input data for the neighborhood modeling function $J(x)$ are the body parts likelihood maps obtained in the first stage $(Y_1' \dots Y_n')$. In the first step of the modeling a set of different gaussian filters is applied on each map. All these multi-resolution decompositions give information about the influence of each body part at different scales along the space. Then, a 8-neighbor sampling is performed for each pixel with sampling distance proportional to its decomposition scale. This allows to take into account the different limbs influence and their context. The

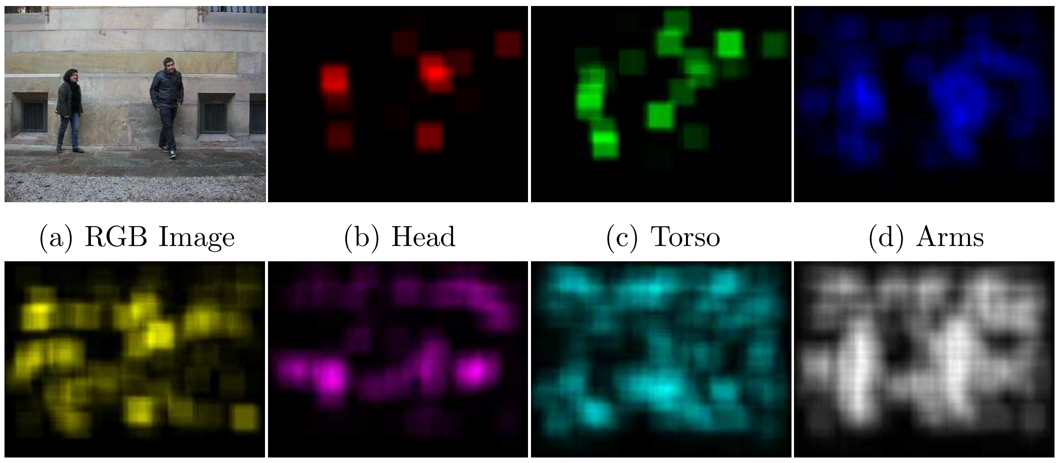

Figure 5.3: Limb-like probability maps for the set of 6 limbs and body-like probability map. Image (a) shows the original RGB image. Images from (b) to (g) illustrate the limb-like probability maps and (h) shows the union of these maps.

extended set X' is formed by stacking all the resulting samplings at each scale for each limb likelihood map (see the extended feature set X' in Fig. 5.1(b)). As a result, X' will have dimensionality equals to the number of samplings multiplied by the number of scales and the number of body parts. In our experiments we use eight neighbor sampling, three scales and six body parts. Notice that contrary to the MSSL traditional framework, we do not fed the second classifier H_2 with both the original X and extended X' features, and only the extended set X' is provided. In this sense, the goal of H_2 is to learn spatial relations among body parts based on the confidences produced by first classifier. As a result, second classifier provides a likelihood of the membership of an image pixel to the class 'person'. Thus, the multiple spatial relations of body parts (obtained as a multi-class classifier in H_1), are labelled as a two-class problem (*person* vs *not person*) and trained by H_2. Consequently, the label set associated to the extended training data X' corresponds to the union of the ground truths of all human body parts. Although, within our method any binary classifier can be considerer for H_2, we use a Random Forest classifier to train 50 random trees that focus on different configurations of the data features. This strategy has shown robust results for human body segmentation in multi-modal data (64). Fig. 5.4 shows a comparative between the union of the likelihood maps obtained by the first classifier and the final likelihoods obtained after the second stage. We can see that a naive fusion of the limb likelihoods produce noisy outputs in many body parts. The last column shows how second stage clearly detects the human body using the same data. For instance, Fig. 5.4 (f) shows how it works well also when two bodies are close one to other, splitting them accurately, preserving the poses. Notice that in Fig. 5.4 (f) a non zero probability zone exists between both silhouettes, denoting the existence of a handshaking. Finally in Fig. 5.4 (c) we can see how the foreground person is highlighted in the likelihood map, while in previous stage (Fig. 5.4 (b)) it was completely missed. This shows that the second stage is able to restore body objects at different scales. Finally, the output likelihood maps obtained after this stage are used as input of a post-process based on graph-cut to obtain final segmentation

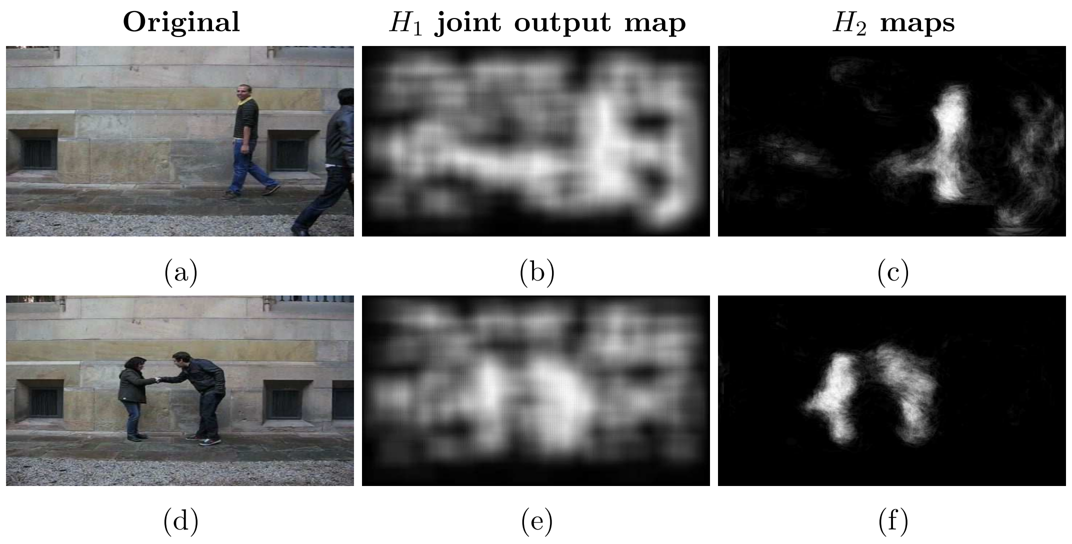

Figure 5.4: Comparative between H_1 and H_2 output. First column are the original images. Second column are H_2 output likelihood maps. Last column are the union of all likelihood map of body parts

5.3 Experimental Results

Before present the experimental results, we first discuss the data, experimental settings, methods and validation protocol.

5.3.1 Dataset

We used *HuPBA* 8*k*+ *dataset* described in (61). This dataset contains more than 8000 labeled images at pixel precision, including more than 120000 manually labeled samples of 14 different limbs. The images are obtained from 9 videos (RGB sequences) and a total of 14 different actors appear in those 9 sequences. In concrete, each sequence has a main actor (9 in total) which during the sequence interacts with secondary actors portraying a wide range of poses. For our experiments, we reduced the number of limbs from the 14 available in the dataset to 6, grouping those that are similar by symmetry (right-left) as arms, forearms, thighs and legs. Thus, the set of limbs of our problem is composed by: *head*, *torso*, *forearms*, *arms*, *thighs* and *legs*. Although labeled within the dataset, we did not include hands and feet in our segmentation scheme. In Fig. 5.5 some samples of the *HuPBA* 8*k*+ dataset are shown.

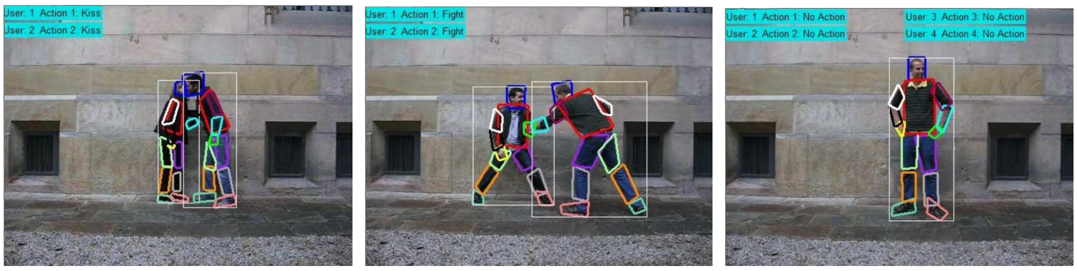
User: 1 Action 1: Kiss
User: 2 Action 2: Kiss
User: 1 Action 1: Fight
User: 2 Action 2: Fight
User: 1 Action 1: No Action
User: 2 Action 2: No Action
User: 3 Action 3: No Action
User: 4 Action 4: No Action

Figure 5.5: Different samples of the HuPBA 8k+ dataset.

5.3.2 Methods

We compare the following methods for Human Segmentation: **Soft Body Parts (SBP) detectors + MSSL + Graphcut**. The proposed method, where the body like confidence map obtained by each body part soft detector is learned by means of MSSL and the output is then fed to a GraphCut optimization to obtain the final segmentation. **SBP detectors + MSSL + GMM-Graphcut**. Variation of the proposed method, where the final GraphCut optimization also learns a GMM color model to obtain the final segmentation as in the GrabCut model (59). **SBP detectors + GraphCut**. In this method the body like confidence map obtained by aggregating all body parts soft detectors outputs is fed to a GraphCut optimization to obtain the final segmentation. **SBP detectors + GMM-GraphCut**. We also use the GMM color modeling variant in the comparison.

5.3.3 Settings and validation protocol

In a preprocessing step, we resized all limb samples to a 32×32 pixels region. Regions are first rotated by main gradient orientation. In the first stage, we used the standard Cascade of Classifiers based on AdaBoost and Haar-like features (67) as our body part multi-class classifier H_1. As model parameters, we forced a 0.99 false positive rate and maximum of 0.4 false alarm rate during 8 stages. To detect limbs with trained cascades of classifiers, we applied a sliding window approach with an initial patch size of 32×32 pixels up to 60×60 pixels. As result of this stage, we obtained 6 likelihood maps for each image. In the second stage, we performed 3-scale gaussian decomposition with $\sigma \in [8, 16, 32]$ for each body part. Then, we generated a extended set selecting for each pixel its 8-neighbors with σ displacement. From this extended set, a sampling of 1500 selected points formed the input examples for the second classifier. As second classifier, we used a Random Forest with 50 decision trees. Finally, in a post-processing stage, binary Graph Cuts with a GMM color modeling (we experimentally set 3 components) were applied to obtain the binary segmentation where the initialization seeds of foreground and background were tuned via cross-validation. For the binary Graph Cuts without a GMM color modeling we directly fed the body likelihood map to the optimization method. In order to assess our results, we used 9-fold cross-validation, where each fold correspond to images of a main actor sequence. As results measurement we used the Jaccard Index of overlapping ($J = \frac{A \bigcap B}{A \bigcup B}$) where A is the ground-truth and B is the corresponding prediction.

5.3.4 Quantitative Results

In Table 5.1 we show overlapping results for the *HuPBA* $8K+$ dataset. Specifically, we show the mean overlapping value obtained by the compared methods on 9 folds of the *HuPBA* $8k+$ dataset. We can see how our MSSL proposal consistently obtains a higher overlapping value on every fold.

Notice that MSSL proposal outperforms in the SBP+GC method in all folds (by at least a 3% difference), which is the state-of-the-art method for human segmentation in the HuPBA $8k+$ dataset (60).

5.3.5 Qualitative Results

In Fig. 5.6 some qualitative results of the compared methodologies for human segmentation are shown. It can be observed how in general SBP+MSSL+GMM-GC obtains a better segmentation of the human body than the SBP + GMM-GC method. This improvement is due to the contextual body part information encoded in the extended feature set. In particular, this performance difference is clearly visible in Fig. 5.6(f) where the human pose is completely extracted from the background. We also observe how the proposed method is able to detect a significative number of body parts at different scales. This is clearly appreciated in Fig. 5.6(c), where persons at different scales

	GMM-GC		GC	
	MSSL	**Soft Detect.**	**MSSL**	**Soft Detect.**
Fold	**Overlap**	**Overlap**	**Overlap**	**Overlap**
1	**62.35**	60.35	**63.16**	60.53
2	**67.77**	63.72	**67.28**	63.75
3	**62.22**	60.72	**61.76**	60.67
4	**58.53**	55.69	**58.28**	55.42
5	**55.79**	51.60	**55.21**	51.53
6	**62.58**	56.56	**62.33**	55.83
7	**63.08**	60.67	**62.79**	60.62
8	**67.37**	64.84	**67.41**	65.41
9	**64.95**	59.83	**64.21**	59.90
Mean	**62,73**	59,33	**62,49**	59,29

Table 5.1: Overlapping results over the 9 folds of the *HupBA8K+* dataset for the proposed MSSL method and the Soft detectors post-processing their outputs with the Graph-Cuts method and GMM Graph-Cuts method.

are segmented, while in Fig. 5.6(b) the SBP+GMM-GC fails to segment the rightmost person. Furthermore, Fig. 5.6(i) shows how the proposed method is able to recover the whole body pose by stacking all body parts, while in Fig. 5.6(h) the SBP+GMM-GC method just detected the head of the left most user. In this pair of images also we can see how our method is able to discriminate the different people appearing in an image, segmenting as background the interspace between them. Although, it may cause some loss, specially in the thinner body parts, like happens with the extended arm. Due to space restrictions, a table with more examples of segmentation results can be found in the supplementary material. Regards the dataset used, it is important to remark the large amount of segmented bodies (more than 10.000) and their high variability in terms of pose (performing different activities and interactions with different people), size and clothes. The scale variations are learnt by H_2 through spatial relationships of body parts. In addition, although background is maintained across the data, H_2 is trained over the soft predictions from H_1 (see the large number of false positive predictions shown in Fig. 5.3), and our method considerably improves those person confidence maps, as shown in Fig. 5.4.

5.4 Conclusions

We presented a two-stage scheme based on the MSSL framework for the segmentation of the human body in still images. We defined an extended feature set by stacking a multi-scale decomposition of body part likelihood maps, which are learned by means of a multi-class classifier based on soft body part detectors. The extended set of features encodes spatial and contextual information of human limbs which combined enabled us to define features with high order information. We tested our proposal on a large dataset obtaining significant segmentation improvement over state-of-the-art methodologies.

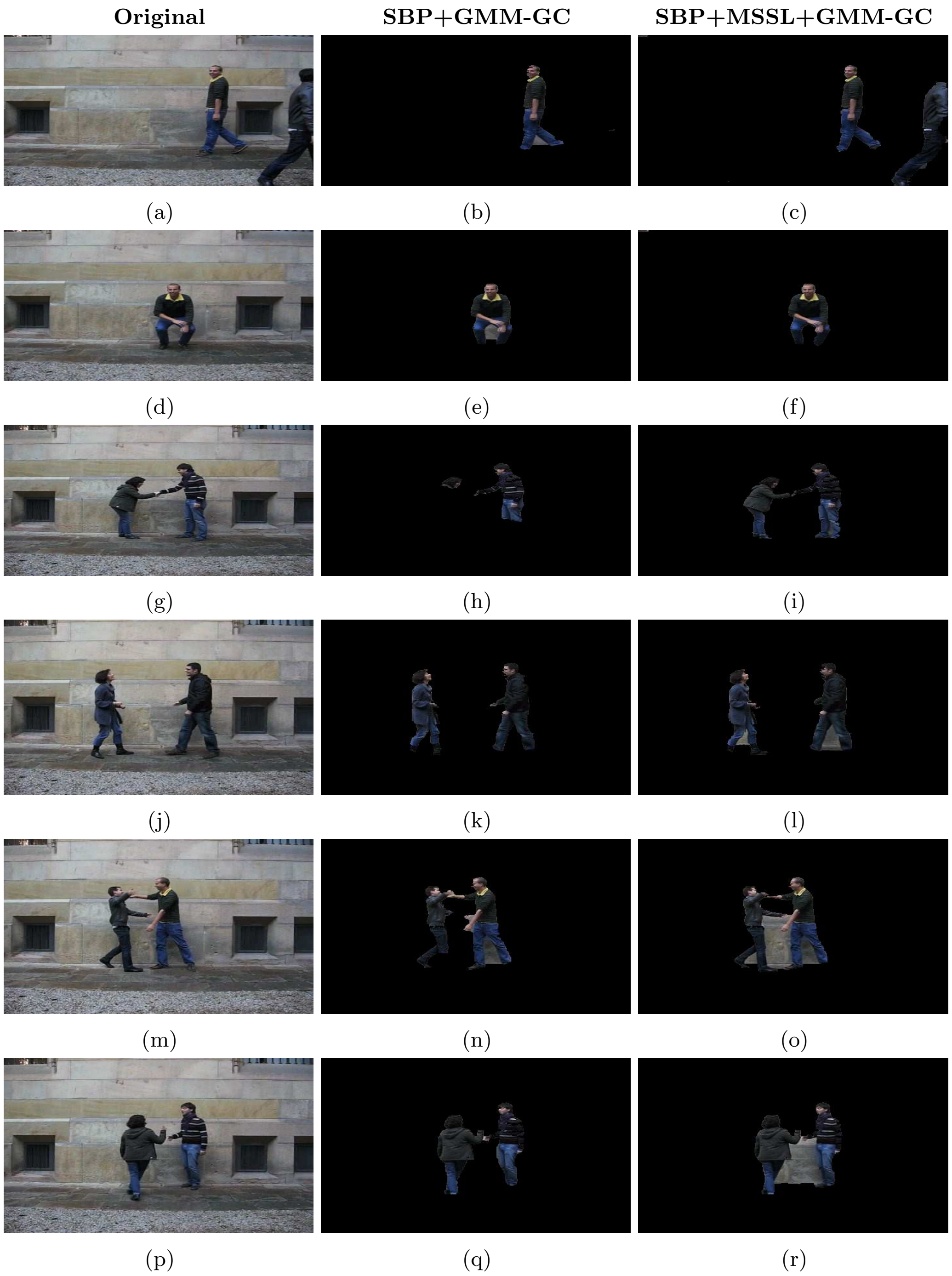

Figure 5.6: Samples of the segmentation results obtained by the compared approaches.

6

Conclusions

This thesis focuses on the problem of sequential learning from a meta-learning perspective.

Chapter 1 introduces the concept of sequential learning and the motivations of this thesis.

Chapter 2 reviews some approaches of sequential learning from different points of view. These approaches mainly comes from machine learning and pattern recognition fields. However, since one of the motivations is to use sequential learning in images classification tasks, we have reviewed some related works appeared in computer vision field.

As a result of the research in this topic, in this thesis the following contributions are proposed:

- In Chapter 3 we present a novel framework for sequential learning problems. Specifically, we generalize the stacked sequential learning framework (SSL) stressing the key role of the neighborhood modeling, in order to apply it in problems such as object recognition or human body parts segmentation. Thanks to the inclusion of function J after first classifier, where the multi-scale decomposition and sampling of predictions is performed, our approach (MSSL) is more efficient and capable to capture longer distance interactions than the original SSL. The method allows to have an explicit trade-off between the resolution of the interactions we desire to model and the number of features; very detailed interactions can be modeled in short distance or long distance patterns can be captured with a coarser resolution using the same number of features in the extended training set. We show that strategies mixing detailed interactions and long ranges can be defined at the cost of adding more features. The proposed method has been tested on two different data sets, the first on a 1D correlation lattice and the second on a 2D correlation lattice. We have compared our methodology with the graphical model CRF. Our method has obtained better results in both datasets, assuming non *a priori* knowledge of the structure of the labels. Even, our methodology is more straight-forward than the graphical models, since the loss function dependency is delegated to the base classifier. This means that the parametrization of our method is only dependent on the base classifier, the number of scales in the multi-resolution step and the number of sampled elements forming the extended data set. This last two parameters can be easily tuned depending on the application dataset and the computation capacity available.

On going research in MSSL is towards to consider non-isotropic and/or non-linear decomposition methods. Recently, Gatta and Ciompi (33) use scale-space Taylor coefficients in order to model the neighborhood relationships, instead of using multi-resolution decomposition. Meanwhile, we have already performed some experiments applying wavelets and bilateral filters instead of multi-resolution decomposition, but in the general case, the results have not been significantly better than the ones obtained using MSSL.

- In Chapter 4 we develop some improvements over MSSL framework. Specifically, we have developed a general and efficient extension of MSSL for the multi-class case by integrating the ECOC framework in the base classifiers. We test our multi-class methodology performing different experiments out from four databases showing different kind of sequential relationships: Sensor motion data database, FAQ database, IVUS image database and e-trims database. We test all the databases with different configurations of our MSSL methodology, including a feature-compression approach based on sub-lineal ECOCs. Finally, we compare our results with Real Adaboost and CRF Multi-label optimization through Graph Cut α-expansion methodologies.

  As future work we going to experiment with other compression approaches, such as compressed sensing or PCA, for the sake of reducing the extended set as much as possible without losing accuracy.

- The last contribution of this chapter is an architecture specifically designed for classification of different sized objects. The challenge in this problem comes by the fact that the classifier has not been necessarily exposed to examples at the different scales found in the testing images. We have used two images dataset for testing our architecture: a data base of pictures of different sized horses and a data base of different types and sized flowers. Adaboost and CRF are also used as baseline experiments in order to compare our achieved results.

As future work we consider a scale and rotation invariant architecture, shifting not only the scales but also the sampled neighborhood patterns.

- Finally, in Chapter 5 we present an application of MSSL for human body segmentation. We presented a two-stage scheme based on the MSSL framework for the segmentation of the human body in still images. We defined an extended feature set based on likelihood maps obtained from soft body part detectors. These features encode spatial and contextual information of human limbs providing high order information to the second classifier. We tested our proposal on a large dataset obtaining significant segmentation improvement over state-of-the-art methodologies.

  Our work in progress is to refine our body segmentation application in order to perform accurate multi-limb body segmentation. This is, to perform correctly segmentation of each part of the body (arms, legs, torso, head...) by using our MSSL framework.

Bibliography

[1] Aas, K., Eikvil, L. & Huseby, R. (1999). Applications of hidden markov chains in image analysis. *Pattern Recognition*, **32**, 703–713. 10

[2] Adelson, E.H., Anderson, C.H., Bergen, J.R., Burt, P.J. & Ogden, J.M. (1984). Pyramid methods in image processing. *RCA Engineer*, **29**, 33–41. 23

[3] Allwein, E., Schapire, R. & Singer, Y. (2002). Reducing multiclass to binary: A unifying approach for margin classifiers. *JMLR*, **1**, 113–141. 17, 48

[4] Andriluka, M., Roth, S. & Schiele, B. (2009). Pictorial structures revisited: People detection and articulated pose estimation. In *Computer Vision and Pattern Recognition, 2009. CVPR 2009. IEEE Conference on*, 1014–1021, IEEE. 76

[5] Bengio, Y. & Frasconi, P. (1996). Input-output HMM's for sequence processing. *IEEE Transactions on Neural Networks*, **7(5)**, 1231–1249. 13, 14

[6] Borenstein, E. & Malik, J. (2006). Shape guided object segmentation. In *CVPR (1)*, 969–976. 36

[7] Borenstein, E. & Ullman, S. (2002). Class-specific, top-down segmentation. In *Proceedings of the European Conference on Computer Vision*, vol. 2351, 109–124, Copenhagen, Denmark. 31, 32, 35, 36

[8] Borenstein, E. & Ullman, S. (2004). Learning to segment. In T. Pajdla & J. Matas, eds., *European Conference on Computer Vision (3)*, vol. 3023 of *Lecture Notes in Computer Science*, 315–328, Springer. 54

[9] Bourdev, L., Maji, S., Brox, T. & Malik, J. (2010). Detecting people using mutually consistent poselet activations. In *Computer Vision–ECCV 2010*, 168–181, Springer. 76

[10] Boykov, Y. & Funka-Lea, G. (2006). Graph cuts and efficient nd image segmentation. *International Journal of Computer Vision*, **70**, 109–131. 58

[11] Boykov, Y., Veksler, O. & Zabih, R. (2001). Fast approximate energy minimization via graph cuts. *IEEE Trans. Pattern Anal. Mach. Intell.*, **23**, 1222–1239. 16, 17

[12] Burt, P. & Adelson, E. (1983). The laplacian pyramid as a compact image code. *IEEE Transactions on Communications*, 532–540. 21

[13] Cai, J. & Liu, Z. (2002). Pattern recognition using markov random field models. *Pattern Recognition*, **35**, 725–733. 14

[14] Casale, P., Pujol, O. & Radeva, P. (2012). Personalization and user verification in wearable systems using biometric walking patterns. *Personal Ubiquitous Comput.*, **16**, 563–580. 57

[15] Chakraborty, B., Bagdanov, A.D., Gonzalez, J. & Roca, X. (2011). Human action recognition using an ensemble of body-part detectors. *Expert Systems*. 75

[16] Ciompi, F., Pujol, O., Gatta, C., Carrillo, X., Mauri, J. & Radeva, P. (2011). A holistic approach for the detection of media-adventitia border in ivus. In *MICCAI (3)*, 411–419. 58

[17] Cohen, W.W. & de Carvalho, V.R. (2005). Stacked sequential learning. *Proc. of IJCAI 2005*, 671–676. 2, 19, 27, 58

[18] Cour, T. & Shi, J. (2007). Recognizing objects by piecing together the segmentation puzzle. In *Proc. IEEE Computer Society Conference on Computer Vision and Pattern Recognition*, 1 – 8, IEEE Computer Society, Minneapolis, Minnesota, USA. 16

[19] Dalal, N. & Triggs, B. (2005). Histograms of oriented gradients for human detection. In *CVPR*, vol. 1, 886 –893. 58, 75

[20] Dantone, M., Gall, J., Leistner, C. & van Gool, L. (2013). Human pose estimation using body parts dependent joint regressors. In *Computer Vision and Pattern Recognition (CVPR), 2013 IEEE Conference on*, 3041–3048. 75

[21] Darroch, J.N. & Ratcliff, D. (1972). Generalized iterative scaling for log-linear models. *The Annals of Mathematical Statistics*, **43**, 1470–1480. 14

[22] Dempster, A.P., Laird, N.M. & Rubin, D.B. (1977). Maximum likelihood from incomplete data via the em algorithm. *JOURNAL OF THE ROYAL STATISTICAL SOCIETY, SERIES B*, **39**, 1–38. 14

[23] Demšar, J. (2006). Statistical comparisons of classifiers over multiple data sets. *J. Mach. Learn. Res.*, **7**, 1–30. 33, 59, 63

[24] Dietterich, T. & Bakiri, G. (1995). Solving multiclass learning problems via error-correcting output codes. In *Journal of Artificial Intelligence Research*, vol. 2, 263–286. 17, 48

[25] Dietterich, T.G. (2002). Machine learning for sequential data: A review. In *Proceedings of the Joint IAPR International Workshop on Structural, Syntactic, and Statistical Pattern Recognition*, 15–30, Springer-Verlag, London, UK. 1, 2, 8, 17

[26] Dietterich, T.G., Ashenfelter, A. & Bulatov, Y. (2004). Training conditional random fields via gradient tree boosting. In *Proceedings of the 21th International Conference on Machine Learning*, 217–224, ACM, Banff, Alberta, Canada. 27, 58

[27] Escalera, S., Tax, D., Pujol, O., Radeva, P. & Duin, R. (2008). Subclass problem-dependent design of error-correcting output codes. *PAMI*, **30**, 1–14. 17, 48, 49

[28] Escalera, S., Pujol, O. & Radeva, P. (2010). On the decoding process in ternary error-correcting output codes. *PAMI*, **32**, 120–134. 49, 77

[29] Fawcett, T. & Provost, F. (1997). Adaptive fraud detection. *Data Mining and Knowledge Discovery*, **1**, 291–316. 9

[30] Felzenszwalb, P.F. & Huttenlocher, D.P. (2000). Efficient matching of pictorial structures. In *Computer Vision and Pattern Recognition, 2000. Proceedings. IEEE Conference on*, vol. 2, 66–73, IEEE. 76

[31] Freund, Y. & Schapire, R. (1995). A decision-theoretic generalization of online learning and an application to boosting. In *EuroCOLT*, 23–37. 58

[32] Friedman, J., Hastie, T. & Tibshirani, R. (2000). Additive Logistic Regression: a Statistical View of Boosting. *The Annals of Statistics*, **38**. 46

[33] GATTA, C. & CIOMPI, F. (2014). Stacked sequential scale-space taylor context. *IEEE Transactions on Pattern Analysis and Machine Intelligence*, **36**, 1694–1700. 88

[34] GATTA, C., PUERTAS, E. & PUJOL, O. (2011). Multi-scale stacked sequential learning. *Pattern Recognition*, **44**, 2414–2426. 4

[35] GKIOXARI, G., ARBELAEZ, P., BOURDEV, L.D. & MALIK, J. (2013). Articulated pose estimation using discriminative armlet classifiers. In *CVPR*, 3342–3349, IEEE. 75

[36] GORELICK, L. & BASRI, R. (2009). Shape based detection and top-down delineation using image segments. *Int. J. Comput. Vision*, **83**, 211–232. 16, 36

[37] HEITZ, G. & KOLLER, D. (2008). Learning spatial context: Using stuff to find things. In *Proceedings of the 10th European Conference on Computer Vision*, 30–43, Springer-Verlag, Marseille, France. 16

[38] HERNÁNDEZ-VELA, A., REYES, M., PONCE, V. & ESCALERA, S. (2012). Grabcut-based human segmentation in video sequences. *Sensors*, **12**, 15376–15393. 76

[39] HERNÁNDEZ-VELA, A., ZLATEVA, N., MARINOV, A., REYES, M., RADEVA, P., DIMOV, D. & ESCALERA, S. (2012). Graph cuts optimization for multi-limb human segmentation in depth maps. In *CVPR*, 726–732. 76

[40] JACCARD, P. (1901). Distribution de la flore alpine dans le bassin des drouces et dans quelques regions voisines. *Bulletin del la Société Vaudoisedes Sciences Naturelles*, **37**, 241–272. 32

[41] KORČ, F. & FÖRSTNER, W. (2009). eTRIMS image database for interpreting images of man-made scenes. Tech. Rep. TR-IGG-P-2009-01, Institute of Geodesy and Geoinformation, Universität Bonn. 58

[42] KUMAR, M.P., TORR, P.H.S. & ZISSERMAN, A. (2005). Obj cut. In *Proceedings of the 2005 IEEE Computer Society Conference on Computer Vision and Pattern Recognition (CVPR'05) - Volume 1 - Volume 01*, CVPR '05, 18–25, IEEE Computer Society, Washington, DC, USA. 36

[43] KUMAR, S. & HEBERT, M. (2003). Discriminative random fields: A discriminative framework for contextual interaction in classification. In *Proceedings of the 2003*

IEEE International Conference on Computer Vision (ICCV '03), vol. 2, 1150–1157, Nice, France. 16

[44] Lafferty, J.D., McCallum, A. & Pereira, F. (2001). Conditional random fields: Probabilistic models for segmenting and labeling sequence data. In *Proceedings of the International Conference on Machine Learning*, 282–289, Williamstown, MA, USA. 13, 14

[45] Lee, C.H., Greiner, R. & Schmidt, M.W. (2005). Support vector random fields for spatial classification. In A. Jorge, L. Torgo, P. Brazdil, R. Camacho & J. Gama, eds., *PKDD*, vol. 3721 of *Lecture Notes in Computer Science*, 121–132, Springer. 57

[46] Levin, A. & Weiss, Y. (2009). Learning to combine bottom-up and top-down segmentation. *International Journal of Computer Vision*, **81**, 105–118. 36

[47] McCallum, A., Freitag, D. & Pereira, F.C.N. (2000). Maximum entropy markov models for information extraction and segmentation. In *Proceedings of the Seventeenth International Conference on Machine Learning*, 591–598, Morgan Kaufmann Publishers Inc., San Francisco, CA, USA. 13, 28

[48] Mitchell, T.M. (1997). *Machine Learning*. McGraw-Hill, Inc., New York, NY, USA, 1st edn. 7

[49] Nilsback, M.E. & Zisserman, A. (2006). A visual vocabulary for flower classification. In *Proc. IEEE Conf. Comput. Vision Pattern Recog.*, vol. 2, 1447–1454, IEEE Computer Society. 55

[50] Nilsson, N. (1965). Learning machines. In *McGraw-Hill*. 17, 49

[51] Pishchulin, L., Andriluka, M., Gehler, P. & Schiele, B. (2013). Poselet conditioned pictorial structures. In *Computer Vision and Pattern Recognition (CVPR), 2013 IEEE Conference on*, 588–595, IEEE. 75, 76

[52] Puertas, E., Escalera, S. & Pujol, O. (2010). Classifying objects at different sizes with multi-scale stacked sequential learning. In *CCIA*, 193–200. 5

[53] Puertas, E., Escalera, S. & Pujol, O. (2013). Generalized multi-scale stacked sequential learning for multi-class classification. *Pattern Analysis and Applications*, 1–15. 5

[54] Puertas, E., Bautista, M., S'anchez, D., Escalera, S. & Pujol, O. (2014). Learning to segment humans by stacking their body parts. In *ChaLearn Looking at people Workshop, ECCV*. 5

[55] Qian, N. & Sejnowski, T.J. (1988). Predicting the secondary structure of globular proteins using neural network models. *Journal of Molecular Biology*, **202**, 865–884. 9

[56] Rabiner, L.R. (1989). A tutorial on hidden markov models and selected applications in speech recognition. *Proceedings of the IEEE*, **77**, 257–286. 10, 12

[57] Ramanan, D., Forsyth, D. & Zisserman, A. (2005). Strike a pose: tracking people by finding stylized poses. In *Computer Vision and Pattern Recognition, 2005. CVPR 2005. IEEE Computer Society Conference on*, vol. 1, 271–278 vol. 1. 75

[58] Ramanan, D., Forsyth, D. & Zisserman, A. (2007). Tracking people by learning their appearance. *PAMI*, **29**, 65 –81. 75

[59] Rother, C., Kolmogorov, V. & Blake, A. (2004). "grabcut": interactive foreground extraction using iterated graph cuts. *ACM Trans. Graph.*, **23**, 309–314. 76, 82

[60] Sanchez, D., Ortega, J.C., Bautista, M.A. & Escalera, S. (2013). Human body segmentation with multi-limb error-correcting output codes detection and graph cuts optimization. In *Proceedings of InPRIA*, 50–58. 76, 77, 83

[61] Sanchez, D., Bautista, M. & Escalera, S. (2014). Hupba 8k+: Dataset and ecocgraphcut based segmentation of human limbs. *Neurocomputing*. 81

[62] Sapp, B., Jordan, C. & Taskar, B. (2010). Adaptive pose priors for pictorial structures. In *Computer Vision and Pattern Recognition (CVPR), 2010 IEEE Conference on*, 422–429, IEEE. 76

[63] Sejnowski, T.J. & Rosenberg, C.R. (1987). Parallel networks that learn to pronounce english text. *Complex Systems*, **1**, 145–168. 9

[64] Shotton, J., Fitzgibbon, A., Cook, M., Sharp, T., Finocchio, M., Moore, R., Kipman, A. & Blake, A. (2011). Real-Time Human Pose Recognition in Parts from Single Depth Images. In *Computer Vision and Pattern Recognition*. 80

[65] Torralba, A. (2003). Contextual priming for object detection. *Int. J. Comput. Vision*, **53**, 169–191. 17

[66] Vineet, V., Warrell, J., Ladicky, L. & Torr, P. (2011). Human instance segmentation from video using detector-based conditional random fields. In *BMVC*. 76

[67] Viola, P. & Jones, M. (2001). Rapid object detection using a boosted cascade of simple features. In *CVPR*, vol. 1. 75, 82

[68] Vishwanathan, S.V.N., Schraudolph, N.N., Schmidt, M.W. & Murphy, K.P. (2006). Accelerated training of conditional random fields with stochastic gradient methods. In *Proceedings of the 23rd International Conference on Machine Learning*, 969–976, ACM, New York, NY, USA. 16, 31, 35

[69] Weiss, Y. (2001). Comparing the mean field method and belief propagation for approximate inference in mrfs. 16

[70] Winn, J. (2005). Locus: Learning object classes with unsupervised segmentation. In *in ICCV*, 756–763. 36

[71] Wolpert, D.H. (1992). Stacked generalization. *Neural Networks*, 241–259. 8, 10, 19

[72] Yang, Y. & Ramanan, D. (2011). Articulated pose estimation with flexible mixtures-of-parts. In *IEEE Conference on Computer Vision and Pattern Recognition*, 1385–1392, IEEE. 76

[73] Yu, C.N.J. & Joachims, T. (2009). Learning structural svms with latent variables. In *Proceedings of the 26th Annual International Conference on Machine Learning*, 1169–1176, ACM. 76